Adsorption and Wetting

experiments, thermodynamics and molecular aspects

40951

Promotor: dr. J. Lyklema

hoogleraar in de fysische chemie, met bijzondere

aandacht voor de grensvlak- en kolloïdchemie

Co-promotor: dr. ir. L.K. Koopal

universitair hoofddocent bij de

vakgroep Fysische en Kolloïdchemie

Adsorption and Wetting

experiments, thermodynamics and molecular aspects

Lucas Jozef Maria Schlangen

Proefschrift

ter verkrijging van de graad van doctor

in de landbouw- en milieuwetenschappen

op gezag van de rector magnificus,

dr. C. M. Karssen,

in het openbaar te verdedigen

op dinsdag 27 juni 1995

des namiddags te vier uur in de Aula

van de Landbouwuniversiteit te Wageningen.

I ▲   ·SITEIT

The White Rabbit put on his spectacles. "Where shall I begin, please your Majesty?" he asked. "Begin at the beginning," the King said, very gravely, "and go on till you come to the end: then stop."

(from: "Alice's Adventures in Wonderland", Lewis Carroll, 1865)

Voorwoord

Hoe korter je nadenkt over een vraag hoe eenvoudiger het antwoord vaak zal zijn. Soms moet je echter juist lang nadenken voor een eenvoudig antwoord, terwijl een eenvoudig antwoord weer aanleiding kan geven tot lang denken. "Hoe staan adsorptie en bevochtiging met elkaar in verband?" was de centrale vraagstelling waaraan ik gedurende vier jaar heb gewerkt. Getuige de omvang van het proefschrift is het antwoord wel wetenschappelijk maar niet echt eenvoudig geworden. Voor eenvoud is of heel weinig of heel veel kennis vereist. Het eerste station is gepasseerd, het tweede is in zicht maar nog niet gehaald.

Het schrijven van een proefschrift vergt veel van één persoon maar is zeker geen eenzaam avontuur, vele mensen zijn er direct of indirect bij betrokken. Een aantal van hen wil ik hier graag met name noemen. Luuk, in (onze) discussies heeft het jou nooit aan stelligheid ontbroken. Met de jou eigen directe en voortvarende wijze van communiceren heb jij mij dikwijls weten te stimuleren, ook op moeilijke momenten. Hiermee heb je zowel mij als het proefschrift veel goedgedaan. Ik kijk met veel plezier terug naar onze samenwerking en hoop nog vaker mensen zoals jij te treffen.

Martien Cohen Stuart heeft met zijn inspirerende ideeënstroom geholpen het onderzoek op de rails te zetten en te houden. Daarnaast bleek hij uitermate bedreven in "la diplomatie française". Hoewel mijn promotor Hans Lyklema zich meesttijds op de achtergrond hield was hij steeds paraat wanneer hem naar zijn mening of advies werd gevraagd. Hans, bedankt voor het in mij gestelde vertrouwen. De theoretische berekeningen waren niet mogelijk geweest wanneer ik niet op de schouders had kunnen staan van Frans, Cas en Peter, mensen die in meerdere opzichten (een) prima gezelschap zijn. Jos en Marc, jullie maakten mijn werkplek tot een thuis waar het uitstekend werken was, ik zal jullie missen.

Dankzij en door de uitermatig plezierige sfeer op het lab en daarbuiten (zoals tijdens feestjes, wandelweekenden en volleyactiviteiten) heb ik de mens in de collega en de collega in de mens mogen ontdekken. In dit verband wil ik (nog) een aantal mensen niet onvermeld laten: Martin TA, Katinka, Janet, Jeannette, Ronald en Anton.....bedankt!

Je tiens à exprimer mes plus profonds remerciements au Dr. Michel Robin pour m'avoir accueilli au Laboratoire de Physico-Chimie Appliquée et d'Analyse de l'Institut Français du Pétrole. Ma reconnaissance va également à Xhuliano, Emmanuelle, Gerard, Albert, Yannick, Yves, Suzanne, Thierry, Didier et Corrine pour leur hospitalité et

leur amitié au travail. J'ai de très bons souvenirs des heures de repas et des petites ballades avec vous. Emanuelle, ton remarquable sens de l'humour (je me souviens des "trucs" comme "le Roi de la soudure" et le "GTT") et ton amitié ont fait de mon sejour à Paris un vrai plaisir, merci.

Zonder mijn vrienden, met name Yvonne, Romke, René, Wendelmoet, Antoine, Elles en Evert, zou ik niet de persoon zijn die ik nu ben. Dit geldt des te meer voor mijn ouders op wie ik zo dikwijls heb mogen bouwen en met wie ik nu nog steeds graag op vakantie mag gaan.

Lieve Anne,
te midden de betrekkelijkheid der woorden,
sta ik trots met jou, zij aan zij.

Luc

Contents

iii

Chapter 1

General Introduction

1.1. Wetting

Wetting refers to the different situations that may arise when a liquid comes into contact with a solid surface originally contacting a gas or another liquid. The liquid may move out over the solid until it comes to a halt when the angle between the liquid-fluid and solid-liquid interface reaches a certain value, the contact angle. Alternatively, the liquid may spread maximally over the solid under displacement of the original contacting liquid or gas.

Wetting of solid substrates by liquids is relevant for many natural and commercial processes. Ducks grease their feathers in order to render them strongly water repellent. If water would completely wet their feathers this would strongly reduce their floatability. This example shows that the wetting properties of a solid can be controlled by changing the "surface composition" of the solid: coating operations allow wettability control. In human invented coating operations teflon (polytetrafluoroethylene) is often used as surface coating material because of its very low affinity for other materials. This low affinity character can easily be demonstrated by putting a water droplet in a teflon coated frying-pan: the droplet tries to minimize its contact area with the pan and will not spread. In special waterproof and breathing outdoor garmets expanded polytetrafluorethylene is often applied as membrane material. The membrane iself is water repellent whereas moisture vapour is still able to pass through the tiny pores in the membrane.

In many industrial technologies wetting (-related) problems are encountered. In coating industry, a decorative or protective coating should spread over the object and give good adhesion. Furthermore, during manufacture the coating formulation should wet, disperse and stabilize the pigments and protective agents. In semiconductor industry, silicon wafers are often cleaned from adhering particles by immersion in liquid prior to processing. When a particle adhering to the wafer passes through the liquid-gas interface the liquid may sweep the particle from the solid. The larger the resistance of the particle to be wetted by the liquid the more efficient the cleaning will be. In flotation processes, as for instance metal extraction from ore, wettability differences between particles, dispersed in a liquid medium, are used to separate the different types of particles from the dispersion. Other examples of processes for which wetting is relevant are the spreading of the liquid droplets on solids formed by spraying

of agricultural chemicals, the penetration and spreading of ink on paper, painting, lubrication and the displacement of oil by water in enhanced oil recovery.

The significance of wetting for many processes and products is now increasingly recognized and this has stimulated much research in the area [1, 2]. Also from a fundamental perspective, wetting studies are challenging as the macroscopic wetting properties of a system are the result of intermolecular interactions acting across fluid-solid and fluid-fluid interfaces. Over the past few decades knowledge of these interactions has increased considerably [3-5]. This renewed scientific interest in both the statics and dynamics of wetting [6].

This thesis concentrates both on the macroscopic conditions and on the molecular interpretation of wetting. To this end wetting and adhesion will be studied in the context of adsorption. Special attention will be paid to linear hydrocarbons as they often serve as standards in wettability and adhesion studies [7, 8].

1.2. Adsorption and wetting

In general, the molecular density and organisation of a fluid in interfacial regions differs from that of bulk fluid. At a hard impenetrable solid surface molecules are restricted in their movement and the number of conformations (shapes and orientations) they can have. When vapour molecules adsorb on a solid this results in a decrease in entropy that has to be compensated for by the adsorption energy. Only when the adsorption energy compensates this entropy loss will molecules accumulate in the interfacial region.

When a liquid contacts a solid surface, two different equilibrium states of wetting can be found. These equilibrium states are denoted as "partial" and "complete" wetting. Partial wetting refers to the situation where the liquid only partially spreads on the solid under formation of a droplet with a finite contact angle θ, as depicted in Fig. 1a. In the case of complete wetting the liquid spreads maximally over the solid substrate. If enough liquid is present, the final equilibrium state is a macroscopic liquid layer which covers the whole solid surface, see Fig. 1b.

Adsorption and wetting are strongly related. This is particularly obvious when considering the adsorption of vapour v of a volatile liquid L onto a solid surface S. Adsorbing vapour molecules form a film which thickens with increasing vapour pressure. At saturation and in the presence of enough vapour, the adsorbed film may grow to a macroscopically thick layer with properties of bulk liquid. In this case the solid is completely wetted by the liquid. When the thickness of the film formed at saturation is not macroscopic we are dealing with partial wetting.
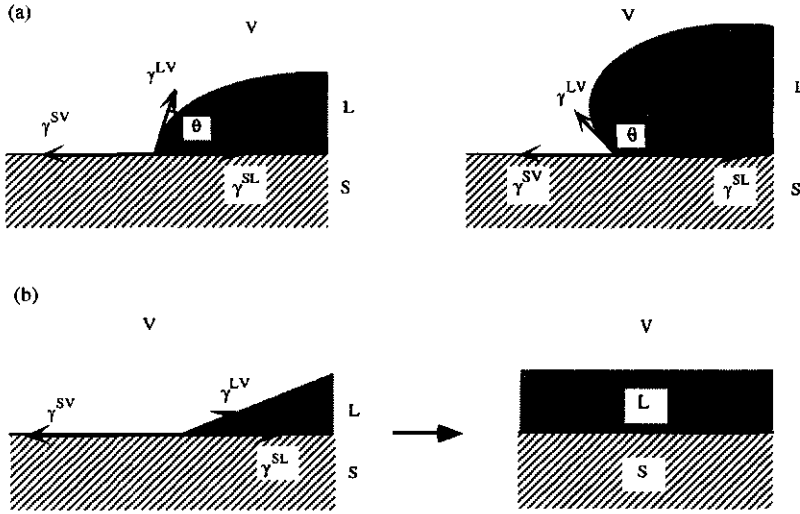
Figure 1. Different equilibrium states of wetting in a solid(S)-liquid(L)-vapour(V) system. (a) Two partial wetting cases; on the left normal partial wetting is shown, on the right hand side a more extreme partial wetting situation is sketched. (b) Complete wetting. The arrows represent the interfacial tensions of the interfaces involved in the wetting process. The left figure is not an equilibrium situation; the net force (due to the sum of the interfacial tensions) is to the left. When enough liquid is present the liquid will spread over the solid until the final equilibrium situation shown on the r.h.s. is attained.

The wetting characteristics of a solid-liquid pair can be identified by the shape of the vapour adsorption isotherm (which is a plot of the adsorbed amount of vapour as a function of the vapour pressure, see Fig. 2). In the case of complete wetting the vapour adsorption isotherm rises gradually with increasing vapour pressure and goes to infinity at the saturated vapour pressure (i.e., condensation occurs), see Fig. 2a. In the case of partial wetting the isotherm intersects the saturation axis with a finite adsorbed amount ($\Gamma = \Gamma_{\ddagger}$); condensation only occurs after the vapour has been supersaturated (see Fig. 2b).

In a partial wetting system, three interfaces are present, a liquid-vapour (LV), a liquid-solid (LS) and a solid-vapour (SV) interface. Each interface contains a certain Gibbs energy per unit area, denoted as the interfacial tension γ. Almost two centuries ago, Young [9] discovered that the contact angle θ can be considered as the result of the mechanical equilibrium between the interfacial tensions of the three interfaces involved.

$$\gamma^{sv} - \gamma^{sL} = \gamma^{LV} \cos \theta \tag{1}$$

3
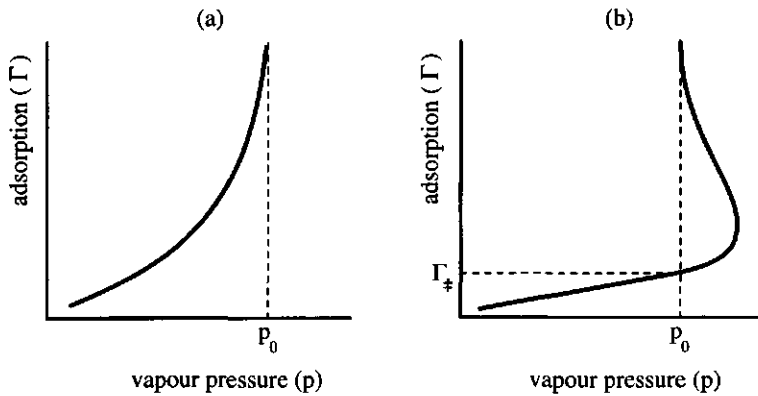
Fig. 2. Vapour adsorption isotherms for (a) complete wetting and (b) partial wetting. The dashed line represents the saturation axis (i.e., the saturated vapour pressure p_0).

The contact angle is a measure of the wettability of a solid-liquid pair. The larger the contact angle the stronger the partial wetting behaviour. If a liquid completely wets a solid the contact angle equals zero. According to Eq. (1) the degree to which a surface is wetted can be assessed from the three interfacial tensions. Liquids with large surface tensions γ^{LV} (i.e., with a high cohesive energy) are rather resistent to spreading (as according to Eq. (1), θ tends to be high for large γ^{LV} values). On solids with large γ^{SV} values, θ tends to be small. For surfaces with low γ^{SV} values (such as teflon) $\cos\theta$ tends to be low and such surfaces usually have a poor wettabilty.

In complete wetting situations (Fig. 1b) the contact angle does not exist (i.e., $\theta = 0$). However, in this case, the wetting of the solid can be translated in terms of spreading tensions $\sigma^{LS(V)}$ defined as

$$\sigma^{LS(V)} = \gamma^{SV} - \gamma^{SL} - \gamma^{LV} \tag{2}$$

The spreading tension can be considered as a measure of the driving force of wetting. Liquid L spontaneously replaces vapour V from the surface if the net force at the three phase contact line in Fig. 1b is directed to the left. Spontaneous spreading of L in the presence of V occurs for $\sigma^{LS(V)} > 0$. On the other hand, for $\sigma^{VS(L)} < 0$ (or $\sigma^{LS(V)} < -2\gamma^{LV}$) the vapour phase remains at the surface. In intermediate cases ($-2\gamma^{LV} \leq \sigma^{LS(V)} \leq 0$) partial wetting occurs with a finite contact angle according to Eq. (1).

Interfacial tensions are not only important with respect to wetting. They are also relevant for adhesion science and technology as they quantify the thermodynamic work

4

of adhesion W_A. For adhesion of liquid L on a solid S that is originally in contact with a vapour V, $W_A^{LS(V)}$ equals

$$W_A^{LS(V)} = \gamma^{SV} + \gamma^{LV} - \gamma^{SL} \tag{3}$$

Interfacial tensions of interfaces involving a solid phase cannot be measured directly. However, the interfacial tension difference between SV and SL interfaces is experimentally accessible (using Eq. (1)) from measurements of $\cos\theta$ and γ^{LV}. It is also possible to determine $\gamma^{SV} - \gamma^{SL}$ from vapour adsorption isotherms, relating the surface concentration Γ (mole/unit area) to the relative equilibrium pressure p/p_0 in the gas phase. According to Gibbs law, the surface pressure of the solid-vapour interface $\pi^{SV}(\Gamma)$ is defined as the difference between the surface tension in vacuum of a pristine surface S, γ^S, and the interfacial tension of the same interface S containing Γ moles of vapour molecules

$$\pi^{SV}(\Gamma) \equiv \gamma^s - \gamma^{SV}(\Gamma) = RT \int_{\Gamma=0}^{\Gamma} \Gamma \, d \ln p/p_0 \tag{4}$$

where R is the gas constant and T is the absolute temperature.

Equation (4) can be extended to include a thick adsorbed layer that has properties of bulk liquid (complete wetting). If a thick liquid layer ($\Gamma = \Gamma_\infty$) is adsorbed on S, the interfacial pressure $\pi^{SV}(\Gamma_\infty)$ equals

$$\pi^{SV}(\Gamma_\infty) = \gamma^s - (\gamma^{SL} + \gamma^L) \tag{5a}$$

In the case of partial wetting meta- and unstable adsorbed states have to be passed before a thick liquid layer is eventually formed at saturation. In Fig. 1b these states correspond to the part of the isotherm behind the saturation axis. This part of the isotherm can not be fully measured. Therefore, $\pi^{SV}(\Gamma_\infty)$ cannot be assessed from experimental vapour adsorption isotherms. Only the interfacial pressure $\pi^{SV}(\Gamma_{\ddagger})$ of the thin film formed at saturation can be determined. The value of $\pi^{SV}(\Gamma_{\ddagger})$ is related to the contact angle according to

$$\pi^{SV}(\Gamma_{\ddagger}) = \gamma^{SV} - (\gamma^{SL} + \gamma^{LV} \cos\theta) \tag{5b}$$

The interfacial pressure of any other vapour (V_1 or V_2) can be obtained in the same way using Eq. (4). In principle, $\gamma^{SL_1} - \gamma^{SL_2}$ can be found by subtraction of $\pi^{SV_1}(\Gamma_\infty)$ from $\pi^{SV_2}(\Gamma_\infty)$ so that liquid(L_1)-liquid(L_2) displacement can be studied using analogues of Eqs. (1) and (2). The use of Gibbs law to describe wetting is not restricted to wetting studies on macroscopically flat surfaces but may also be applied to powdered solids.

In general, many solid surfaces are charged which affects the wetting properties of the solid. The surface charge develops due to adsorption of charged species. This means that the effect of the surface charge on the solid-liquid interfacial tension can be established thermodynamically by means of Gibbs law. Together with Eqs. (1) and (2), this provides a means to characterize the influence of the surface charge on the wettability of a solid substrate.

1.3. Lattice theory for adsorption and wetting

At saturation, partially wetting liquids have a stable state with a finite adsorbed amount. Meta- and unstable states have to be passed before condensation occurs and a stable macroscopic liquid layer is formed at the saturated vapour pressure. The unstable region of adsorption isotherms cannot be measured and theoretical models have to be invoked to allow extrapolation of the part of the isotherm beyond $\Gamma_{\dagger}$ (see Fig. 2b).

The quality of adsorption models is determined by the extent to which certain physical premises (e.g. homogeneity of the surfaces, architecture of the molecules, localized or mobile adsorption, lateral interactions) are considered. For short chain molecules such as alkanes, the physics of adsorption will be strongly determined by the chain nature of the molecules and the conformations they can assume in their vapour phase or adsorbed state. In most adsorption models (e.g., Langmuir, Volmer, BET [10]) the adsorbing molecules are considered as sperical particles, this makes such models inapt to describe adsorption of chain molecules correctly.

By means of lattice theories the properties of chain molecules in complex systems can be investigated at relatively low computational cost. Lattice theories have been applied quite succesfully to investigate fluid mixtures and interfaces [11], polymeric melts, polymeric solutions and polymer adsorption [12], solid-fluid interfaces and polymeric brushes [13], lipid bilayers [14] and surfactant behaviour [15, 16]. This wide diversity of applications suggests that lattice theories provide a versatile theoretical framework for the description of adsorption and wetting of fluids composed of chain molecules.

In this thesis the properties of liquid and vapour phases composed of chain molecules will be studied using an equilibrium lattice theory for chain molecules, originally developed by Scheutjens and Fleer [17, 18]. In the theory, a chain molecule is represented as a flexible chain of beads (the segments), each bead representing a repeating unit of the molecule. The chains are placed on a lattice (see Fig. 3) so that the configurational statistics of the molecules can be evaluated relatively easily, in our case by combining Markov chain statistics with a random mixing (mean field)
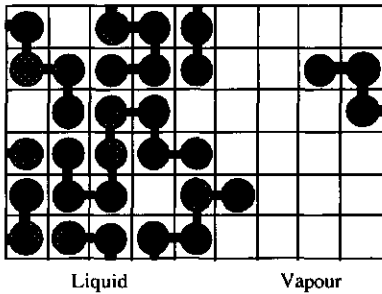
Figure 3. A lattice representation of chain molecules and their liquid-vapour interface; the circles represent the segments of the chain molecules.

Liquid   Vapour

approximation. Each chain experiences an average potential energy field generated by all other molecules in the system. In the potential energy field intermolecular interactions are accounted for by Flory-Huggins parameters. The potential energy field both depends on and determines the volume fractions in the system. Numerical methods are applied to find the self-consistent potential energy field and the (corresponding) volume fraction distribution. The equilibrium volume fraction profiles, in the direction perpendicular to the interface, of the different components are obtained by minimizing the total free energy of the system. From the equilibrium volume fraction profiles the adsorbed amounts can be calculated together with the mechanical- (such as pressure and energy) and thermodynamic properties (e.g. interfacial tensions) of the system.

1.4. Contents and outline of this thesis

As stated in the introductory section, the central aim of the project is to understand and predict wettability starting from vapour adsorption. Special attention is paid to chain molecules (e.g. n-alkanes) at solid interfaces.

In Chapter 2 the thermodynamics of wetting and adsorption and their relations are discussed. Spreading tensions of individual liquids are derived from vapour adsorption isotherms using the Gibbs equation. For complete wetting this is straightforward. However, in those cases where the liquid does not wet the solid completely, the isotherm has an unstable branch which is experimentally inaccessible. This implies that the spreading tension has to be obtained in an alternative way, namely by combining the solid-liquid-vapour contact angle with the (measurable) stable part of the vapour adsorption isotherm. The wetting characteristics of a solid with respect to a pair of immiscible liquids L_1 and L_2 can be deduced from the difference between the spreading tensions $\sigma^{L_1,S(V_1)}$ and $\sigma^{L_2,S(V_2)}$ of the individual liquids.

In Chapter 3 thermodynamic relations between the surface charge of a solid and its wetting and adhesion behaviour will be derived starting from the Gibbs equation. The

7

relations are used to investigate the water wettability of silica as a function of its surface charge as measured by potentiometric titrations.

Chapter 4 describes the gravimetric determination of (alkane and water) vapour adsorption isotherms on two substrates: powdered (pyrogenic) silica (Aerosil-OX50) and the same adsorbent, after modification by (complete) methylation. The formation of thin adsorbed layers onto both substrates is investigated for different (linear and cyclic) alkanes. The measured isotherms are compared with data available in the literature and transformed into surface pressure and disjoining pressure isotherms. The surface pressure isotherms allow us to derive the work of adhesion and to obtain information on the components of the solid surface tension. The disjoining pressure isotherms are interpreted in terms of interaction forces acting in adsorbed (thin) films.

In Chapter 5 the self-consistent-field (SCF) theory of Scheutjens and Fleer [17, 18] is extended to serve as a lattice fluid theory for the description of aliphatic chains. The liquid and vapour phases of chain molecules (e.g., n-alkanes) are described as a binary mixure of chains and free volume entities, the vacancies. The input parameters (i.e., chain lengths and interactions) required are derived from the experimental temperature dependence of the n-alkane vapour pressures. With these parameters, the critical temperatures, liquid and vapour densities, heats of vaporization, LV interfacial tensions of n-alkanes of different chain lengths are inferred. Also the temperature dependency of the heat of vaporization, the interfacial structure and interfacial tensions are investigated.

In Chapter 6 the SCF theory is used to describe alkane vapour adsorption on homogeneous solids. The influence of differences in the adsorption energies of chain end and middle segments is investigated, together with the effect of chain flexibility. The contact angles of chain molecular liquids on rigid and "soft" solids (i.e., with end-attached chains) are scrutinized. On rigid solids, the contact angles are studied as a function of the chain length of the liquid molecules so that the critical surface tension (for wetting) of the solid can be determined. The calculations are performed at different temperatures. Moreover, the adsorption isotherms of an octamer on a rigid solid are calculated at different temperatures. Also, the temperature dependence of the interfacial tension of the rigid solid-octameric fluid interface (with the pristine solid as a reference state) is investigated and used to infer the contact angle as a function of temperature. Furthermore, the effect of alkylation (i.e, surface grafting with terminally attached chains) on the adsorption isotherm and contact angles of an octameric liquid on solids

with grafted chains is investigated as a function of the grafting density and the grafted chain length.

The results calculated in Chapters 5 and 6 are compared with experimental data. In general a good qualitative and in some cases even a good quantitative agreement is found. The advantage of the SCF theory is that macroscopic and molecular aspects of wetting are described simultaneously while taking into account both the structure and the interactions of the substrate and the fluid molecules.

References

[1]   Berg, J. C. (Ed.), *"Wettability"*; Marcel Dekker Inc.: New York, **1993**.

[2]   Schrader, M. E., Loeb, G. I. (Eds.), *"Modern Approaches to Wettability Theory and Applications";* Plenum Press: New York, **1992**.

[3]   Hough, D. B. and White, L. R., *Adv. Colloid Interface Sci.*, 14, **1980**, p. 3-41.

[4]   Derjaguin, B. V., Churaev, N. V. and Muller, V. M., in *"Surface Forces";* Consultants Bureau: New York, **1987**.

[5]   Israelachvili, J. N., in *"Intermolecular & Surface Forces";* Acedemic Press: London, **1992**.

[6]   Mittal, L. K. (Ed.), *"Contact Angle, Wettability and Adhesion";* VSP BV.: Utrecht, **1993**.

[7]   Zisman, W. A., in *"Contact Angle, Wettability and Adhesion"* Gould, R. F. (Ed.); American Chemical Society: Washington, D. C., **1964**: p. 1-51.

[8]   Fowkes, F. M., in *"Contact Angle Wettability and Adhesion"* Gould, R. F. (Ed.); American Chemical Society: Washington, D. C., **1964**: p. 99-111.

[9]   Young, T., *Phil. Trans. Roy. Soc. London*, 95, **1805**, p. 65.

[10]   Young, D. M. and Crowell, A. D., in *"Physical Adsorption of Gases";* Butterworths: London, **1962**.

[11]   Guggenheim, E. A., in *"Mixtures";* Clarendon: Oxford, **1952**.

[12]   Flory, P. J., in *"Principles of Polymer Chemistry";* Cornell University Press: Ithaca (N. Y.), **1953**.

[13]   Fleer, G. J., Cohen Stuart, M. A., Scheutjens, J. M. H. M., Cosgrove, T. and Vincent, B., in *"Polymers at Interfaces";* Chapman & Hall.: Cambridge, **1993**.

[14]   Leermakers, F. A. M. and Scheutjens, J. M. H. M., *J. Phys. Chem.*, 89 (5), **1988**, p. 3264-3274.

[15]   Böhmer, M. R., Koopal, L. K. and Lyklema, J., *J. Phys. Chem.*, 95 (23), **1991**, p. 9569-9578.

[16]   Böhmer, M. R. and Koopal, L. K., *Langmuir*, 8 (11), **1992**, p. 2660-2665.

[17]   Scheutjens, J. M. H. M. and Fleer, G. J., *J. Phys. Chem.*, 83, **1979**, p. 1619-1635.

[18]   Scheutjens, J. M. H. M. and Fleer, G. J., *J. Phys. Chem.*, 84, **1980**, p. 178-190.

Chapter 2

Thermodynamics of Wetting and Vapour Adsorption*

Abstract

Starting from the Gibbs adsorption equation the thermodynamic relations between vapour adsorption and wetting are derived. The surface pressure of a film formed by vapour adsorption on a solid surface is calculated from the vapour adsorption isotherm and related to the spreading tension and contact angle in the solid-liquid-vapour system. The surface pressure at the saturated vapour pressure determines, together with the interfacial tension of the liquid, the difference between the interfacial tension of a (clean) solid and a solid-liquid interface. The individual surface pressure values of two different immiscible liquids allow to predict the wettability in a solid-liquid-liquid system. The procedure is illustrated for a silica-water-octane system.

2.1. Introduction

Wettability is important for many practical processes such as dying, painting, coating and lubrication. In oil recovery, the wettability of reservoir rocks by aqueous drive fluids determines the effectiveness of displacement and the amount of oil recovered. Because of its many applications wettability is a widely studied subject [1]. In general, two cases of wetting can be distinguished: partial wetting and complete wetting. Partial wetting refers to the situation where at equilibrium a drop of liquid (with a finite contact angle) is formed on the solid. In the case of complete wetting the solid is fully covered by a macroscopically thick liquid layer and the value of the contact angle equals zero.

Often, wettability is investigated without recourse to adsorption studies. However, adsorption and wettability are strongly related. The formation of (wetting) layers or a films on solid surfaces is the result of an adsorption process. Adsorption decreases the surface tension of the solid by an amount that is denoted the solid-vapour surface pressure π^{SV} [2]. The value of the surface pressure can be calculated from the adsorption isotherm. It is also possible to obtain the surface pressure from the disjoining pressure isotherm [3].

Surface pressure values at the saturated vapour pressure are useful to study either the spreading tension or the contact angle in a vapour-liquid-solid system. Starting from a model for vapour adsorption isotherms, Adamson has discussed the relation between the isotherm and the spreading tension (complete wetting) or the contact angle (partial

wetting) in liquid-vapour-solid systems [4-6]. In combination with contact angle studies, surface pressures can be used to investigate the composition of a film that is in equilibrium with a droplet [7]. Some investigators have used the surface pressure to calculate the Lifshits-van der Waals contribution to the interfacial tension of the solid γ_{LW}^S [7, 8].

In the present work the thermodynamic relations derived by Adamson are extended in order to investigate the competitive wetting of a solid in presence of two different liquids. The surface pressures calculated from the adsorption of the vapours of both individual liquids will be used for this goal. As the thermodynamic relations are generally valid the approach covers wetting on both flat and powdered solids. Wetting on flat surfaces can be studied directly as contact angles can be easily measured. However, on powders, wettability studies are more complicated [9] and the analysis of vapour isotherms on powders provides at least a good complementary tool to investigate wetting. To illustrate the procedure we will briefly investigate a silica-water-octane system which can be considered a primitive model of an oil reservoir.

2.2. Thermodynamic relations between adsorption and wetting

Adsorption occurring on a solid affects the interfacial Gibbs energy to an extent depending on the nature of the adsorbing molecules and the adsorbed amount. The change in interfacial tension upon adsorption (the surface pressure) can be both positive or negative depending on the occurrence of positive or negative adsorption. For vapour adsorption on a solid the surface pressure $\pi^{SV}(\Gamma)$ has a positive value defined as the difference between the interfacial tension of the clean (i.e., in vacuum) solid surface S denoted by γ^S and the interfacial tension $\gamma^{SV}(\Gamma)$ of the same surface in contact with adsorbing vapour V of liquid L with chemical potential μ and adsorbed amount Γ:

$$\pi^{SV}(\Gamma) = \gamma^S - \gamma^{SV}(\Gamma) \tag{1}$$

The excess Gibbs energy G^σ of a flat interface of area A at temperature T (according to the Gibbs convention the volume of the interface equals zero) can be expressed as

$$G^\sigma = \sum \mu_i n_i^\sigma \tag{2}$$

where μ_i is the chemical potential of component i and n_i^σ is the molar excess amount of i (with respect to the Gibbs dividing plane) present at the interface. According to the first and second law of thermodynamics, the differential of the excess Gibbs energy depends on the interfacial excess of entropy S^σ, the interfacial excess of pressure (i.e., the interfacial tension γ) and the excess adsorbed amount n_i^σ and reads

$$dG^\sigma = -S^\sigma \, dT - A \, d\gamma + \sum \mu_i \, dn_i^\sigma \tag{3}$$

Since Eqs. (2) and (3) are simultaneously valid it follows that

$$d\gamma = -S_a^{\sigma} dT - \sum_i \Gamma_i d\mu_i \tag{4}$$

where S_a^{σ} is the interfacial excess entropy of the surface per unit area and Γ_i is the excess adsorbed amount of component i per unit surface, n_i^{σ}/A. Equation (4) is the Gibbs adsorption equation (for a more detailed discussion see ref. [10]).

In the case of vapour adsorption on insoluble, non-volatile solids, the Gibbs dividing plane is fixed so that the surface excess of solid with respect to the dividing plane equals zero. This means that for pure vapour adsorbing on a solid at constant temperature the Gibbs adsorption equation only contains the $\Gamma d\mu$ term of the vapour. The surface pressure can now be obtained directly by integration of Eq. (4). At constant temperature we have

$$\pi^{SV}(\Gamma) = \int_{\Gamma=0}^{\Gamma} \Gamma(\mu) \, d\mu \tag{5}$$

If the vapour behaves ideally $d\mu = RT \, d \, ln \, p/p_0$ with p/p_0 is the relative vapour pressure, so that we may write

$$\pi^{SV}(\Gamma) = RT \int_{\Gamma=0}^{\Gamma} \Gamma \, d \, ln \, p/p_0 \tag{6}$$

According to Eq. (6) the surface pressure at a certain vapour pressure equals the area under the adsorption isotherm plotted as Γ versus $ln \, p/p_0$.

Near saturation ($p/p_0 = 1$) adsorption isotherms for partial and complete wetting are differently shaped. In the partial wetting case the amount adsorbed at saturation can be finite and a stable thin film (with a thickness of one or a few monolayers) can be formed. In the complete wetting case the adsorption goes to infinity at saturation and a macroscopically thick liquid layer is formed on the solid. The high pressure regions of some adsorption isotherms corresponding to the different kinds of wetting behaviour are sketched in Fig. 1. The most simple case is shown in Fig. 1a, curve 1: the isotherm goes smoothly to infinity at the saturation condition, $\mu^{\ddagger}$. Curve 2 is a somewhat more complicated isotherm: there is a step in the surface concentration when going to saturation. This step occurs at a value of the chemical potential where the areas enclosed by the dashed isotherm and the normal at μ^{jump} are equal. Both curves eventually result in complete wetting and a macroscopically thick layer of liquid L. The adsorbed amount

13
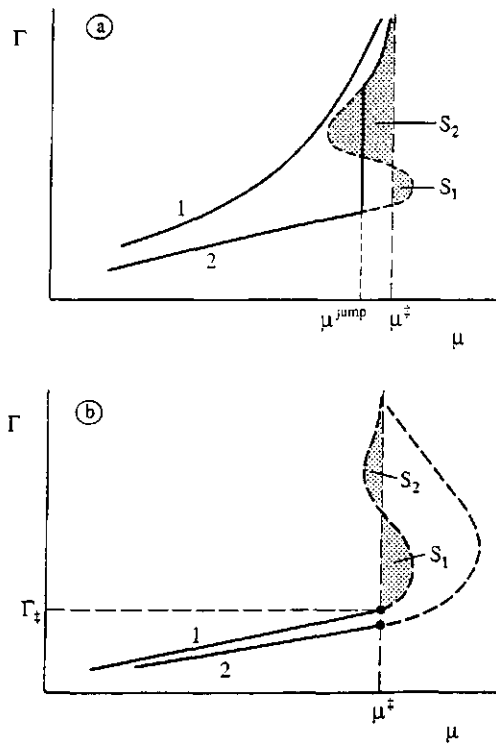
Figure 1. Different types of vapour adsorption isotherms near the saturated vapour pressure (at $\mu^{\ddagger}$). The curves in (a) correspond to complete wetting. Isotherm 1 continuously increases and reaches Γ_{∞} at the saturation pressure. Isotherm 2 shows a step at μ^{jump} and approaches Γ_{∞} at saturation. In the case of complete wetting, the area S_2 bounded between isotherm 2 and the $\mu^{\ddagger}$ axis, exceeds the area S_1. The curves in (b) represent partial wetting. At saturation, the isotherm has a stable state with a finite adsorbed amount ($\Gamma_{\ddagger}$). The isotherm continues in the supersaturation region and finally approaches Γ_{∞}. At saturation, bulk liquid (Γ_{∞}) can be in equilibrium with a thin film ($\Gamma_{\ddagger}$) through the curved interface of a droplet with a finite contact angle. In general partial wetting occurs when the area S_1 of an isotherm exceeds the area denoted S_2.

in this situation is Γ_∞, where ∞ is used to denote that the film is macroscopically thick and has properties of bulk liquid. The surface pressure at saturation $\pi^{SV}(\Gamma_\infty)$ equals therefore

$$\pi^{SV}(\Gamma_\infty) = \gamma^S - (\gamma^{SL} + \gamma^L) \tag{7}$$

In the case of partial wetting (see Fig. 1b, curves 1 and 2) the vapour adsorption can be finite (denoted $\Gamma_{\ddagger}$) at saturation. The stable states of the adsorbed film correspond to those parts of the isotherm for which $d\Pi/d\mu > 0$. After passing supersaturation (and the meta- and unstable regions) some vapour may condense on the solid surface. In a closed system the adsorbed film at the saturation pressure can therefore be in equilibrium with a liquid droplet characterized by its contact angle θ (between $0°$ and $180°$). This equilibrium is given by the Young-Dupré relation

$$\gamma^{SV}(\Gamma_{\ddagger}) = \gamma^{SL} + \gamma^L \cos\theta \tag{8}$$

where γ^L is the surface tension of the liquid (or: the liquid-vapour interfacial tension). This equation is valid for homogeneous, smooth surfaces that are chemically inert and insoluble in the liquids they contact. If this is not the case the equation still holds but the parameters of Eq. (8) vary with the location on the surface and with time. By combining Eqs. (1) and (8) we obtain for the surface pressure $(\pi^{SV}(\Gamma_{\ddagger}))$ due to the thin adsorbed film formed at saturation:

$$\pi^{SV}(\Gamma_{\ddagger}) = \gamma^S - (\gamma^{SL} + \gamma^L \cos\theta) \tag{9}$$

If the vapour pressure is further increased above the saturated vapour pressure (i.e. the vapour is supersaturated) eventually a phase transition will occur and the vapour condenses leading to the formation of a macroscopic liquid layer on the surface. The surface pressure $(\pi^{SV}(\Gamma_\infty))$ of this layer is given by Eq. (7). According to Eqs. (7) and (9), the difference in surface pressure between the film and the condensed layer, that may coexist at saturation, equals

$$\pi^{SV}(\Gamma_\infty) - \pi^{SV}(\Gamma_{\ddagger}) = \gamma^L(\cos\theta - 1) \tag{10}$$

Formally this difference can also be written as

$$\pi^{SV}(\Gamma_\infty) - \pi^{SV}(\Gamma_{\ddagger}) = \int_{\Gamma=0}^{\Gamma_\infty} \Gamma \, d\mu - \int_{\Gamma=0}^{\Gamma_{\ddagger}} \Gamma \, d\mu = \int_{\Gamma_{\ddagger}}^{\Gamma_\infty} \Gamma \, d\mu \tag{11}$$

Hence in the case of partial wetting it follows

$$\gamma^L (\cos\theta - 1) = \int_{\Gamma_{\ddagger}}^{\Gamma_\infty} \Gamma(\mu) \, d\mu \tag{12}$$

15

Provided the measured isotherm can be extended to the supersaturation region, Eq. (12) allows the calculation of the contact angle from the difference in areas enclosed by the saturation axis ($\mu^{\ddagger}$) and the isotherm. For curve 1 in Fig. 1b the r.h.s of Eq. (12) equals $S_2 - S_1$. This difference is slightly negative and $0° < \theta < 90°$. Curve 2 shows a more extreme situation, the area S_1 is large and S_2 is negligible so that $-2 \gamma^L < S_2 - S_1 < -\gamma^L$. In this case $cos\ \theta$ becomes negative and $90° < \theta < 180°$.

Since a range of unstable film thicknesses has to be passed when going from the film formed at saturation to the thick condensed layer, the exact behaviour of this part of the adsorption isotherm is hard to determine experimentally. One way to solve this problem is to use an adsorption model which is fitted to the measured isotherm and also predicts the adsorbed amounts after passing saturation. Adamson and co workers [5, 6] fitted an adsorption model based on a potential theory adsorption function (a four-constant equation) to experimentally measured isotherms and contact angles and obtained fairly reasonable values for the parameters describing the interactions in his model. However, by also using the measured contact angles, predicting a contact angle with the obtained equation is of course trivial. In the discussion we will return to the problems related to the prediction of the course of the partial wetting isotherm around the saturation pressure.

Before continuing, it is instructive to summarise the various adsorption and wetting conditions in an energy diagram. Figure 2 shows such a diagram for the complete wetting case. The initial situation is the bare surface, with interfacial tension γ^S. In the beginning of the adsorption process, at low relative pressures, an adsorbed film will be formed on the surface (with interfacial tension $\gamma^{SV}(\Gamma)$) and the surface pressure changes with adsorption according to Eq. (6). As the saturated vapour pressure is approached a macroscopically thick liquid layer is formed and the surface pressure levels off to the value given by Eq. (7) (the interfacial tension of the solid with this thick liquid layer equals $\gamma^{SL} + \gamma^L$). The lowest energy state, with interfacial tension γ^{SL}, is obtained upon immersion. The corresponding diagram for the partial wetting case is shown in Fig. 3. For low vapour pressures the situation is comparable to the one in Fig. 2. At saturation a thin film (finite adsorbed amount) can be in equilibrium with a drop of liquid with a curved interface. The decrease in interfacial tension due to the adsorbed film is given by $\pi^{SV}(\Gamma_{\ddagger})$. After supersaturation Γ_{∞} is reached and the interfacial tension in the system equals $\gamma^{SL} + \gamma^L$. For partial wetting this state has a higher interfacial tension level than $\gamma^{SV}(\Gamma_{\ddagger})$ (see Eq. (8)). The interfacial tension upon immersion, γ^{SL}, is lower than $\gamma^{SV}(\Gamma_{\ddagger})$ if the contact angle is smaller than 90°, whereas γ^{SL} is larger than $\gamma^{SV}(\Gamma_{\ddagger})$ for $\theta > 90°$.

clean solid (S)

γ^S

$$\pi^{SV}(\Gamma) = \int_{\Gamma=0}^{\Gamma} \Gamma(\mu)\,d\mu$$

thin adsorbed film
or submonolayer
(Γ)

$\gamma^{SV}(\Gamma)$

$$\pi^{SV}(\Gamma_\infty) = \int_{\Gamma=0}^{\Gamma_\infty} \Gamma\,d\mu$$

macroscopically
thick liquid layer
(Γ_∞) of L on S

$\gamma^{SL} + \gamma^L$

γ^L

immersion
of S
in liquid L

γ^{SL}

vacuum

vapour at μ

saturated
vapour
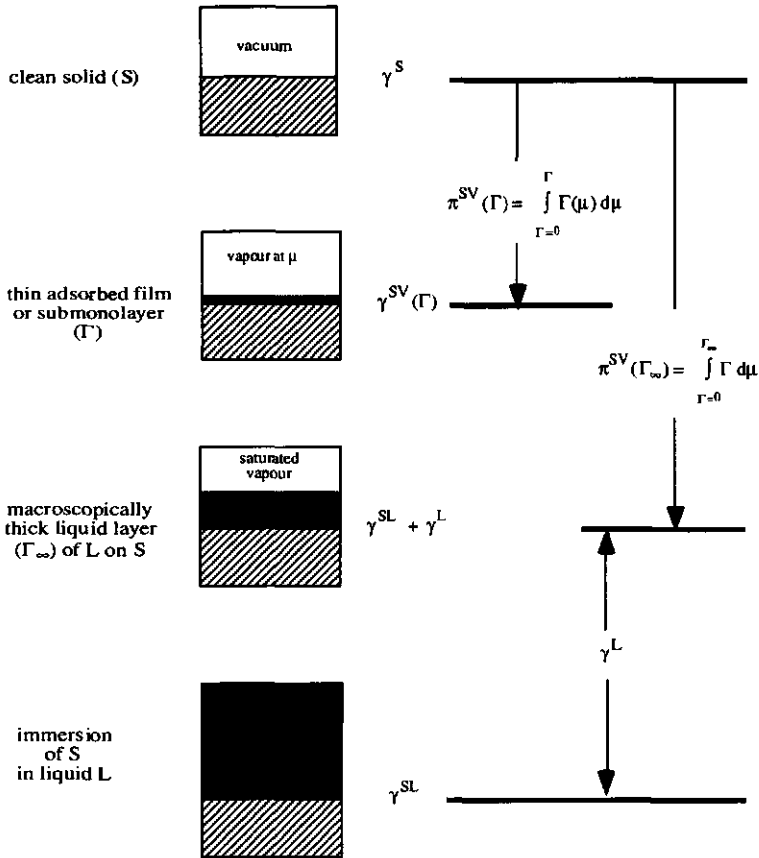
Figure 2. Schematic representation of the values of the interfacial tensions of the solid (S), liquid (L) and vapour (V) interfaces involved in the adsorption and wetting process in the case of complete wetting. Vapour (of chemical potential μ) adsorbing on the solid reduces the interfacial tension. Eventually, at saturation (at μ‡), this results in a thick liquid layer Γ_∞ with energy state $\gamma^{SL} + \gamma^L$. Full immersion of S in L leads to a still lower Gibbs energy state γ^{SL}.

17
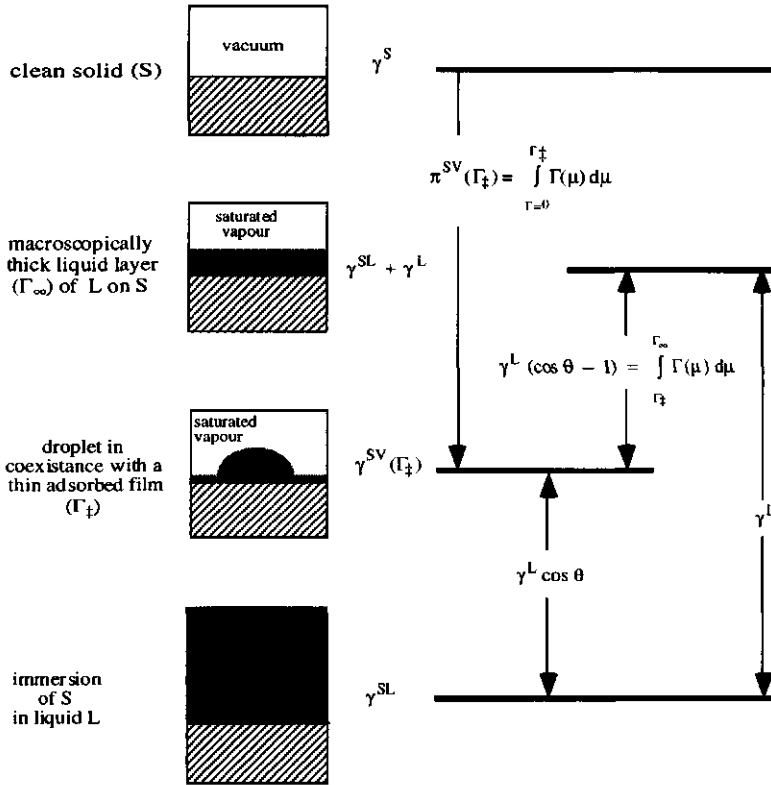
Figure 3. Schematic representation of the values of the interfacial tensions of the solid (S), liquid (L) and vapour (V) interfaces involved in the adsorption and wetting process in the case of partial wetting. At saturation, the adsorption at the solid is finite ($\Gamma_{\ddagger}$) and the SV interfacial tension equals $\gamma^{SV}(\Gamma_{\ddagger})$. The adsorbed layer formed at saturation ($\Gamma_{\ddagger}$) can be in equilibrium with a drop of contact angle θ. After passing supersaturation a macroscopic layer (Γ_{∞}) is formed with energy level $\gamma^{SL} + \gamma^{L}$. The difference between $\gamma^{SV}(\Gamma_{\ddagger})$ and $\gamma^{SL} + \gamma^{L}$ is related to the contact angle. The contact angle also determines the difference between $\gamma^{SV}(\Gamma_{\ddagger})$ and γ^{SL} (the energy state after immersion). The contact angle for the scheme lies between 0 and 90°. If the contact angle lies between 90 and 180° cos θ will be negative and the scheme has to be modified so that $\gamma^{SV}(\Gamma_{\ddagger}) < \gamma^{SL} < (\gamma^{SL} + \gamma^{L})$.

Spreading tension and wettability

It has been shown that, in principle, the surface pressure and the contact angle in a solid-liquid-vapour system can be obtained from the adsorption isotherm. When complete wetting occurs the surface pressure at the saturated vapour pressure equals the spreading tension. The spreading tension is a parameter used to characterise the wettability of a surface. It is defined as the difference in interfacial tensions of the initial and final state of the wetting process.

Consider a surface S originally covered by fluid 1 that is brought into contact with fluid 2, fluids 1 and 2 are immiscible. To describe the displacement of 1 by 2 the spreading tension $\sigma^{2S(1)}$ in such a system is defined by

$$\sigma^{2S(1)} \equiv \gamma^{S1} - (\gamma^{12} + \gamma^{S2}) \tag{13}$$

Spreading of 2 on S occurs if $\sigma^{2S(1)} > 0$. Rewriting Eq. (13) as

$$\sigma^{2S(1)} = \pi^{S2} - \pi^{S1} - \gamma^{12} \tag{14}$$

shows that the spreading tension is related to the interfacial pressures $\pi^{S1} \equiv \gamma^{S} - \gamma^{S1}$ and $\pi^{S2} \equiv \gamma^{S} - \gamma^{S2}$. Alternatively, we can also define the spreading tension $\sigma^{1S(2)}$ for the reverse situation of a surface S initially covered by fluid 2, and brought into contact with fluid 1. This quantity is related to $\sigma^{2S(1)}$ by

$$\sigma^{1S(2)} + \sigma^{2S(1)} = -2\gamma^{12} \tag{15}$$

The wetting possibilities of a two fluid-solid system can be expressed in terms of the spreading tension. The following cases may be distinguished:

 a) When $\sigma^{2S(1)} > 0$ (or $\sigma^{1S(2)} < -2\gamma^{12}$) fluid 2 will tend to displace 1 from the solid surface, eventually 2 will totally cover (or wet in case of a liquid) the solid.
 b) When $\sigma^{1S(2)} > 0$ (or $\sigma^{2S(1)} < -2\gamma^{12}$) fluid 1 will tend to completely cover the solid surface, under displacement of 2.
 c) Partial wetting will occur in the intermediate cases, i.e. when the spreading tension lies between $-2\gamma^{12}$ and 0. The contact angle θ is given by the Young-Dupré equation (Eq. (8)).

The conditions for the different wetting situations are given schematically in Table 1. Consider 2 to be a liquid and 1 the vapour of the liquid.

Table 1. *Spreading tensions and the corresponding wetting behaviour. Two spreading tensions are given, the spreading tension $\sigma^{2S(1)}$ of a solid S originally covered by phase 1 and brought into contact with phase 2 and the spreading tension $\sigma^{1S(2)}$ of solid S originally contacting 2 brought into contact with 1.*

Wetting behaviour	Spreading	tension
	$\sigma^{2S(1)} = \gamma^{S1} - (\gamma^{12} + \gamma^{S2})$	$\sigma^{1S(2)} = \gamma^{S2} - (\gamma^{12} + \gamma^{S1})$
Complete wetting:		
2 displaces 1 from the surface	$\sigma^{2S(1)} > 0$	$\sigma^{1S(2)} < -2\gamma^{12}$
1 displaces 2 from the surface	$\sigma^{2S(1)} < -2\gamma^{12}$	$\sigma^{1S(2)} > 0$
Partial wetting:	$-2\gamma^{12} < \sigma^{2S(1)} < 0$	$-2\gamma^{12} < \sigma^{1S(2)} < 0$
formation of a droplet of 1	$cos\,\theta_1 = (\gamma^{S2} - \gamma^{S1})/\gamma^{12}$	
formation of a droplet of 2	$cos\,\theta_2 = (\gamma^{S1} - \gamma^{S2})/\gamma^{12}$	

Liquid-liquid displacement

The wetting behaviour and the occurrence of displacement on a solid contacting two immiscible liquids can be studied analogously since the same relations are valid if phase 1 is another liquid instead of a vapour. From the interfacial tensions of the solid-liquid and liquid-vapour interfaces involved in the wetting process, the wettability or displacement in a liquid-liquid-solid system can be evaluated using the expression for the spreading tension (Eq. (13)).

For pure vapour of different liquids adsorbing on a given solid, Eqs. (7) or (9) can be used to calculate π^{SV} for different individual vapours. Once the π^{SV} values are known the interfacial pressure π^{SL} of the liquid on the solid can be found. In the case of complete wetting, Eq. (7) applies and π^{SV} is given by

$$\pi^{SL} \equiv \gamma^{S} - \gamma^{SL} = \pi^{SV}(\Gamma_\infty) + \gamma^{L} \tag{16}$$

In the case of partial wetting, Eq. (9) holds and

$$\pi^{SL} \equiv \gamma^{S} - \gamma^{SL} = \pi^{SV}(\Gamma_{\!f}) + \gamma^{L}\,cos\theta \tag{17}$$

This means that the π^{SL} values for different liquids can be obtained from the surface pressures that follow from the adsorption isotherms.

For a two-liquid-solid system the spreading tension can be evaluated using the individual π^{SV} values for the different liquids. If each of the individual liquids 1 and 2 completely wets the surface, the spreading tension $\sigma^{2S(1)}$ of the liquid-liquid pair can be calculated by combining Eqs. (14) and (16) to

$$\sigma^{2S(1)} = \gamma^2 - \gamma^1 - \gamma^{12} + \pi^{SV_2}(\Gamma_\infty) - \pi^{SV_1}(\Gamma_\infty) \tag{18}$$

where $\pi^{SV_i}(\Gamma_\infty)$ is the surface pressure at saturation for adsorption of pure fluid i on S. The values of γ^1, γ^2 and γ^{12} are easily measurable interfacial tensions of the pure liquids 1 and 2 and the 12 interface. If one of the individual liquid phases (say 2) partially wets the surface we have for the liquid-liquid pair

$$\sigma^{2S(1)} = \gamma^2 \cos\theta_2 - \gamma^1 - \gamma^{12} + \pi^{SV_2}(\Gamma_{\neq,2}) - \pi^{SV_1}(\Gamma_\infty) \tag{19}$$

θ_2 being the contact angle of a drop of 2 on the solid S in equilibrium with its vapour. If we have a situation that, individually, both liquids partially wet the surface we can calculate the spreading tension according to

$$\sigma^{2S(1)} = \gamma^2 \cos\theta_2 - \gamma^1 \cos\theta_1 - \gamma^{12} + \pi^{SV_2}(\Gamma_{\neq,2}) - \pi^{SV_1}(\Gamma_{\neq,1}) \tag{20}$$

In principle, the surface pressures π^{SV_1} and π^{SV_2} and the contact angles θ_1 and θ_2 can be determined from the individual vapour adsorption isotherms using Eqs. (6), (10) and (12).

Based on Eqs. (18), (19) and (20) the wetting state of a two liquid-solid system can be evaluated. As explained above and summarised in Table 1, three different cases can be distinguished, depending on the value of $\sigma^{2S(1)}$: (i) 2 displaces 1 from the surface for $\sigma^{2S(1)} > 0$, (ii) 1 stays on the surface if $\sigma^{2S(1)} < -2\gamma^{12}$ or (iii) partial wetting occurs in the intermediate case.

Work of different types of wetting

If complete wetting occurs for a liquid on a solid, different wetting processes can be distinguished, each with its own amount of work. The work of spreading W_S, defined as the work performed when a clean solid is brought into contact with a liquid (in equilibrium with its vapour) which spreads on the surface, equals

$$W_S \equiv \gamma^S - (\gamma^{SL} + \gamma^L) = \pi^{SV}(\Gamma_\infty) \tag{21}$$

Immersion of the solid in liquid corresponds to the work of immersional wetting W_I defined as

$$W_I \equiv \gamma^S - \gamma^{SL} = \gamma^L + \pi^{SV}(\Gamma_\infty) \tag{22}$$
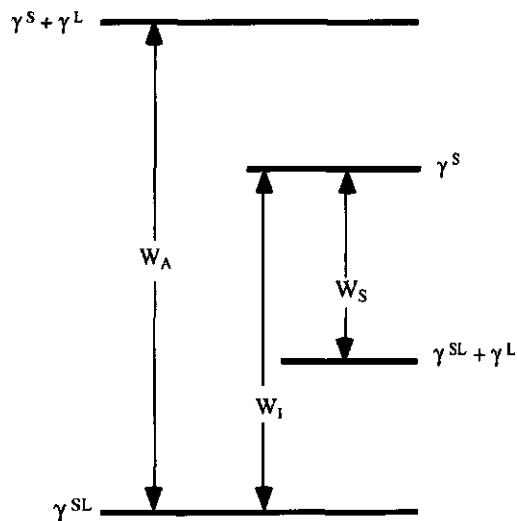
Figure 3. The work of adhesional wetting W_A, immersional wetting W_I and spreading wetting W_S is expressed schematically as a function of the differences in interfacial tensions of the SV, LV and SL interfaces.

When a solid and a liquid interface are brought into contact we speak of adhesional wetting. The work of adhesional wetting W_A or the work of adhesion is defined according to

$$W_A \equiv \gamma^S + \gamma^L - \gamma^{SL} = 2\gamma^L + \pi^{SV}(\Gamma_\infty) \tag{23}$$

The relations between W_S, W_I and W_A are shown schematically in Fig. 4, the sum of the interfacial tensions of the system decreases in the downward direction of the figure. Eqs. (21)-(23) show that the work performed during a wetting process can be obtained from the interfacial tension of the liquid and $\pi^{SV}(\Gamma_\infty)$ as determined from the vapour adsorption isotherm.

2.3. Discussion

It has been shown that, in principle, quantities such as $cos\ \theta$, π^{SL}, $\sigma^{2S(l)}$ and the various works of wetting can be obtained from the vapour adsorption isotherms of the liquids under consideration. These quantities characterize the wetting behaviour of a single liquid on a solid. Furthermore, from the wetting behaviour of individual liquids the displacement of a liquid from a solid by another liquid (immiscible with the first) can be

predicted. The approach followed is based on equilibrium thermodynamics, it does not provide information on the kinetics of the wetting processes. For the interpretation of the thermodynamically found contact angle we refer to Good [11].

Wetting of silica from vapour adsorption data

To illustrate the method described, we will anticipate the gravimetrical octane and water vapour adsorption isotherms measured at 17°C on powdered silica Aerosil OX-50 (see Chapter 4). The silica/octane/water system is chosen as a primitive model to investigate the wettability in an oil reservoir (i.e., rock containing brine and crude oil). The adsorption and surface pressure isotherms, calculated according to Eq. (6) from the area under the adsorption isotherms, are shown in Figs. 2 and 6a of Chapter 4, respectively. The n-octane (O) and water (W) adsorption isotherms on silica Aerosil OX-50 (Si) both rise sharply as saturation is approached. Asumming complete wetting of both water and n-octane, the π^{SV} values near saturation (see Table 1 in chapter 4) and the interfacial tensions of the pure liquids are used to calculate the π^{SL} values for the silica-octane (SiO) and the silica-water (SiW) interface according to Eq. (16). The π^{SL} values for the SiO and SiW interface are 39 and 159 mJ/m^2, respectively. Since water and octane hardly mix, both the π^{SL} values and the interfacial tensions of the silica-pure water and silica-pure octane interface will be hardly affected by the presence of the other liquid.

The value of the spreading tension $\sigma^{WSi(O)}$ in a solid/water/octane system calculated from Eq. (18) equals 69 mJ/m^2. Hence on the basis of Gibbs energy considerations it is concluded that the silica surface will be preferentially wetted by water. The calculated values of the various works of wetting, W_S, W_I and W_A, for water on silica are 86, 159 and 232 mJ/m^2 respectively, those for octane on silica 17, 39 and 60 mJ/m^2. Also here we see that the water silica values are much larger than the octane-silica values indicating the preference of the silica surface for water. The high values of the water-silica system are due to hydrogen bond formation between water and the OH groups of the silica surface.

In practice with oil recovery the situation is considerably less simple than in the silica/water/octane system. In a typical oil reservoir the wettability on the pore scale will be affected by the heterogeneity of the reservoir rock. There may be some areas where the rock is water wet and some where the rock is oil wet. In such a reservoir negative values of $\sigma^{WS(O)}$ occur locally. The displacement of oil from these regions by waterflooding will be enhanced by the addition of a surfactant that mainly reduces the interfacial tensions of the water-oil and solid-water interface (whereas the surfactant should have minor effects on the oil-solid interfacial tension).

Another complication encountered in practice is that brine and crude oils usually contain various electrolytes and natural surface active components (f.i., asphaltenes), respectively. Adsorption of the surface active components and/or salts on the reservoir minerals influences the wettability of the rock material [12]. In general this adsorption can be taken into account in the Gibbs adsorption equation (see also Chapter 3). Moreover, impurities present in the liquids and dissolution of the solid in the contacting liquid(s) can in principle, all be taken into account as extra components in the Gibbs equations for the different interfaces involved. In practice this is not an easy task, but qualitative predictions are still possible.

Partial wetting adsorption isotherms

In the treatment we discussed it has been assumed that the total vapour adsorption isotherm is known. In the case of complete wetting, the whole isotherm can be measured. In the case of partial wetting, the isotherm crosses the saturated vapour pressure axis, and knowledge of the isotherm around $p/p_0 = 1$ (including the meta-and unstable part) is not obvious. In practice it may sometimes be more easy to measure the contact angle directly instead of predicting its value from the vapour adsorption isotherm. When combining this the contact angle with $\pi^{SV}(\Gamma_{\ddagger})$, liquid-liquid displacement can be predicted according to Eqs. (19) and (20). Due to supersaturation effects, it may sometimes be necessary to estimate the surface pressure $\pi^{SV}(\Gamma_{\ddagger})$ by extrapolation of the isotherm close to the saturated vapour pressure. If the value of the contact angle is not known one can try to model the course of the isotherm in the meta - and unstable region. One way to do this is to use the potential theory for adsorption [4]. The meta- and unstable regions of the adsorption isotherm can also be modelled using the concept of disjoining pressure, which is defined as the additional pressure in a thin film in thermodynamic equilibrium. For an adsorbed film of a volatile liquid the disjoining pressure is proportional to ln p/p_0 and knowledge of the disjoining pressure as a function of film thickness implies knowledge of the adsorption isotherm. The disjoining pressure and its various contributions due to electrostatic, dispersive and structural interaction forces are well studied [13-15]. A third alternative way to obtain the required information is the use of models for the work of adhesion [16]. Once W_A and $\pi^{SV}(\Gamma_{\ddagger})$ are known the contact angle can be calculated and displacement can be predicted. In the models for W_A always some estimation of γ^S is required. Hence, this method is only suited for well studied solids.

In general, prediction of the adsorption isotherm on the basis of a sophisticated model seems the most elegant way to asses the meta- and unstable region in the partial wetting adsorption isotherm. Moreover, this renders wetting (and displacement) studies feasible.

References

[1]   Gennes, P. G., *Rev. Mod. Phys.*, 57 (3), **1985**, p. 827-863.

[2]   Bangham, D. H. and Razouk, R. I., *Trans. Faraday Soc.*, 33 , **1937**, p. 1459-1472.

[3]   Derjaguin, B. V., Churaev, N. V. and Muller, V. M., in *"Surface Forces"*; Consultant Bureau: New York, **1987**: p. 79.

[4]   Adamson, A. W., *J. Colloid Interface Sci.*, 27 (2), **1968**, p. 180-187.

[5]   Adamson, A. W., *J. Colloid Interface Sci.*, 44 (2), **1973**, p. 273-281.

[6]   Tadros, M. E., Hu, P. and Adamson, A. W., *J. Colloid Interface Sci.*, 49 (2), **1974**, p. 184-195.

[7]   Janczuk, B., Chibowski, E. and Bialopiotrowicz, T., *J. Colloid Interface Sci,*, 102 (2), **1984**, p. 533-538.

[8]   Fowkes, F. M., *Ind. Eng. Chem.*, 12, **1964**, p. 40.

[9]   Dunstan, D. and White, L. R., *J. Colloid Interface Sci.*, 111 (1), **1986**, p. 60-64.

[10]   Everett, D. H., *Pure Appl. Chem.*, 53, **1981**, p. 2181-2198.

[11]   Good, R. J., in *"Surface and Colloid Science, Vol. 11"*, Good, R. J. and Stomberg, R. R. (Eds.), Plenum Press: New York, **1979**: p. 1-29.

[12]   Salathiel, R. A., *J. Pet. Technol.*, 25, **1973**, p. 1216.

[13]   Derjaguin, B. V., Churaev, N. V. and Muller, V. M., in *"Surface Froces"*; Consultant Bureau: New York, **1987**.

[14]   Churaev, N. V. and Derjaguin, B. V., *J. Colloid Interface Sci.*, 103 (2), **1985**, p. 542-553.

[15]   Churaev, N. V. and Zorin, Z. M., *Adv. Colloid Interface Sci.*, 40 , **1992**, p. 109-146.

[16]   Mittal, K. L. (Ed.), *"Contact Angle, Wettability and Adhesion"*; VSP: Utrecht, **1993**.

Chapter 3

Wetting and Adhesion on Charged Solids:
interfacial thermodynamics and surface charge

Abstract

Starting from the Gibbs adsorption equation a thermodynamic framework is developed which describes the surface charge (and electrolyte concentration) dependence of the water contact angle on surfaces exposing ionizable groups. According to this framework, the solid-(aqueous)liquid-vapour contact angle in the case of partial wetting is maximal at the point of zero charge of the solid. The contact angle (and the work of adhesion) decrease with increasing surface charge. In the case of complete wetting the presence of charge on a surface increases its tendency to be water wetted. The derived equations are used to study the wetting of silica, a primitive model for sandstone. The surface charge density of silica Aerosil OX-50 is determined from potentiometric titrations at a series of indifferent electrolyte (KCl) concentrations ranging from 0.01 M to 1M. The silica surface charge becomes increasingly negative with increasing ionic strength and/or increasing pH. At the point of zero charge silica is already completely wetted by water. Charging of the surface results in a still better water wettability although this cannot be observed experimentally. At pH=9 and 1 M KCl the silica-water interfacial tension is 22 mJ/m^2 lower than that of the uncharged silica-water interface (pH=3).

3.1. Introduction

The adhesion and wetting behaviour of solids depends on their surface properties such as roughness, charge and heterogeneity. In many fundamental and technological situations, such as the wetting of oil-reservoir rocks, mineral flotation and contact angle studies on functionalized (polymeric) surfaces, charged surfaces are dealt with. In order to understand and predict the wettability and adhesion of charged substrates a basic understanding of the influence of electrostatics on the interfacial tension of the solid-liquid interface is required.

When a charged solid contacts a liquid in which ions are present, ions will accumulate at or near the surface in order to neutralize the surface charge. The combination of the surface charge and its countercharge in solution is called the electrical double layer. The electrical double layer has a large influence on the macroscopic (solid-liquid-vapour) contact angle [1, 2]. On functionalized surfaces and monolayers the water contact angle depends on the hydrophilicity of the functionalizing group [3]. So-called contact angle titrations show that the water wettability of functionalized surfaces improves for pH values at which (more) interfacial groups

become ionized [4, 5]. On alkanethiol-monolayers bearing carboxylic groups the water wettability at low pH values decreases with increasing pH, upon a further rise in pH the water contact angle reaches a maximum after which it decreases with a further increase in pH [6]. This behaviour probably arises from conformational changes in the carboxylate groups upon surface ionization.

In the present paper we will discuss wetting on charged interfaces from a general thermodynamic point of view, based on the Gibbs adsorption equation. The approach will be outlined for silica which is often used as a model mineral substrate because of its optical properties. Moreover, it can be readily rendered more hydrophobic by alkylation [7]. The silica surface charge as a function of pH and salt concentration is determined by means of potentiometric titrations and correlated to the water wettability of silica. As the approach outlined is based on thermodynamics it is universally valid and therefore suited for application to other substrates.

3.2. Surface charge and wetting and adhesion

The surface charge

Solids in aqueous electrolyte solutions may build up a surface charge due to adsorption of charge-determining electrolyte. When the concentration of indifferent electrolyte is much larger than the concentration of charge determining electrolyte, the surface excess of charge-determining ions equals the surface charge. Consider a solid for which H^+ and OH^- are the charge determining ions. The charge density σ_o^{SL} of the solid-liquid interface (SL) then follows from

$$\sigma_o^{SL}(pH) = F \left(\Gamma_{HCl}^{SL} - \Gamma_{KOH}^{SL} \right) \tag{1}$$

where F is the Faraday constant and Γ_{HCl}^{SL} and Γ_{KOH}^{SL} are the adsorption densities (per m^2 SL interface) of the hydrogen and hydroxyl ions and their counter ions, respectively. As Γ_{HCl}^{SL} and Γ_{KOH}^{SL} depend on the proton concentration the surface charge is pH dependent. Amphoteric materials have a certain pH at which the surface charge equals zero. This pH is called the point of zero charge (p.z.c.). In the absence of specific adsorption [8] and patchwise surface heterogeneity [9] the p.z.c. can be determined from the common intersection point in curves of the surface charge vs. pH at different ionic strengths. The common intersection point occurs because an increase in indifferent electrolyte concentration will increase the screening of the surface charge on the left and right side of the p.z.c. resulting in an increase of the (negative or positive) surface charge, at the p.z.c. there is nothing to screen and electrolyte has no effect [10].

Wetting and adhesion

When a macroscopic amount of liquid comes into contact with a solid a number of situations may arise. Complete wetting referes to the situation where the liquid spreads maximally over the solid. When enough liquid is present the solid will eventually be totally covered with a macroscopically thick liquid layer. The situation where at equilibrium a liquid droplet, with a finite contact angle, is formed at the interface is referred to as partial wetting. The wettability of an interface can be characterized by the spreading tension. For a solid S, originally contacting vapour V, brought into contact with liquid L the spreading tension $\sigma^{LS(V)}$ is defined as

$$\sigma^{LS(V)} \equiv \gamma^{SV} - (\gamma^{LV} + \gamma^{SL}) \tag{2}$$

where γ is the interfacial tension of the interface denoted by the superscripts. Liquid L completely wets the solid if $\sigma^{LS(V)} > 0$. For $-2\gamma^{LV} < \sigma^{LS(V)} < 0$, partial wetting occurs [11] with a macroscopic contact angle θ. According to the Young-Dupré relation, the contact angle in the solid-liquid-vapour system can be related to the interfacial tensions in the system

$$cos\ \theta = (\gamma^{SV} - \gamma^{SL}) / \gamma^{LV} \tag{3}$$

The work of adhesion $W_A^{LS(V)}$ of L on S, originally in contact with V, is related to the interfacial tensions and the contact angle according to

$$W_A^{LS(V)} = \gamma^{SV} + \gamma^{LV} - \gamma^{SL} = \gamma^{LV}(1 + cos\ \theta) \tag{4}$$

Equations (2) - (4) show that the influence of a surface charge on wetting and adhesion properties follows from the surface charge dependence of the interfacial tensions involved.

Interfacial tension of charged interfaces

Adsorption of a component i onto an interface changes the interfacial tension according to Gibbs law. The change depends on the change in chemical potential $d\mu_i$ upon adsorption and the interfacial excess amount of i, Γ_i^{SL}, with respect to the Gibbs dividing plane. For a rigid solid (i.e. a solid which does not dissolve or deform) in contact with a liquid at constant pressure and temperature, the SL interfacial tension will change upon adsorption of component(s) i from L according to

$$d\gamma^{SL} = -\sum_i \Gamma_i^{SL} d\mu_i \tag{5}$$

When liquid L is an aqueous electrolyte solution of indifferent electrolyte (KCl) and charge determining electrolyte (HCl or KOH) Eq. (5) can be written as

$$d\gamma^{SL} = - \left(\Gamma_{KCl}^{(w)SL} \, d\mu_{KCl} + \Gamma_{HCl}^{(w)SL} \, d\mu_{HCl} + \Gamma_{KOH}^{(w)SL} \, d\mu_{KOH} \right) \quad (6)$$

where $\Gamma_i^{(w)SL}$ denotes the relative surface excess (with respect to water) [12] of species i at the SL interface. At sufficiently high concentrations of KCl, addition of HCl or KOH does not affect the activity of KCl, $d\mu_{KCl} \approx 0$, and $d\mu_{KOH} \approx d\mu_{OH^-}$, moreover, $d\mu_{HCl} \approx d\mu_{H^+} = -2.303 \, RT \, dpH$. According to the water dissociation equilibrium, we have $d\mu_{OH^-} = -d\mu_{H^+}$ and for constant $\mu_{KCl} \gg \mu_{HCl}, \mu_{KOH}$ Eq. (6) reduces to

$$d\gamma^{SL} = 2.303 \, RT \, (\Gamma_{HCl}^{(w)SL} - \Gamma_{KOH}^{(w)SL}) \, dpH = 2.303 \, RT \, (\sigma_o^{SL}(pH)/F) \, dpH \quad (7)$$

For normal charging behaviour, the solid-liquid interfacial tension is maximal at the point of zero charge ($\sigma_o^{SL} = d \, pH = 0$). The interfacial tension of a charged solid-liquid interface $\gamma^{SL}(pH)$ follows by integration of Eq. (7) from the pH at the point of zero charge pH^0 to the actual pH value of the solution in contact with the solid

$$\gamma^{SL}(pH) - \gamma^{SL}(pH^0) = 2.303 \, (RT/F) \int_{pH^0}^{pH} \sigma_o^{SL}(pH) \, dpH \quad (8)$$

where $\gamma^{SL}(pH^0)$ denotes the interfacial tension of the SL interface at the p.z.c..

   In principle, addition of electrolyte to water affects the (saturated) vapour pressure and therefore changes the adsorption of water vapour onto the solid. However, at constant and sufficiently high concentrations of indifferent electrolyte, the addition of charge determining electrolyte hardly affects the ionic strength and the vapour pressure. Adsorption of water and electrolyte at the solid-vapour (SV) interface affects the SV interfacial tension analogously to Eq. (5). If the adsorbed film formed at the saturated vapour presure is very thin (i.e., below the thickness of the electrical double layer) the adsorbed water layer has a rather low dielectric constant which prevents adsorption of charge detemining species ($\Gamma_{KCl}^{SV} = \Gamma_{HCl}^{SV} = \Gamma_{KOH}^{SV} \approx 0$). In this case, we may put $d\gamma^{SV} \approx$ 0. If thicker adsorbed films are formed at the saturated vapour presure the adsorbed water layer will be more comparable to bulk water. In this case $d\gamma^{SV}$ depends on the thickness of the adsorbed film. Normally, electrolyte adsorption at the SV interface is lower than for the SL interface and $d\gamma^{SV}$ maximally equals $d\gamma^{SL}$. Therefore, when changing the pH in a droplet at fixed p, T and salt concentration, we may write for $d\gamma^{SV}$:

$$d\gamma^{SV} = f \, d\gamma^{SL} = f \, 2.303 \, RT \, (\sigma_o^{SL}(pH)/F) \, dpH \quad (9)$$

where f is a proportionality factor depending on the thickness of the sv film formed at the saturated vapour pressure. For very thin sv films $f = 0$, for very thick sv films/layers f approaches unity. Charge determining ions have no particular affinity for the liquid-vapour interface and at constant (and sufficiently high) indifferent electrolyte concentration γ^{LV} is virtually independent of the pH.

From the surface charge dependence of the interfacial tensions we are able to study the role of the surface charge in wetting and adhesion. Combining Eqs. (2), (7), (8) and (9) directly reveals that normally (i.e., for $f < 1$) the spreading tension $\sigma^{LS(V)}$ in a solid-liquid-vapour system increases with increasing surface charge density. In other words, the water wettability of a solid increases with the solid surface charge. By combining Eqs. (3), (7), (8) and (9) we obtain for the pH dependence of the contact angle

$$
\begin{aligned}
cos\ \theta(pH) - cos\ \theta(pH^0) &= \frac{d\gamma^{sv} - d\gamma^{sL}}{\gamma^{LV}} \\
&= \frac{f - 1}{\gamma^{LV}}\ 2.303\ (RT/F) \int_{pH^0}^{pH} \sigma_o^{sL}(pH)\ dpH
\end{aligned}
\tag{10}
$$

Normally $f < 1$, hence, according to Eq. (10), the contact angle has a maximum at the p.z.c. and decreases with increasing surface charge in either direction.

With the thermodynamic framework presented above, the effect of surface charge on the work of adhesion can be characterized separately. Combining Eqs. (4), (7), (8) and (9) yields:

$$
W_A^{LS(V)}(pH) - W_A^{LS(V)}(pH^0) = (f - 1)\ 2.303\ (RT/F) \int_{pH^0}^{pH} \sigma_o^{sL}(pH)\ dpH
\tag{11}
$$

The treatment discussed above is based on thermodynamics, hence, it is also valid for substrates with charge determining ions other than H^+ and OH^-. In this case the pH in the equations presented above has to be replaced by pX, X representing the charge determining species of the substrate.

3.3. Surface charge and wettability of silica

The nature of the silica surface

The surface properties of silica are primarily determined by the density and arrangements of the surface silanol (-Si-O-H) groups. These surface silanol groups can occur isolated or hydrogen bonded to other surface silanols. Isolated silanol groups

have no possibility of forming hydrogen bonds with neighbouring surface silanol groups. Both types of silanols can be identified by their infrared absorption bands [13]. The surface concentration of both types of silanols depends on the methods used for prepararing and cleaning the silica. Upon thermal dehydroxylation of silica the hydrogen bonded silanols form siloxane (-Si-O-Si-) groups under evolution of water. Dehydroxylation of the hydroxyl groups on the silica surface is reversible up to $\pm$ 400 °C [14]. When a silica is dehydroxylated well above this temperature (> 850 °C) the siloxane groups are not rehydrated upon exposure to water vapour. However, in alkaline solutions, surface Si atoms dissolve rather easily and rehydration of the surface siloxane groups may occur. The surface siloxane groups are rather hydrophobic; on a heat dehydroxylated silica water adsorption occurs mainly on the few remaining isolated silanol groups [14]. A heat treatment reduces the number of surface hydroxyl groups and increases the silica-water contact angle.

The silica used in this study is Aerosil OX-50, a pyrogenic (or fumed) silica, prepared from oxidation of a gaseous $SiCl_4$ at high temperature. In general, pyrogenic silica particles are not porous. They have a high fraction of siloxane bonds and a few isolated silanol groups at their surfaces that account for their hydrophilicity. The surface charge density of a silica-water interface originates from the deprotonation of the silanol groups present at (or under) the silica surface. At ambient pH values a silica surface is negatively charged. The precise point of zero charge of silica is rather difficult to obtain from the common intersection point of the surface charge vs. pH curves at different ionic strengths. The common intersection point is not very distinct; the point of zero charge (in the acidic region) is approached asymptotically. However, this also means that the surface charge versus pH curves are rather insensitive to the exact choice of the p.z.c.. In the literature the pH at the iso electric point is often assigned a value of 2-3 [15]. In the absence of specific adsorption this i.e.p. equals the point of zero charge.

Potentiometric titrations of silica

Surface charge-pH curves of silica Aerosil OX-50 in aqueous KCl solutions of different ionic strength are determined at 25 °C using an automated titration set up. A (Metrohm) combined glass electrode is used for the titrations, which are performed in a well closed thermostatted, double-walled vessel under a CO_2 free, water vapour saturated, nitrogen atmosphere. The behaviour of the cell was checked by performing blank titrations and comparing these to calculated blank curves. For the suspension titrations 50 ml of KCl solution was added to about 0.6 g silica. The suspension is placed in an ultrasonic bath for 60 minutes in order to reduce any aggregation of the silica particles. Before starting

the titration the solution was brought to *pH* 3 and purged with (extremely pure) nitrogen for at least 45 minutes. The silica suspension was then titrated between *pH* 3 and *pH* 9 with 0.1 M KOH and back with 0.1 M HCl. In order to determine the extent of the proton and hydroxyl ion adsorption on the sample as a function of the *pH*, the proton/hydroxyl consumption of the blank solution was subtracted from the overal suspension consumption.

The (potentiometric) titration curves were measured at salt concentrations of 0.01, 0.1 and 1 M KCl respectively. Small deviations between the hydroxyl ion and the (reverse) proton titrations are ascribed to dissolution of the silica at higher *pH* values (pH > 8.5), by a rather rapid titration (in our case for titration runs of ± 2 hours) these differences are minimized [16].

3.4. Results and discussion

The absolute magnitude of the surface charge density is calculated from the potentiometric titration curves assuming the surface charge of silica to be negligibly small at *pH*=3. In order to convert the adsorption of charge determining ions from mole/g silica to mole/m^2 the (BET(N$_2$)) surface area of 45 m^2/g was used.

The surface charges for different concentrations of KCl are given in Fig. 1. For *pH* < 6 the surface charge is low, at higher *pH* values a larger charge is build up at the silica surface. Increasing the salt concentration improves the screening of the electrostatic interactions so that, at given *pH*, more charge can be accommodated at the surface. The magnitude of the surface charges found for bare Aerosil OX-50 compare very well with those found by Abendroth [17] for silica CAB-O-SIL M7 (a pyrogenic silica). This indicates that both silicas have a similar surface chemistry. On precipitated BDH silica, considerably higher (up to 1.9 C/m^2) surface charges have been measured [16]. A pyrogenic silica has a low concentration of surface silanol groups so that a rather modest surface charge develops with increasing *pH*. A fully dehydroxylated silica (treated at 900 °C) has roughly one surface silanol group per nm^2 [18]. On a precipitated (i.e., a non-heat-treated and porous) silica, previous studies have shown a density of 8-10 hydroxyl groups per nm^2 [13, 19]. A "fully" hydrated and annealed silica surface contains approximately 5 hydroxyl groups per nm^2, if larger silanol group densities are found on a silica surface these are probably due to the presence of internal SiOH groups which were assumed to be present at the surface [20]. When solely all surface silanols of the heat-dehydroxylated and the fully hydrated annealed silica would dissociate, this results in surface charges of –0.16 and –0.80 C/m^2, respectively. The surface charge of a pyrogenic silica is expected to be comparable to that of a heat dehydroxylated silica.
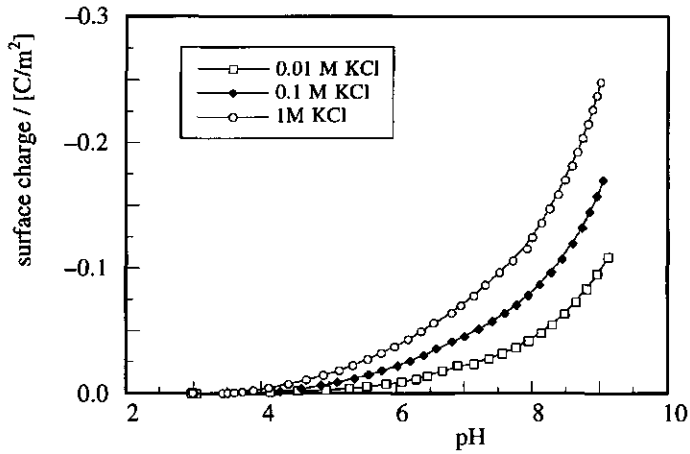
Figure 1. The surface charge densities at 25 °C of silica Aerosil OX-50 in KCl solution as a function of pH and ionic strength.
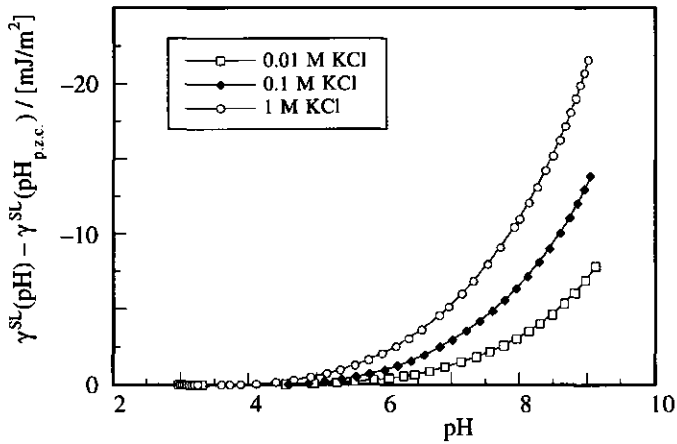
Figure 2. Surface pressures at 25 °C of silica Aerosil OX-50 as a function of the pH, calculated from an integration (see Eq. 8) of the surface charge curves given in Fig 1.

However, rehydration might render the pyrogenic silica more comparable to a fully hydrated annealed silica. Furthermore, titration of a pyrogenic silica until rather high *pH* values (i.e., at which the silica starts to dissolve) could easily increase the number of surface silanol groups.

By integrating the surface charge as a function of the *pH* the decrease in silica-water interfacial tension upon charging the solid can be calculated according to Eq. (8). The results are plotted in Fig. 2. According to Eqs. (8), (10) and (11), the surface charge dependency of the contact angle and the work of adhesion, respectively, directly follows from Fig. 2. The presence of charge (i.e., adsorption of potential determining ions) at the silica surface increases the surface pressure and reduces the silica-water interfacial tension. For *pH* > 4 the addition of salt reduces the silica-water interfacial tension.

In general, the interfacial tension of any charged solid-water interface is decreased upon the addition of electrolyte. Therefore, the water spreading tension on charged solids normally increases when increasing the surface charge (i.e., by raising the *pH* and/or the salt concentration), see also Eqs. (2), (7) and (9).

Relevance of the surface charge for oil recovery

In order to demonstrate the implications of the thermodynamic framework presented above, the wettability in an oil reservoir (reservoir rock/oil/brine) will be briefly discussed. Many rock surfaces are charged, and their surface charge depends on the salinity, *pH* and specific adsorption of species from the oil or brine phase [21]. Although the exact electrolyte composition of the brine and the exact behaviour of the (heterogeneous) reservoir rock surface charge are not known, the present approach can be used to predict some trends. The presence of salt will increase the preference of a charged surface to be wetted by the aqueous (brine) phase. This means that the efficiency of an aqueous solution to displace oil from a charged surface increases when the salt content of the aqueous phase is increased. In order to evaluate the influence of the *pH* on the reservoir wettability, knowledge of the location of the p.z.c. or of the electrokinetically measurable isoelectric point of the reservoir rock is required. Finally, the polarizability of the liquid medium close to the surface, determines the screening and the surface charge. Organic adsorbates usually have a lower dielectric permittivity than water and their adsorption will, in general, suppress the surface charge (see f.i. ref. [22]). Hence, both uncharged and charged adsorbates affect the surface charge. Asphaltene (apolar species present in crude oils) adsorption on reservoir rocks will, in general, decrease the surface charge and decrease the waterflooding efficiency in tertiary oil recovery.

35

The work of adhesion on charged solids

Many authors split up the substrate-liquid work of adhesion in two additive parts, a Lifshits-van der Waals part, denoted by $W_{A, LW}$ and a rest term, non Lifshits-van der Waals, denoted by $W_{A, nLW}$, according to [23]

$$W_A = W_{A, LW} + W_{A, nLW} \tag{12}$$

However, W_A is a Gibbs energy and contains both enthalpic and entropic contributions. In general the entropic contributions contain configurational entropy terms that are not additive, i.e. Eq. (12) is an approximation. For a better analysis the configurational entropy contribution has to be considered separately (by, for instance, a statistical thermodynamic treatment).

In Eq. (12), all non Lifshits-van der Waals interactions are included in $W_{A, nLW}$. Many authors (mainly) attribute $W_{A, nLW}$ to acid-base interactions and various semi-empirical models describing acid-base interactions have been proposed [23-25]. The input parameters of such models are usually defined within a certain concept of acid-base interactions whereas several concepts may be interplaying. Furthermore, in many cases reliable experimental data are lacking so that the input parameters for the various acid-base models are uncertain. Moreover, such acid-base models are fairly crude approximations for complicated interactions.

It should be noted that the possible long range electrostatic and structural contributions to the work of adhesion are both included in $W_{A, nLW}$. The former can be easily described by means of Eq. (11).

3.5. Conclusions

The contact angle and the work of adhesion in a solid-liquid-vapour system are maximal at the point of zero charge of the solid-liquid interface. The effect of the surface charge (and changing electrolyte concentrations) on the work of adhesion and the contact angle can be evaluated quantitatively by integrating the surface charge as a function of the (logarithm of the) concentration of charge detemining electrolyte at constant indifferent electrolyte concentration.

On a pyrogenic silica the surface charge increases with increasing pH and salt concentration. At 1M KCl and $pH = 9$ the surface charge of the pyrogenic silica equals -0.25 C/m^2. Compared to the uncharged silica (i.e., for $pH = 3$), this surface charge increases the solid-liquid interfacial tension by 22 mJ/m^2, whereas this surface charge decreases the work of adhesion by maximally 22 mJ/m^2.

The *pH* dependency of water contact angles on substrates exposing ionizable groups is usually interpreted qualitatively from the degree of ionization of the functional groups at the surface. However, it is worthwhile to determine the (absolute) surface charge on these substrates. Together with the thermodynamic framework presented here this allows a quantitative explanation.

The surface charge on solids can also be studied in terms of (theoretical) adsorption equations for charge determining ions. In combination with the thermodynamic approach outlined this indulges one to investigate the influence of different types of solid charging behaviour (e.g. monofunctional, zwitterionic or amphoteric surfaces [26]) on the adsorption, adhesion and and wetting properties of such solids.

References

[1]   Billet, D. F., Hough, D. B. and Ottewill, R. H., *J. Electroanal. Chem.*, 74, **1976**, p. 107-120.

[2]   Fokkink, L. G. and Ralston, J., *Colloids Surfaces A*, 36, **1989**, p. 69-76.

[3]   Holmes-Farley, S. R., Bain, C. D. and Whitesides, G. M., *Langmuir*, 4 (4), **1988**, p. 921-937.

[4]   Holmes-Farley, S. R., Reamey, R. H., McCarthy, T. J., Deutch, J. and Whitesides, G. M., *Langmuir*, 1 (6), **1985**, p. 725-740.

[5]   Whitesides, G. M., Biebuyck, H. A., Folkers, J. P. and Prime, K. L., *J. Adhesion Sci. Techn.*, 5 (1), **1991**, p. 57-69.

[6]   Lee, T. R., Carey, R. I., Biebuyck, H. A. and Whitesides, G. M., *Langmuir*, 10 (3), **1994**, p. 741-749.

[7]   Hair, M. L. and Hertl, W., *J. Phys. Chem.*, 73 (7), **1969**, p. 2372-2378.

[8]   Lyklema, J., *J. Colloid Interface Sci.*, 99 (1), **1984**, p. 109-117.

[9]   Koopal, L. K. and van Riemsdijk, W. H., *J. Colloid Interface Sci.*, 128 (1), **1989**, p. 188-200.

[10]   de Keizer, A., Böhmer, M. R., Mehrian, T. and Koopal, L. K., *Colloids Surfaces A*, 51, **1990**, p. 339-357.

[11]   Schlangen, L. J. M., Koopal, L. K., Cohen Stuart, M. A. and Lyklema, J., *Colloids Surfaces A*, 89, **1994**, p. 157-167, most of this work is included as Chapter 2 in this Thesis.

[12]   Everett, D. H., *Pure & Appl. Chem.*, 53, **1981**, p. 2181-2198.

[13]   Kiselev, A. V. and Lygin, V. I., in *"Infrared Spectra of Surface Compounds";* Wiley and Sons: New York, **1975**: p. 80.

[14]   Young, G. J., *J. Colloid (Interface) Sci.*, 13, **1958**, p. 67-85.

[15]   Parks, G. A., *J. Phys. Chem.*, 65, **1969**, p. 177.

[16]   Tadros, T. F. and Lyklema, J., *J. Electroanal. Chem.*, 17, **1968**, p. 267.

[17]   Abendroth, R. P., *J. Colloid Interface Sci.*, 34, **1970**, p. 591-596.

[18]   Hair, M. L., in *"Silanes, Surfaces and Interfaces";* Leyden, D. E. (Ed.), Gordon and Beach Science Publishers: New York, **1986**: p. 25-43.

[19]   Nishiokoka, G. M. and Schramke, J. A., *J. Colloid Interface Sci.*, 105 (1), **1985**, p. 102-111.

[20]   Iler, R. K., in *"The Chemistry of Silica: Solubility, Polymerization, Colloid and Surface Properties and Biochemistry";* John Wiley & Sons Inc.: New York, **1979**: p. 635-640.

[21]   Anderson, W. G., *J. Petr. Tech.*, Oct. **1986**, p. 1125.

[22]   Szczypa, J., Kajdewicz, I. and Kosmulski, M., *J. Colloid Interface Sci.*, 137 (1), **1990**, p. 157-162.

[23]   Fowkes, F. M., *J. Adhesion Sci. Techn.*, 1 (1), **1987**, p. 7-27.

[24]   Mittal, K. L. and Anderson(Jr.), H. R. (Eds.), *"Acid-Base Interactions: Relevance to Adhesion Science and Technology"*; VSP: Utrecht, **1991**.

[25]   Berg, J. C., in *"Wettability"*, Berg, J. C. (Ed.); Marcel Dekker Inc: New York, **1993**: Chapter 2.

[26]   Koopal, L. K., in *"Coagulation and Flocculation: Theory and Applications"*; Surfactant Science Series ,Vol 47; Dobias, B (Ed.), Marcel Dekker Inc.: New York, **1993**: chapter 4.

Chapter 4

Thin Hydrocarbon and Water Films on Bare and Methylated Silica: vapour adsorption, wettability, adhesion and surface forces *

Abstract

The vapour adsorption of different n-alkanes, cyclohexane, toluene and water on bare and methylated pyrogenic silica (Aerosil OX-50) has been studied gravimetrically. Linear adsorption isotherms of the n-alkanes and of cyclohexane on both substrates are found until high relative vapour pressures, the same holds for toluene on methylated silica. The linearity of the isotherms indicates relatively weak lateral interactions between adsorbed molecules. On bare silica, the adsorption, expressed in moles/m², of the n-alkanes studied (C7-C9) is independent of chain length. The adsorption strongly increases after the coverage corresponding to a monolayer of alkanes oriented perpendicular to the surface has been reached. Methylation of the silica decrease the adsorption of all adsorptives studied. On methylated silica the octane isotherm lies below the coverage of a monolayer parallel to the surface until just before saturation. From the adsorption data surface pressure isotherms are constructed and the work of adhesion is obtained. The work of adhesion reveals that the Lifshits-van der Waals part of the silica surface tension is reduced from 44 mJ/m² for bare (pyrogenic) silica to 30 mJ/m² for methylated silica. The adsorption data are also converted to disjoining pressure isotherms. At small film thicknesses, the disjoining pressure can be described by an exponential short-range interaction.

4.1. Introduction

Adsorption is often used as a tool to modify the physico-chemical properties of interfaces. Practical applications of adsorption include steric stabilisation, flotation, coating, lubrication, wetting and oil recovery. Such applications benefit from detailed studies on the adsorption mechanism and the interaction forces involved. Adsorption can be studied either from a macroscopic or from a more molecular point of view. The former approach focuses, for example, on adhesion, wetting and thin film behaviour in terms of the spreading tension, contact angle and surface pressures. The latter is based on a molecular interpretation of macroscopic properties. Information on these macroscopic properties can be obtained from, for instance, adsorption studies, surface force measurements, colloidal stability or disjoining pressure measurements.

Adsorption of liquids that are sufficiently volatile at ambient temperature is often investigated by studying the vapour adsorption on a solid. On flat interfaces, techniques

41

like crystal resonant frequency change [1] and ellipsometry [2-4] are used for this goal. With these techniques it is difficult to determine the adsorption accurately in the steep isotherm part near saturation, because of difficulties with the vapour pressure control. However, this range can be studied by measuring disjoining pressures, for instance by pressing a vapour bubble against a solid-liquid interface [5].

Many vapour adsorption studies have been performed on silica and related substrates [2, 4, 6, 7]. In this study the influence of the alkane chain length and cyclicity on the formation of thin adsorbed layers onto silica is investigated. Furthermore, the adsorption behaviour on bare and methylated silica will be compared. Gravimetric vapour adsorption experiments have been carried out on a pyrogenic silica and on the same adsorbent, after modification by (complete) methylation. When rather volatile liquids are used, the difficulties encountered with the control and measurement of the low vapour pressures of the adsorptive are minimal. The measured isotherms are compared with data available in the literature and transformed into surface- and disjoining pressure isotherms. The surface pressure isotherms are related to the tangential component of the pressure tensor whereas disjoining pressure isotherms refer to its normal component. Surface pressure isotherms allow interpretation in terms of two-dimensional equations of state and can be used to obtain information on components the solid surface tension [8]. The disjoining pressure isotherms can be used to assess the interaction forces acting in (thin) films [5].

4.2. Experimental

Adsorptives

The adsorptives used in this study were n-heptane (Merck), n-octane (SDS), n-nonane (Merck), cyclohexane (Aldrich), toluene (Aldrich) and water. All the alkanes were p/a (> 98%) grade and used without further purification. The water was of ultra high quality (UHQ, resistivity 18 MΩ cm at 25 °C), obtained using an Elgastat UHQ II system.

Substrates

A powdered pyrogenic non-porous silica Aerosil OX-50 (Degussa) and fully methylated Aerosil OX-50 have been used as substrates. Prior to methylation, the Aerosil OX-50 was cleaned by rinsing for two hours under reflux with a hot 50%-50% mixture of nitric acid and sulfuric acid, followed by prolonged rinsing with UHQ water until pH 7 had been reached. After this treatment the Aerosil OX-50 was dried overnight under vacuum at 150 °C. The clean Aerosil OX-50 was methylated by overnight immersion in a 15% (v/v) solution of HMDS (hexamethyldisilazane, Fluka) in refluxing toluene (for the reaction mechanism, see Refs. [9, 10]). After methylation the powder was successively rinsed with dry toluene, acetone and UHQ water. Finally, the methylated Aerosil OX-50 was dried under vacuum at 100 °C overnight. The

Cahn 1000 elektrobalance

MKS 128
pressure gauge

MKS 220
pressure gauge

Drytel 30
vacuumpump

adsorptive
supply

cold trap

liquid
thermostat
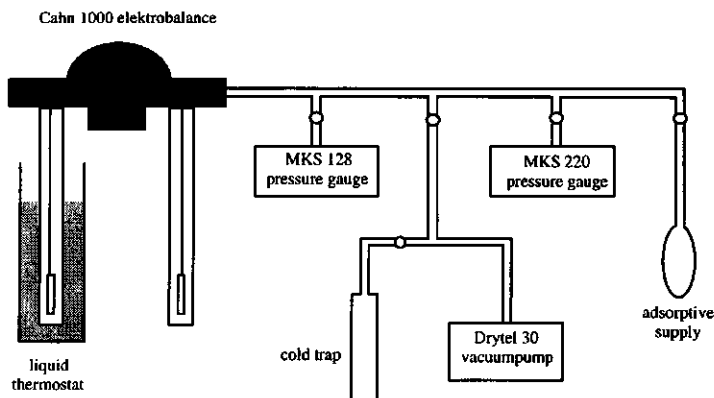
Fig. 1. The gravimetric set-up for adsorption measurements.

surface areas of the Aerosil OX-50 and the methylated Aerosil OX-50, as determined by BET(N_2) gas adsorption, were 45 m^2/g and 36 m^2/g, respectively. Before measuring an adsorption isotherm, each sample was outgassed by overnight heating in the gravimetric set-up at 150°C under a pressure lower then 10^{-3} mbar, in order to remove any physically adsorbed molecules (especially water) [11].

Gravimetry

The adsorption isotherms of the n-alkanes, cyclohexane, toluene and water on the substrates were determined by measuring the increase in weight at equilibrium as a function of the relative vapour pressure. In Fig. 1 the general set-up of the gravimetric equipment is shown. A Cahn 1000 electrobalance (sensitivity 0.1 μg) is connected to two pressure gauges (MKS Baraton 220, 0-5000 mbar and MKS Baraton 128, 0-100 mbar), a (liquid nitrogen) cold trap in connection with a Drytel 30 vacuum pump (oil-free, two-stage pumping system) and the adsorptive supply, a liquid reservoir (at saturated vapour pressure) at room temperature.

The weighing unit of the balance is made vibration-free by placing it on a sand-filled case. The substrate is placed in a cylindrical aluminium sample bucket (height: 60 mm, outer- and inner diameter: 13 mm and 12 mm, respectively). The bucket acts as a radiator [12], draining the heat of adsorption. The bucket is surrounded by a glass outer tube placed in a liquid thermostat at 17 °C. In order to prevent condensation, the rest of the set-up is kept at room temperature. The temperature in the sample bucket was 17 °C; this value is determined by filling the sample bucket with liquid and measuring the equilibrium pressure attained in the set-up. For the measurement of the water vapour adsorption isotherms, silanisation of the inside of the glass outer tube was necessary.

In order to avoid spurting of the sample from the bucket upon evacuation of the set-up some pieces of aluminium foil were inserted in the sample bucket. The time needed for the recording of an isotherm is minimized by a stepwise introduction of adsorptive,

43

instead of a more time-consuming (quasi-equilibrium) continuous introduction [13]. A small amount of vapour is admitted to the sample via a tap, connecting the adsorptive supply and the balance. Once equilibrium has been reached (i.e., the adsorbed mass and the vapour pressure reading had become constant) the mass and vapour pressure are recorded. Vapour admissions are repeated until close to saturation.

In the gravimetric experiment, the mass reading has a contribution due to the buoyancy force. Calibration with nitrogen (assuming ideal behaviour of the gas present in the set-up) showed that, in a typical experiment, the buoyancy correction could be safely ignored compared to the change in the adsorbed mass (see Appendix I).

4.3. Results

Although the electrobalance had a sensitivity of 0.1 μg, the weight fluctuations registered during the measurements indicated a standard deviation of about 4 μg for hydrocarbon adsorption and circa 40 μg for water adsorption. For a typical isotherm this corresponds to a maximum absolute error of about 0.02 μmole/m² for the alkane- and 0.9 μmole/m² for the water adsorption isotherm. The precision of the measured pressure was in the order of 0.005 mbar.

Adsorption on silica

The equilibrium adsorbed amounts (in μmoles/m²) for the n-alkanes, cyclohexane, toluene and water on the bare silica are plotted in Fig. 2. Figure 2a shows that for the n-alkanes on silica, the adsorption increases approximately linearly with the vapour pressure until relative pressures of about 0.75. The isotherms coincide within experimental error. Figure 2b shows the adsorption of octane, cyclohexane, toluene and water on Aerosil OX-50. The adsorption isotherms of the linear alkanes and cyclohexane also coincide up to about $p/p_0=0.75$. The hydrocarbon adsorption isotherms exhibit a continuous, monotoneous increase. The shape of the toluene and water adsorption isotherms differs from those of the alkanes; for both a weak knee-bend is found at $p/p_0\approx 0.1$. For toluene the adsorption levels at intermediate pressures are about twice as high as for the alkanes, whereas for water about four times as much moles are adsorbed. As the vapour pressure approaches saturation, all isotherms, except that for water, show a steep increase without intersection with the saturation axis ($p/p_0=1$).

Adsorption on methylated silica

The adsorption isotherms for octane, toluene, cyclohexane and water on methylated Aerosil OX-50 are given in Fig. 3. In Fig. 3a the entire isotherms is plotted, Fig. 3b displays the initial parts more clearly. All adsorption isotherms in Fig. 3a increase rather sharply as saturation is approached. Comparing Figs. 2b and 3 it is evident that methylation of the Aerosil OX-50 leads (for all adsorptives studied) to a lower
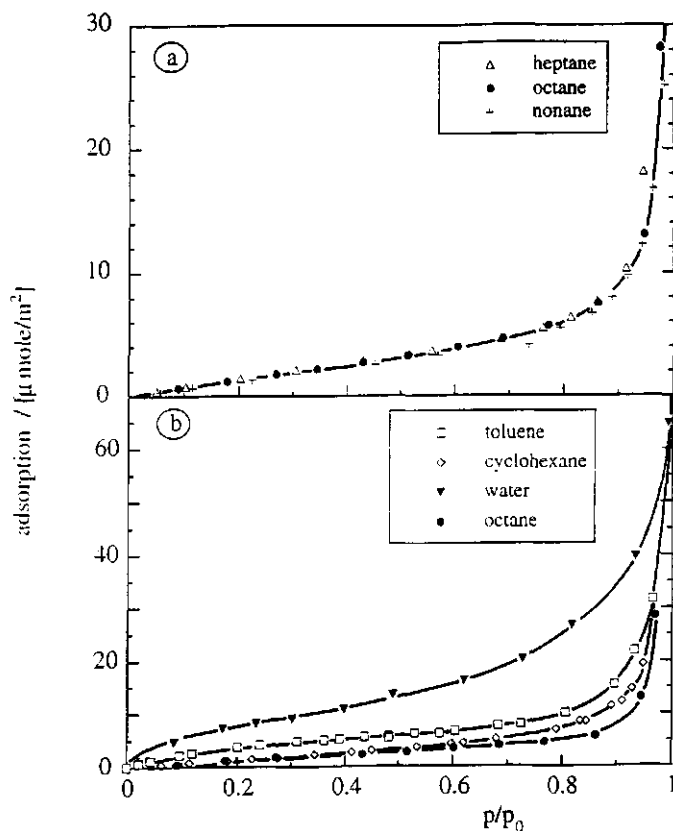
Fig. 2. Gravimetric adsorption isotherms (at 17 °C) of various hydrocarbons and water on bare silica Aerosil OX-50. In (a) the adsorption of the n-alkanes heptane, octane and nonane is shown. In (b) the adsorption of cyclohexane, toluene, water is plotted together with that of octane.

adsorption. The isotherms of n-octane and toluene on methylated Aerosil OX-50 are approximately linear up to $p/p_0 \approx 0.7$. The adsorption levels for octane and toluene are very similar. The adsorption of cyclohexane remains very low up to $p/p_0 = 0.4$, (however, this may be an artefact due to the limited experimental accuracy if small adsorbed amounts are measured) after which a linear increase occurs up to $p/p_0 \approx 0.8$. The water isotherm deviates considerably from the others, both with respect to shape and adsorbed amount.
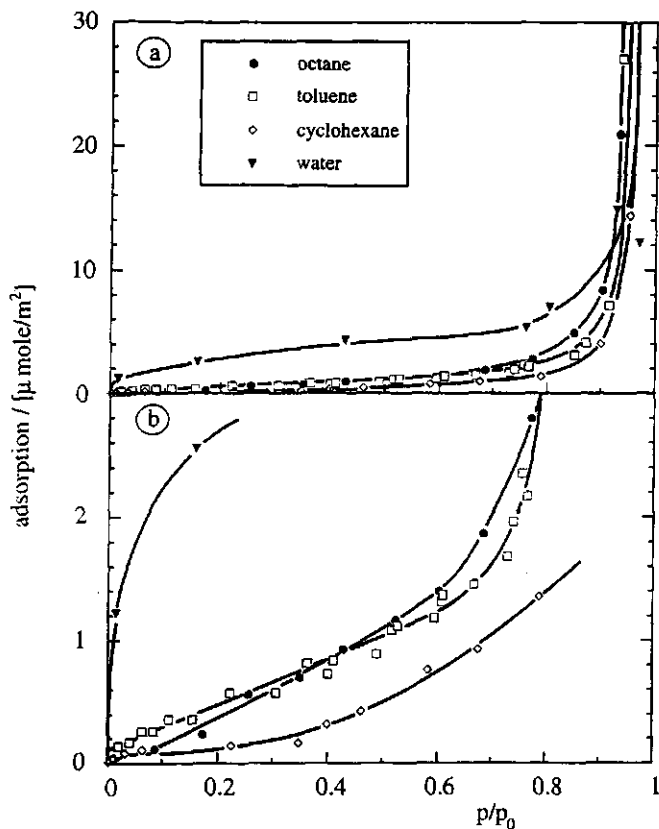
Fig. 3. Adsorption isotherms (at 17 °C) of octane, cyclohexane, toluene and water on methylated silica Aerosil OX-50. In Fig. (a) the complete isotherm is plotted whereas Fig. (b) is an enlargement of the low adsorption region.

4.4. Comparison with other measurements

In order to enable comparison of the present results with ellipsometric studies, the average thickness h of the adsorbed layer is obtained from the adsorbed amount (Γ) and the molar volume for which the molar volume in bulk liquid was chosen. In ellipsometry, a similar assumption is made when the refractive indices of the adsorbed layer and of bulk liquid are equated. In Figs. 4 and 5 our film thicknesses are compared to data from ellipsometric and gravimetric adsorption measurements available in the literature.[4, 6, 7, 14-16] Anticipating further discussion, we point out that the overall agreement is satisfactory, particularly in the range of low p/p_0. Generally, above $p/p_0=0.8$, the gravimetric isotherms on the powdered Aerosil OX-50 are sligthly higher than the ellipsometric ones on flat substrates. These discrepancies found for powdered

Aerosil OX-50, are probably due to the occurrence of inter-particle condensation (in the section "surface pressure isotherms" we will return to this issue).

I: Hydrocarbon and water adsorption on silica

Before comparing adsorption studies on different silica substrates we briefly discuss the surface properties of the various silicas. The Hamaker constants for quartz (anhydrous crystalline silica) and (anhydrous amorphous) silica are alike [17]. Furthermore, both substrates have a similar surface-silanol and -siloxane group density [18] (a normal, fully hydroxylated SiO_2 surface has about 4.6 surface silanol groups per nm^2, i.e. a surface density of 7.6 $\mu mol/m^2$) so that adsorption on these surfaces may be comparable. The pyrogenic (anhydrous amorphous) Aerosil OX-50 is expected to have a similar surface silanol group density and distribution as a heat-dehydroxylated silica/quartz on which only isolated silanol groups remain at the surface (about one surface silanol group per nm^2) [18]. Rehydration of such a heat-dehydroxylated SiO_2 can be quick or extremely slow depending on the duration and temperature of the heat dehydroxylation treatment. Rehydration of a heat-dehydroxylated SiO_2 (heated 10 hours at 900°C) in water under ambient circumstances took several years [18].

Water on silica

Water vapour adsorbs rather strongly onto silica due to the possibility of hydrogen bond formation between the water molecules and the surface silanol groups. It is known that the adsorption and wetting (characteristics) of water on SiO_2 are affected by the surface density of the silanol groups. Dehydroxylation results in a lower surface silanol density and hence in a lower water adsorption [14], without affecting the $BET(N_2)$ area [19]. In Fig. 4a it can be seen that the current water vapour adsorption data are in good agreement with gravimetric experiments of water adsorption at 25 °C on ground quartz reported by Whalen [15] and the ellipsometric results by Beaglehole and Christenson [4]. The latter authors measured the adsorption of water at 18.1 °C on a silicon wafer covered with a thin SiO_2 layer, formed by a HNO_3 treatment. Beaglehole and Christenson found that their SiO_2 layer was moderately hydrophobic and they considered their substrate to resemble a heat-dehydroxylated quartz. At saturation they measured a film of limited thickness (0.64 nm). The present water vapour adsorption isotherm shows a rather steep increase in adsorbed amount as saturation is approached and appears to intersect the saturation axis at a film thickness of about 1.25 nm. At saturation, ellipsometrically determined water film thicknesses on quartz range between 2 and 8 nm, depending on the temperature [20]. However, if extreme care is taken in cleaning the quartz surface, a continuous increase in film thickness with vapour pressure up to about 150 nm at $p/p_0=1$ is found [3]. A meticulously cleaned quartz surface is relatively hydrophilic and completely wetted by water (contact angle $\approx 0°$). The lower film thicknesses found for less elaborately cleaned quartz are likely due to hydrophobic contaminants. These contaminants oppose the effect of the surface silanol

47
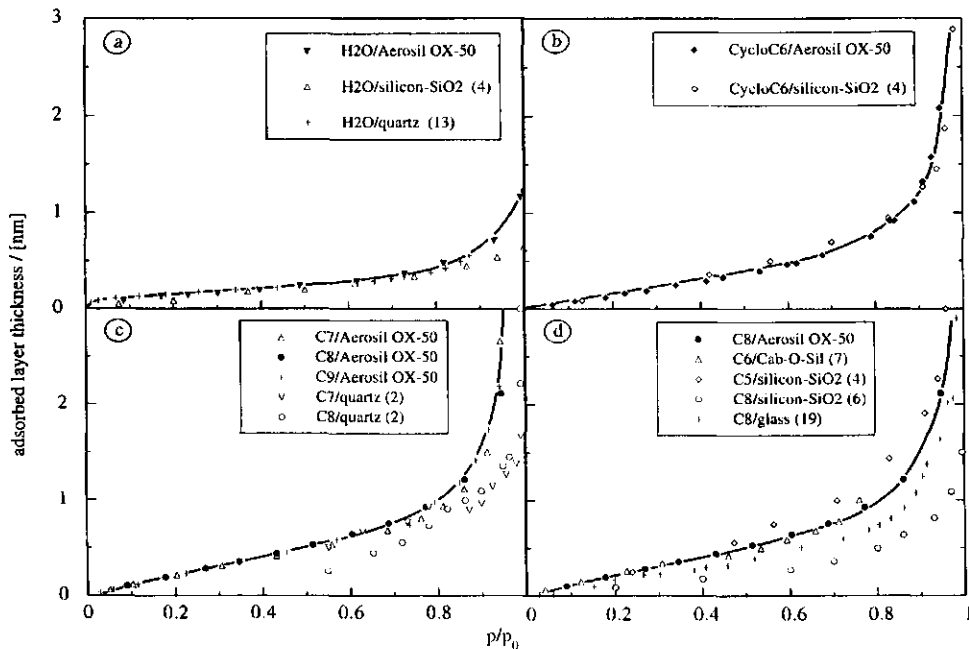
Fig. 4. Comparison of the average adsorbed layer thicknesses as a function of the relative vapour pressure on different SiO₂ surfaces. (a) Water on Aerosil OX-50, on a silica covered silicon [4] and on quartz [15]. (b) Cyclohexane on silica Aerosil OX-50 and on silica covered silicon [4]. (c) n-Alkanes on silica Aerosil OX-50 and on quartz [2]. (d) Octane on Aerosil OX-50, hexane on Cab-O-Sil [7], pentane and octane on silicon covered with silica [4, 6] and octane on glass [21].

groups and render the surface more hydrophobic so that it behaves more comparable to a heat-dehydroxylated SiO_2. This might explain why the quartz studied by Whalen [15] is similar to the pyrogenic silica studied here. Alternatively, some rehydroxylation of Aerosil OX-50 could have occurred so that its adsorption behaviour rather resembles that of normal (hydroxylated) SiO_2, sponaneous dehydroxylation of quartz is unlikely.

Alkanes on silica

The adsorption isotherm of cyclohexane on Aerosil OX-50, plotted in Fig. 4b, is comparable to the isotherm, at 18.1 °C, of cyclohexane on a silicon wafer covered with a thin SiO_2 layer, measured ellipsometrically [4]. The adsorption isotherms of various

n-alkanes on Aerosil OX-50 and on other SiO_2 substrates are plotted in Figs. 4c and d. The n-alkane adsorption isotherms on Aerosil OX-50 (Fig 4c) are very similar to that for cyclohexane (Fig. 4b). Those of the n-alkanes on Aerosil OX-50 are in fair agreement (see Fig. 4c) with ellipsometric studies by Gee et al. [2] of n-heptane on hydroxylated quartz at 21 °C. The shape of the n-octane isotherm by Gee et al. is similar to ours although we found higher adsorbed amounts. Figure 4d shows that the isotherms of the n-alkanes on Aerosil OX-50 coincide with the gravimetric one of n-hexane on heat (800°C)-dehydroxylated pyrogenic silica (Cab-O-Sil) measured, at 22 °C, by Hair and Hertl [7]. The n-octane adsorption isotherm in Fig. 4d by Levinson and coworkers [6] was measured ellipsometrically on a silicon wafer (at 17.2 °C) which has been heated in air at 850 °C so that it became covered by a silica layer of about 100 nm thick. Levinson and coworkers [6] measured a lower adsorbed amount for octane than we did on Aerosil OX-50, but the shapes of the isotherms are similar. In relation to the observed absolute differences between the ellipsometric and gravimetric studies we note that the adsorbed amounts plotted in the gravimetric isotherms depend on the specific surface areas assigned to the substrates. There is always the possibility that nitrogen, alkane and water molecules each "see" a different surface area. Figure 4d shows the adsorption of octane on glass, obtained ellipsometrically at 25 °C [21]. The differences in n-alkane adsorption between glass and pure SiO_2 are minor. The ellipsometric adsorption at 18.1 °C of n-pentane on a SiO_2-covered silicon wafer [4] shown in Fig 4d, is in fair agreement with the current results.

Comparing Figs. 4c and 4d we note that, despite the differences in the degree of surface dehydroxylation of the adsorbing SiO_2, the adsorption isotherms below p/p_0=0.8 are rather similar. Gee et al. [2] have also confirmed this for n-pentane. However, it should be realized that the similarity of alkane adsorption on a heat-dehydroxylated and a hydroxylated SiO_2 could be due to rehydration of the dehydroxylated SiO_2 surface. Secondly, the presence of hydrophobic impurities or physisorbed water at the hydroxylated SiO_2 surface might neutralize (part of) the influence of the surface silanols on hydrocarbon adsorption (it has been observed that bulk water has a significantly lower pentane adsorption compared to silica [22]). For a more detailed comparison of the present results with those from the literature a better knowledge of the way of preparing, storing, the pretreatment and outgassing conditions of the various SiO_2 surfaces is required.

In general, it can be concluded that, for vapour pressures below p/p_0=0.8, the gravimetric adsorption isotherms on powdered Aerosil OX-50 are consistent with adsorption studies on similar flat surfaces, available in the literature. In an ellipsometric experiment, the film thickness is a reflection of the optical contrast and assumptions concerning the refractive index n or $dn/d\Gamma$ have to be made. The gravimetric isotherms are directly available experimentally, without any assumptions except the choice of the specific surface area. The consistency shows that the assumptions made to obtain ellipsometric layer thicknesses are quite reasonable. Furthermore it endorses the linearity of alkane adsorption isotherms on silica up to p/p_0=0.75.

II: Water and hydrocarbon adsorption on alkylated silica

Water on alkylated silica

In Fig. 5a the water adsorption on methylated Aerosil OX-50 is compared to water adsorption at 22°C on methylated Cab-O-Sil as measured gravimetrically by Hair and Hertl.[7] Up to p/p_0=0.8, the isotherms are in fair agreement and show a very low water adsorption, as is expected from the low surface tension of a methylated surface.

n-Alkanes on alkylated surfaces

In Fig. 5b our octane film thicknesses on methylated Aerosil OX-50 are plotted, together with other results. Blake et al. [16] performed a gravimetric study (at 22°C) of octane adsorption on aluminium foil modified by exposure to pentanol. Exposure of an alumina surface to an alcohol (R-OH) vapour results in adjacent surface -OR and -OH groups and provides a means of hydrophobizing the alumina surface. When the five shortest n-alcohols are used for this treatment, three surface -OR groups per nm^2 can be introduced, independent of R [23]. The alcohol treatment creates a low-energy surface with an alkane affinity that depends on the chain length of the alcohol used for hydrophobization [16]. Blake et al. found that the differences between decane adsorption on a propanol- and on a pentanol-modified aluminia are large, whereas the differences between decane adsorption on a pentanol- and on a dodecanol-modified alumina are small. This suggests that alcohols larger than pentanol are able to screen most of the aluminium surface. Some differences in adsorption between methylated silica (which has only CH_3 groups in the grafted layer) and the pentanol-modified alumina could be expected due to the presence of CH_2 groups at the modified alumina. Furthermore, the solid substrate itself could also cause some differences in adsorption behaviour. Figure 5b shows that, with respect to n-octane, an alcohol-modified alumina surface is comparable to methylated Aerosil OX-50.

In Fig. 5b, the adsorption of hexane on methylated Cab-O-Sil, measured gravimetrically by Hair and Hertl (at 22°C) [7], is also shown. Figure 5b shows that, on methylated Cab-O-Sil, hexane adsorbs to a larger extent than octane on methylated Aerosil OX-50. A similar increase in adsorbed amount has been found by Blake et al. [16] on their pentanol-treated aluminium foil when going from n-hexane to n-dodecane.

Cyclohexane on alkylated silica

The cyclohexane film thicknesses, measured gravimetrically on methylated Aerosil OX-50, are in good agreement with those obtained ellipsometrically on a silicon wafer covered with a silica layer bearing grafted (by means of HMDS treatment) methyl groups [6], see Fig. 5b. The gravimetrically determined adsorption is somewhat higher than the ellipsometric one. Both isotherms increase in a rather linear way up to p/p_0=0.8.

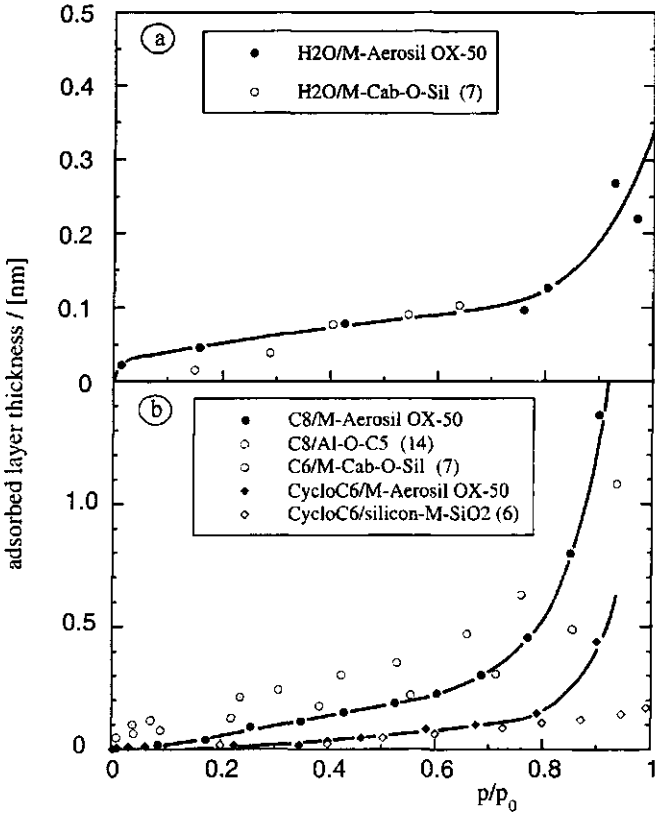Fig. 5. Same as Fig. 4, but for various methylated (M-) SiO₂ surfaces.
(a) Water on M-Aerosil OX-50 and on M-Cab-O-Sil [7]. (b) Octane
and cyclohexane on M-Aerosil OX-50, octane on alcohol modified
aluminum foil [16], hexane on M-Cab-O-Sil [7] and cyclohexane on a
methylated silica layer on silicon [6].

51

4.5. Alkane adsorption mechanism

Bare silica

The comparison made above indicates that the linear (Henry) region of the n-alkane adsorption isotherms on silica, which extends much further (up to p/p_0=0.8) than usually observed, can be considered as an established fact. Furthermore it shows that n-alkane adsorption onto silica is hardly chain length dependent. If n-alkanes were perpendicularly oriented, a monolayer would correspond to 8.3 μmole/m², a monolayer of molecules oriented parallel to the surface to about 4.0, 3.5 and 3.0 μmole/m² for n-heptane, n-octane and n-nonane, respectively [24]. Figure 2a shows that the amount of linear alkanes adsorbed on bare silica is below the value for a perpendicular monolayer of alkanes up to p/p_0=0.9. From these observations it can be inferred that the n-alkanes have a relatively low affinity for silica and do not adsorb in a flat conformation. In order to maximize their adsorption energy, the alkanes will tend to adsorb parallel to the surface, but this tendency is opposed by the incurred conformational entropy loss. For n-alkanes of different chain length these opposing effects lead to very similar molar adsorbed amounts.

The linearity of the alkane adsorption isotherms at lower vapour pressures points towards weak lateral interactions between the adsorbed alkane molecules. This is also in line with the low adsorption and could result from the fact that adsorption is restricted to certain sites. If these sites are spaceously distributed over the surface or separated by sites that are energetically less favourable or unfavourable for alkane adsorption (e.g. due to entropic reasons), lateral interactions between the adsorbate molecules will be absent or small. On silica the free surface silanols might play the role of the strongly adsorbing sites (since free hydroxyls are strongly adsorbing sites and hydrocarbon molecules interact on a 1:1 basis with free silanols [7]), whereas the surface siloxanes could act as the less- or unfavourable sites. Furthermore, with increasing vapour pressure, the adsorbed molecules increasingly protrude in the gas phase, so that lateral interactions remain small and a linear isotherm results. The tendency of adsorbate molecules to protrude into the vapour phase increases with increasing surface coverage. Above p/p_0=0.75, and above a limiting adsorbed amount of 5 μmole/m², irrespective of the chain length of the n-alkane, the adsorption starts to increase above the linear isotherm. At p/p_0=0.9 the adsorption rises sharply and condensation occurs. The adsorbed amount of 8.3 μmole/m² at this relative vapour pressure agrees well with the area of 0.19-0.25 nm² per n-alkane molecule adsorbed perpendicularly to the surface, given by Fowkes [24]. This suggests that multilayer formation only occurs after completion of a monolayer of perpendicularly oriented molecules.

Alkylated surfaces

The comparison of several adsorption studies on alkylated surfaces shows that alkylation decreases the alkane adsorption as compared to the bare surface. For alkylated substrates the attractive forces of the bulk solid are (at least partially) screened by the grafted layer, covering the solid. Longer alkanes adsorb to a lesser extent than shorter ones. Until close to saturation the adsorption remains below the value for a parallel n-alkane monolayer. This points to a rather low alkane affinity of an alkylated substrate and suggests that, on a methylated silica, hydrocarbon molecules adsorb predominantly parallel to the surface, possibly becoming partially embedded within the grafted layer. Presumably, an increasing chain length of the adsorbing n-alkane gives a stronger decrease in conformational entropy upon adsorption, so that the adsorption is lower for longer n-alkanes.

On a methylated silica, cyclohexane has a lower adsorption (in moles/m^2) than n-octane. A cyclic molecule is less flexible than a chain molecule of the same number of carbon atoms so that it has fewer possibilities to adapt its structure to the grafted layer.

4.6. Discussion

Modelling alkane adsorption

The quality of equations to describe adsorption (e.g., Langmuir, BET, Polyani [25]) is determined by the extent to which certain physical premises (e.g. homogeneity of the surfaces, architecture of the molecules, localized or mobile adsorption, lateral interactions) are considered. For alkanes, the physics of adsorption will be strongly determined by the conformations they can assume. Simple adsorption equations are inadequate to describe such adsorption. In Chapter 6 a self-consistent-field theory for adsorption of chain molecules, originally developed for polymer adsorption [26], will be used for a detailed molecular and thermodynamic interpretation of the hydrocarbon adsorption isotherms.

Adsorption and wettability

Adsorption can result in the formation of wetting layers and is very important in relation to wettability. If enough adsorptive is present, complete and partial wetting can be distinghuished. In the case of complete wetting, a macroscopic liquid layer will be formed spontaneously at the substrate. In the case of partial wetting, the liquid forms a droplet with a finite contact angle on the substrate. The critical surface tension γ_c is an empirical parameter that can be used to characterize these two wetting situations [27]. Liquids with a surface tension lower than the critical value completely wet the substrate, liquids with an interfacial tension higher than the critical surface tension partially wet the substrate. The two types of wetting can also be distinguished by the shape of the adsorption isotherm. In the case of complete wetting, the vapour

adsorption gradually increases with increasing vapour pressure until at saturation the adsorption rises very steeply to infinity. Partially wetting liquids form a thin film (finite adsorption) on the substrate at the saturation vapour pressure.[28] When enough liquid is present, macroscopic droplets are formed. Such droplets coexist with the thin adsorbed film.

In Fig. 2 all adsorption isotherms on Aerosil OX-50 approach the saturation axis asymptotically. Hence, all liquids studied completely wet the silica surface, which is not very striking (the spreading and wetting of liquid on a substrate is favoured by a high substrate surface tension [29]). The vapour adsorption isotherms measured on the methylated Aerosil OX-50 (see Fig. 3) also rise sharply close to saturation, suggesting complete wetting. The critical surface tension γ_c of a surface covered entirely by CH_3 groups (determined from the contact angles of a series of homologous alkanes [27]) lies between 22 and 24 mJ/m^2 , depending on the degree of order present in the layer. The interfacial tension of n-octane lies below γ_c, hence, octane is expected to wet the methylated silica completely. However, the liquid surface tensions of cyclohexane, toluene and water exceed γ_c. According to this reasoning, a finite adsorbed amount is expected at saturation, in contrast to the experimental results.

The sharp increase in adsorption close to saturation, found for partially wetting liquids, may be due to an insufficiently accurate vapour pressure control. During the vapour adsorption measurements close to saturation, supersaturation might have occurred. Upon supersturation the meta- and unstable range of the isotherm can be passed so that the adsorbed amount "jumps" from the stable thin film branch of the isotherm (with a finite adsorbed amount at saturation) to the stable thick film branch of the isotherm. Once on the stable thick-film branch of the isotherm, the adsorption rises continuously with a further increase in vapour pressure. At saturation the adsorption rises indefinitely although the liquid is only partially wetting. For completely wetting liquids the occurrence of supersaturation has no effect on the shape of the isotherm. In addition, a (relatively small) interparticle condensation effect could contribute to the rise in adsorption close to saturation. Therefore, the data are not good enough to decide on the wetting behaviour.

From individual vapour adsorption isotherms surface pressures can be calculated. The surface pressure is useful to study the contact angle and spreading tension for a solid contacting a liquid. Furthermore, in the case of two non-miscible adsorptives, the occurrence of liquid-liquid displacement on a solid can be assessed [29]. The surface pressure only indirectly depends on the adsorbent-adsorbate interactions. It is primarily a property of the adsorbate.

The surface pressure is defined as the difference between the interfacial tension of the "clean" solid (i.e., in vacuum) and the same in contact with an (adsorbing) vapour. At constant temperature, assuming ideal behaviour of the vapour, we can write for the surface pressure π^{SV} as a function of adsorption Γ

$$\pi^{SV}(\Gamma) = RT \int_{\Gamma=0}^{\Gamma} \Gamma \, d \ln p/p_0 \qquad (1)$$
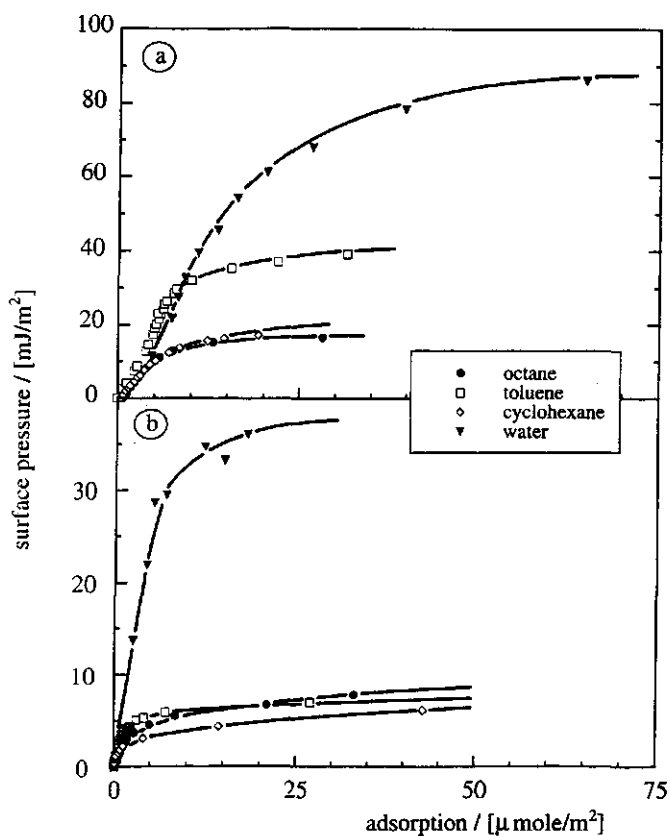
Fig. 6. The surface pressures of the various liquids on bare silica (Fig. a) and methylated silica (Fig. b) obtained from an integration of the adsorption isotherms shown in Figs. 2 and 3.

where p/p_0 is the relative vapour pressure. According to Eq. (1), the surface pressure follows directly from the area under the vapour adsorption isotherm if Γ is plotted versus $\ln p/p_0$.

In the case of complete wetting, the surface pressure approaches asymptotically its saturation value denoted by $\pi^{SV}(\Gamma_\infty)$. The symbol Γ_∞ is used to indicate that the adsorbed layer is macroscopically thick and has the properties of bulk liquid. In the case of partial wetting only a thin (non macroscopic) film is adsorbed at saturation. If enough adsorptive is present this film can be in equilibrium with a droplet and $\pi^{SV}(\Gamma_\infty)$ must be derived from the surface pressure of this thin film $\pi^{SV}(\Gamma_f)$ and the cosine of the contact angle [29].

55

Table 1. Surface pressures near saturation, wetting properties of the liquid, work of adhesion of the liquid Eq. (2), Lifshitz-van der Waals part of the solid interfacial tension (calculated using Eq. (4)). The values in brackets refer to partial wetting situations where the surface pressures near saturation do not neccesarily correspond to $\pi^{SV}(\Gamma_\infty)$.

adsorptive vapour of liquid L	γ^L mJ/m^2	wetting	π^{SV_L} at saturation mJ/m^2	W_A mJ/m^2	γ^S_{LW} mJ/m^2
adsorption on silica Aerosil OX-50					
heptane	20.4	complete	22	62	
octane	21.8	complete	17	60	44 ± 3
nonane	22.8	complete	16	61	
cyclohexane	25.5	complete	17	68	
toluene	28.5	complete	39	96	–
water	72.8	?	(86)	(232)	–
adsorption on methylated Aerosil OX-50					
octane	21.8	complete	8	51	30
cyclohexane	25.5	partial	(6)	(58)	–
toluene	28.5	partial	(7)	(63)	–
water	72.8	partial	(36)	(182)	–

The surface pressures were calculated according to Eq. (1). Henry's adsorption law ($\pi = \Gamma RT$) was used to estimate the magnitude of the initial surface pressure in the first point of the experimental isotherm, this initial value was used to start the numerical integration from the first point of the adsorption isotherm. In Figs. 6a and 6b the results are shown for bare and methylated Aerosil OX-50, respectively. In Table 1 the values of the highest surface pressures, obtained close to saturation, are summarized. Due to the possible occurrence of interparticle condensation the measured adsorption and surface pressures may be too high close to saturation. However, in the case of complete wetting, this hardly contributes to the surface pressure value since interparticle condensation falls within the plateau of the surface pressure isotherm. For partially wetting liquids, the possible occurrence of supersaturation implies that the surface pressures close to saturation do not necessarily correspond to $\pi^{SV}(\Gamma_\ddagger)$ or $\pi^{SV}(\Gamma_\infty)$. The highest surface pressures of the alkanes and water on Aerosil OX-50 are in fair agreement with those for octane and water on glass (15 and 119 mJ/m^2 respectively) determined ellipsometrically (at 25 °C) by Chibowski et al. [21].

Characterization of bare and methylated silica

The surface pressure at infinite adsorption $\pi^{SV}(\Gamma_\infty)$ can be used to investigate the work of adhesion W_A of the liquid-substrate pair under consideration according to Eq. (2) [29]

$$W_A = \pi^{SV}(\Gamma_\infty) + 2\,\gamma^L \tag{2}$$

where γ^L is the interfacial tension of the liquid L -vapour interface. In order to characterize intermolecular interactions of a substrate, many authors split up the substrate-liquid work of adhesion in two additive parts, a Lifshits-van der Waals (LW) part, denoted by $W_{A,\,LW}$ and a rest term, non Lifshits-van der Waals, denoted by $W_{A,\,nLW}$, according to [30].

$$W_A = W_{A,\,LW} + W_{A,\,nLW} \tag{3}$$

It should be realized that W_A is a Gibbs energy and contains both enthalpic and entropic contributions. In general the entropic contributions contain configurational entropy terms that are not additive, i.e. Eq. (3) is an approximation. For a better analysis the configurational entropy contribution has to be considered separately (as can be done in, for instance, a statistical thermodynamic treatment). Often $W_{A,\,LW}$ is expressed (following the Berthelot principle) as the geometric mean of the Lifshits-van der Waals contributions to the interfacial tensions involved

$$W_{A,\,LW} \approx 2\,\sqrt{\gamma_{LW}^L\,\gamma_{LW}^S} \tag{4}$$

where γ_{LW}^L and γ_{LW}^S are the Lifshits-van der Waals contributions to the surface tension of liquid L and solid S respecitvely. In general, these values are determined by bringing the surfaces into contact with apolar liquids (aL) for which it is assumed that only dispersive forces are operative so that $\gamma^{aL} = \gamma_{LW}^{aL}$ and $W_{A,\,nLW} \approx 0$. However, the Berthelot principle is correct for surface enthalpies but not for surface tensions (surface Gibbs energies) since entropic contributions do not obey this principle. Furthermore, contact with another phase may change the molecular orientation and density profiles of interfacial regions. These changes will depend on the two phases that are brought into contact. Hence γ_{LW}^L and γ_{LW}^S should be considered as approximate constants only.

Despite the approximations inherent to Eqs. (3) and (4), the approach has proven to be quite useful in practice [31]. Combining Eqs. (3) and (4) allows to determine γ_{LW}^S of bare and methylated silica using the $\pi^{SV}(\Gamma_\infty)$ values of the different apolar (non-aromatic) vapours. For bare silica Aerosil OX-50, the values are rather consistent (see Table 1) and a mean γ_{LW}^S value of 44 ± 3 mJ/m^2 is found.

The γ_{LW}^S values obtained from different experiments may depend on the experimental conditions such as the presence of physisorbed water and impurities. The γ_{LW}^S value detemined for silica Aerosil OX-50 is considerably less than the

values of 78 mJ/m^2 [32] and 71.8 mJ/m^2 [33] reported for quartz but in good agreement with the values of 39.8 mJ/m^2 and 41.1 mJ/m^2 for laboratory and commercial SiO$_2$ respectively, as determined by liquid penetration (through a wick) into a thin horizontal powder layer [34]. For glass, Chibowski et al. [21] found γ_{LW}^S values of 32 mJ/m^2 and 25 mJ/m^2, depending on the experimental method used. The values of Chibowski et al. are rather low due to the fact that an inflection point near the second monolayer in their surface pressure isotherm was taken for the calculation of γ_{LW}^S instead of the surface pressure of the macroscopically thick liquid layer formed at saturation. Taking Chibowski et al.'s value of the surface pressure near saturation of 15 mJ/m^2 for silica-octane would give a γ_{LW}^S for glass of 39 mJ/m^2, in good agreement with the present result.

Given the critical interfacial tension of a methylated surface, only octane is expected to completely wet such a surface and to form a macroscopic layer at saturation spontaneously. Hence, the surface pressure $\pi^{SV}(\Gamma_\infty)$ of octane is directly available from the adsorption isotherm and using Eqs. (2) and (4) a Lifshits-van der Waals part of the interfacial tension of 30 mJ/m^2 is obtained for the methylated silica. This value is identical to that reported in the literature for a flat interface constituted of $-CH_3$ groups only [35]. The value of γ_{LW}^S for methylated Aerosil OX-50 is considerably lower than that for bare Aerosil OX-50, but not as low as the liquid surface tension of pure alkanes.

Using the values of the surface pressure at saturation of toluene and water, given in Table 1, and setting γ_{LW}^S = 44 mJ/m^2 for Aerosil OX-50, $W_{A, nLW}$ can be calculated from Eqs. (2) to (4). The Lifshits-van der Waals component of the toluene surface tension is considered equal to γ^L, the surface tension of water is split up in a γ_{LW}^L of 21.8 mJ/m^2 and a non-LW part of 51.0 mJ/m^2 [36]. For silica-toluene and silica-water $W_{A, nLW}$ values of 25 and 170 mJ/m^2, respectively, are obtained. The non zero value for toluene is likely due to its aromatic nature allowing π-electron exchange with the substrate. Water is able to form hydrogen bonds, therefore the non-LW interactions at the silica-water interface will be stronger than at the silica-toluene interface.

A polar phase has other interactions besides Lifshits-van der Waals interactions. All these interactions are included in $W_{A, nLW}$ but also entropic effects differing from those occurring for apolar liquids (with the same γ_{LW}^L as the polar liquid) are included in $W_{A, nLW}$. Many authors (mainly) attribute $W_{A, nLW}$ to acid-base interactions and various semi-empirical models describing acid-base interactions have been developed [8,37,38]. Comparing these models with the present experimental data did not lead to consistent results (see Appendix II) and no firm conclusions could be drawn. The input parameters of the models are usually defined within a certain concept of acid-base interactions whereas several concepts may be interplaying. Furthermore, in many cases reliable experimental data are lacking so that the input parameters for the various acid-base models are uncertain. Moreover, acid-base models are fairly crude approximations of the reality for complicated systems.

Disjoining pressure isotherms of adsorbed films

In the literature, adsorbed films are often investigated in terms of the difference in chemical potential between the film and the corresponding bulk liquid. This difference is reflected in the disjoining pressure. According to its definition the disjoining pressure, $\Pi(h)$, can be expressed as [5]

$$\Pi(h) = - (dG(h)/dh)_{P, T} \tag{5}$$

The symbol $G(h)$ stands for the excess Gibbs energy of the film (per unit area) as a function of the film thickness h. The disjoining pressure can also be defined as the additional external pressure that is needed to keep a film of thickness h in mechanical equilibrium with its surroundings [5]

$$\Pi(h) = - \frac{RT}{V_m} ln(p/p_0) \tag{6}$$

where V_m is the molar volume of the bulk liquid. The disjoining pressure varies with p/p_0 and, hence, with the film thickness. The dependence of the disjoining pressure on the layer thickness is the disjoining pressure isotherm. It emphasises (in contradistinction to adsorption isotherms) the decay of the interactions with the film thickness.

Disjoining pressure isotherms on bare and methylated Aerosil OX-50 are calculated from the measured adsorption isotherms according to Eq. (6), assuming that the molecular volume in the adsorbed film equals that of bulk liquid. The resulting isotherms are plotted semilogarithmically in Fig. 7. This figure shows that, in general, the first part of the disjoining pressure isotherms on bare and methylated Aerosil OX-50 can be described by a short range exponential interaction of the form

$$\Pi_s = K e^{-h/l} \tag{7}$$

where K is a constant and l a characteristic decay length. The straight lines through the experimental points in Fig. 7 describe this short range exponential interaction with the parameters K and l given in Table 2. A comparison of the K values in Table 2 with the corresponding adsorption isotherms shows that the K value is a measure of the affinity of the adsorption: the larger its value the higher the affinity.

For the n-alkanes and cyclohexane on bare Aerosil OX-50, similar values of K and l apply. Compared to these values, the K value of toluene is higher whereas the decay length is comparable. For water l is considerably smaller than in the case of alkanes whereas K is much higher.

On methylated Aerosil OX-50, the K value of octane is not significantly different from that on bare Aerosil OX-50 whereas the decay length is considerably shorter. For cyclohexane the first experimental points (below 0.05 nm) are omitted since they may be due to an artefact (see results). The values of K and l for cyclohexane on methylated
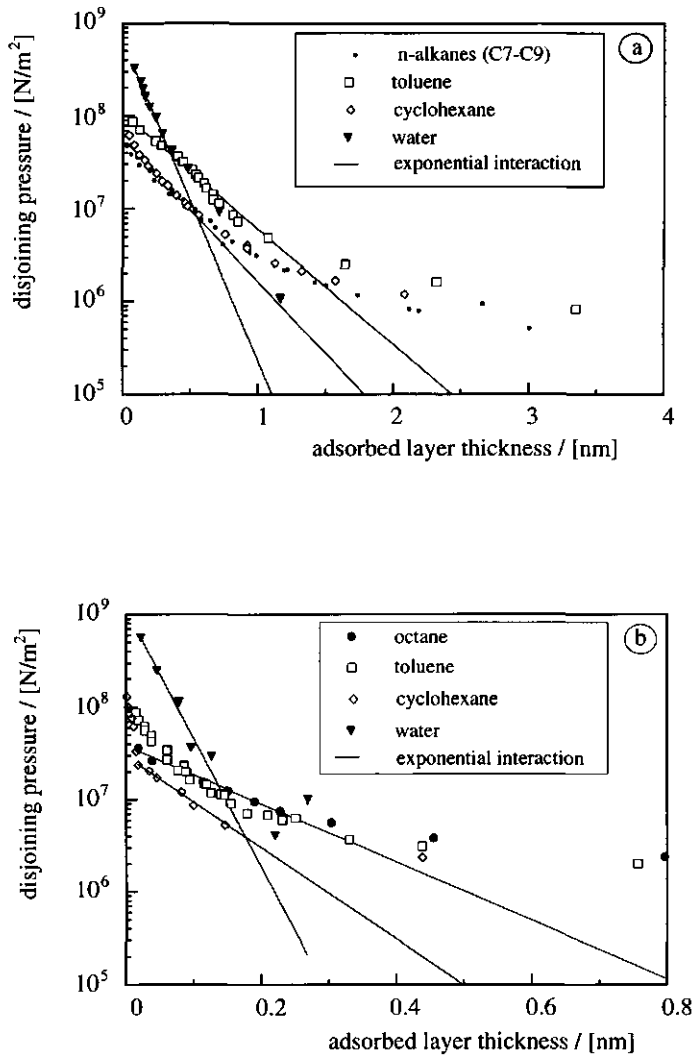
Fig. 7. Semilogarithmic disjoining pressure isotherms. The symbols are the experimental results, the solid curves are the exponential short range interaction according to Eq. (7), using the parameters shown in Table 2. (a) n-alkanes, cyclohexane, toluene and water on silica Aerosil OX-50. (b) octane, toluene, cyclohexane and water on methylated Aerosil OX-50.

Table 2. The parameters K and l that are used in Eq. (7) in order to describe the disjoining pressure isotherms that are shown in Fig. 8.

liquid	bare Aerosil OX-50		methylated Aerosil OX-50	
	K 10^7 N/m^2	l nm	K 10^7 N/m^2	l nm
n-alkanes & cyclohexane	5.7	0.28	–	–
n-octane	–	–	3.8	0.14
cyclohexane: $h > 0.02$ nm	–	–	2.9	0.088
toluene: all h	10.6	0.35	–	–
$h > 0.1$ nm	–	–	± 3.8	± 0.14
water	64.1	0.13	113.2	0.031

Aerosil OX-50 are smaller than those on bare silica. For thin (below 0.1 nm) toluene films on methylated silica the K value is rather high whereas a shorter decay length is found than for octane and cyclohexane. At film thicknesses beyond 0.1 nm the toluene parameters are comparable to those of octane.

In general it should be noted that the validity of Eq. (7) on the methylated silica extends over a shorter interval of film thicknesses as compared to bare Aerosil OX-50 (compare Figs. 7a and 7b). Moreover, the exponential short-range interactions observed here have a shorter decay length (l) than the interaction due to structural forces as calculated by Churaev and Derjaguin [37].

Anisotropic dispersion forces (of which the existence has been suggested by f. i. Fowkes [38]) occurring for oriented molecules (that are anisotropic in polarizability) might play a role in the occurrence of the exponential short range force. With respect to the exponential short range interaction observed here, we also refer to the work of Adamson [39, 40] who treated the adsorption of molecules onto a surface as a compression of vapour in the potential field of the solid surface. He described the van der Waals forces within the first few monolayers (of alkanes on teflon) by a short range exponential interaction instead of the standard inverse cube law.

Disjoining presure isotherms can also be calculated on the basis of interaction forces. In general, van der Waals- (Π_m), electrostatic-(Π_e) and structural- (Π_s) force contributions are distinghuished, assuming them to be additive [5]. However, in the range of thin (close to molecular size) film thicknesses the disjoining pressure may only be formally used and the equations used to calculate the different contributions to Π may be incorrect. By considering the disjoining pressure isotherm for the n-alkanes and cyclohexane, that are dominated by the van der Waals forces, we can easily show that

61
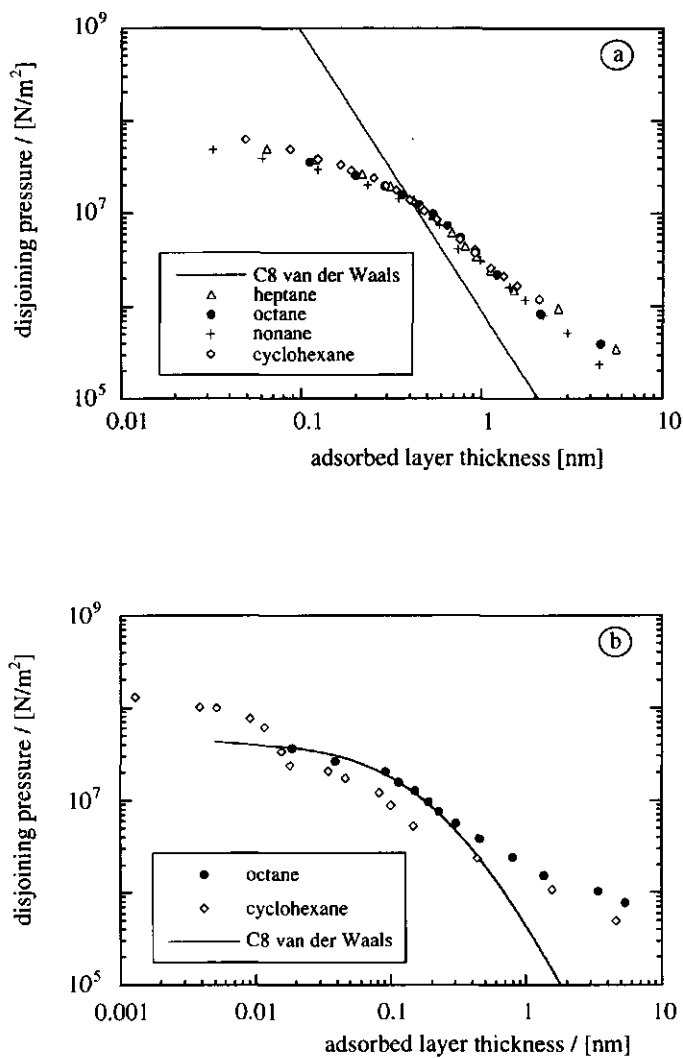
Fig. 8. Double logarithmic plot of the disjoining pressure, the symbols are the experimental results for the hydrocarbons, the curves are calculated theoretically. (a) Bare Aerosil OX-50, the line shown is calculated using Eq. (8a) with $A = -1.67 \ 10^{-20}$ J. (b) Disjoining pressures on methylated Aerosil OX-50. The drawn curve is calculated using Eq. (8b) with $A = -1.67 \ 10^{-20}$ J and $g = 0.27$ nm.

the classical description does not match with the thin films observed here. The classical equation for the van der Waals part relates Π_m to the Hamaker constant $A(h)$ according to

$$\Pi_m(h) = - \frac{A(h)}{6\pi h^3} \tag{8a}$$

The Hamaker constant can be derived from the Lifshits theory [41, 42], for $h \leq 12$ nm, $A(h)$ = constant. For octane on quartz the Hamaker constant equals $-1.67 \ 10^{-20}$ J (calculated theoretically [43]). This value is expected to apply also to n-heptane, n-nonane and cylohexane. On grafted surfaces the thickness (g) of the grafted layer can be taken into account according to

$$\Pi_m(h) = \frac{-A(h)}{6\pi(h+g)^3} \tag{8b}$$

The value of $A(h)$ in Eq. (8b) is assumed to be unaffected by the presence of the grafted layer (i.e., with respect to dispersive interactions, the grafted layer is considered comparable to the adsorbing liquid). The disjoining pressures for the n-alkanes and cyclohexane, calculated according to Eqs. (8a) and (8b), are plotted double logarithmically in Figs. 8a and 8b and compared to the experimental results. In a double logarithmic plot Eq. (8a) results in a straigth line, for Eq. (8b) a straigth line is obtained as soon as $h >> g$. The solid curve in Fig. 8b is obtained from Eq. (8b) using g=0.27 to fit the experimental results around $h = 0.1$ nm.

The comparison made in Figs. 8a and 8b shows that the experimental results for thin films cannot be described with the classical equations for the van der Waals contribution to Π. However, for adsorbed films formed near saturation (for $p/p_0 > 0.8$) this conclusion can not be drawn from the present experiment as interparticle condensation effects can not be excluded.

4.7. Conclusions

Adsorption isotherms of n-alkanes and cyclohexane (expressed in μmole/m^2) on bare SiO_2 are linear up to p/p_0=0.75. Within experimental accuracy, the n-alkane isotherms (of C7-9) on bare SiO_2 are independent of chain length. The toluene and water adsorption isotherms on SiO_2 have a knee and the molar adsorbed amounts found are higher compared to the alkanes.

Methylation of SiO_2 leads to a lowering of the adsorption of all adsorptives studied. The adsorption isotherms of octane, cyclohexane and toluene on methylated silica are linear up to p/p_0=0.7. Methylation of silica Aerosil OX-50 decreases γ_{LW}^s from 44 mJ/m^2 (for bare Aerosil OX-50) to 30 mJ/m^2.

The linearity of the isotherms points to weak or even absent lateral interactions. The chain length-independency of n-alkane adsorption on bare silica suggests that the adsorbed molecules are protruding in the gas phase. Until close to saturation, the

63

n-alkane adsorbed amounts on bare silica are below monolayer adsorption for perpendicularly oriented molecules, on methylated silica the adsorption lies below a monolayer of molecules oriented parallel to the surface. This suggests that on bare silica n-alkanes dominatingly adsorb end-on, perpendicular to the surface, whereas on methylated silica, parallel adsorption dominates.

Because of the chain architecture of the alkanes simple adsorption theories cannot describe their adsorption adequately. In Chapter 6 we will discuss the adsorption isotherms in more depth by comparing the experimental results with a self-consistent-field theory for the adsorption of chain molecules [26]. This theory also allows to investigate the wetting behaviour of chain molecule liquids.

For thin film thicknesses (i.e., below a few tenth of a nm) the disjoining pressure isotherms of apolar molecules on bare and methylated Aerosil OX-50 can be described in terms of a short-range exponentially decaying interaction. The ordinary macroscopic models are not very suited for the description of thin films, since the molecular organization and the discrete character of the adsorbed layer are extremely important. However, the gap between the continuum and discrete, molecular description of interactions can be bridged using, for instance, a self-consistent-field theory [26] for adsorption.

Appendix I

In a gravimetric experiment the magnitude of the buoyancy force varies with the vapour pressure p of the adsorptive and can be calculated from the difference in upthrust (Δw) between the two sides of the balance. Assuming ideality of the adsorptive gas, this difference can be calculated from the weight of the displaced fluid according to

$$\Delta w = \frac{M}{R} \, p \, (V_c/T_c \; - \; V_s/T_s) \tag{I.1}$$

where M is the relative molar mass of the adsorptive, R the gas constant, V_c and V_s indicate the volume of the bucket plus counterweights and the volume of the sample bucket plus sample, respectively, their temperatures being T_c and T_s. In principle, buoyancy can be eliminated by arranging that $V_c/T_c = V_s/T_s$ (this can be done by adjusting the volume of the counterweights). However, in practice this is not very convenient, it is more easy to admit a gas of negligible adsorption to the system and to plot the mass of the bucket as a function of the vapour pressure. From this plot $V_c/T_c - V_s/T_s$ can be determined by means of Eq. (I.1). Depending on the temperature, helium, argon or nitrogen are commonly used as calibrating gas [44]. The buoyancy correction follows from this calibration in combination with the molecular mass ratio of the adsorptive over the calibrating gas.

The effect of the buoyancy force in our gravimetric experiments has been measured using nitrogen as inert gas. Typically, the difference in upthrust was in the order of

0.4 µg per mbar (N_2) vapour pressure increase. This means that, for all adsorptives studied, the measured adsorbed mass is too low by an amount that corresponds to 0.014 µmol adsorptive for each mbar vapour pressure (increase). For a typical adsorption isotherm the substrate surface area equals roughly 2.5 m^2. This means that at saturation the adsorbed amounts measured for n-octane and water will be too low by 0.07 and 0.12 µmole/m^2, respectively. Therefore, the boyancy correction can be safely ignored compared to the change in the adsorbed mass.

Appendix II

Various theories describing acid-base interactions have been developed [45-47]. Fowkes [45] suggested to express the acid-base contribution to the work of adhesion $W_{A, AB}$ as

$$W_{A, AB} = -f n_{AB} \, \Delta(H_m)_{AB} = f n_{AB}(E_A E_B + C_A C_B) \qquad (\text{II.1})$$

where n_{AB} is the interfacial concentration of acid-base bonds (in mole/m^2), $\Delta(H_m)_{AB}$ is the molar enthalpy of acid-base complexation and f is an enthalpy-to-free-energy correction factor [48]. The enthalpy of acid-base complexation can be expressed in the Drago constants C_A, C_B, E_A and E_B (C and E representing the covalent and electrostatic contribution of the acid A or base B, in (kJ/mole)$^{1/2}$, to the adduct stability, respectively) [49]. Drago parameters for toluene are (to our knowledge) not available in literature. However, toluene is expected to behave, with respect to acid-base interaction capacity, similarly to benzene, for which the Drago constants are available. For silica the Drago constants are $E_A = 8.93$ and $C_A = 2.32$ for silica [50], for benzene $E_B = 0.75$ and $C_B = 1.8$ [51]. Taking f (arbitrary) equal to unity, we have $\Delta(H_m)_{AB} = -10.9$ kJ/mole. If $W_{A, AB}$ is considered equal to the $W_{A, n LW}$ value for silica-toluene of 25 mJ/m^2, the interfacial concentration of acid-base bonds is calculated to be about 1.4 acid-base bonds per nm^2. If only one acid-base bond is formed per toluene this corresponds to an occupied surface of 0.72 nm^2 per adsorbed toluene, consistent with a molecular area of about 0.48 nm^2 as measured for a flatly adsorbed toluene molecule [52].

Silica in water is negatively charged, which means that in this case the silica has an acidic character and water acts as a base. In Drago's studies only the acid character of water has been assessed [53] and no literature data on the Drago constants of water as a base could be found.

In another method, developed by Bolger and Michaels [46, 48], the Gibbs energy change per mole acid-base contact $\Delta(G_m)_{AB}$ and $W_{A, AB}$ is assessed from the iso-electric-point of the substrate (pH_{iep}) and minus the logarithm of the proton association or dissociation constants of the base or acid adhering to the surface. For silica interacting with a base we have

$$W_{A, AB} = n_{AB} \, (-\Delta(G_m)_{AB}) = n_{AB} \, 2.303 \, RT \, (pK_b - pH_{iep}) \qquad (\text{II.2})$$

Table I.1. The electron donor and acceptor components of the interfacial tension of laboratory and commercial silica and toluene and water (taken from Ref. [34]) that are used for the calculation of the acid-base component of the work of adhesion according to Eq. (II.3).

	γ_- [mJ/m^2]	γ_+ [mJ/m^2]
silica		
lab. SiO$_2$	43.7	2.4
com. SiO$_2$	62.4	0.13
water	25.5	25.5
toluene	2.7	0

For water acting as a base the proton association constant pK_b equals -1.7, the pH_{iep} of silica is roughly 3 (see also Chapter 3) so that $\Delta(G_m)_{AB}$ equals -26 kJ/mole. Assuming that the maximum value of $W_{A,\,nLW}$ for silica-water found in this study (170 mJ/m^2) roughly equals $W_{A,\,AB}$ would imply 3.9 acid-base contacts per nm^2. This value is close to the amount of silanols present at the surface of a fully hydroxylated and annealed silica and would suggest that the silica Aerosil OX-50 used is (at least partially) rehydroxylated. For silica-toluene a similar procedure can be followed (considering toluene as an acid!) leading to $\Delta(G_m)_{AB} = -198$ kJ/mole for silica-toluene so that, according to Eq. (II.2) with $W_{A,\,AB} = W_{A,\,nLW} = 25$ mJ/m^2, 0.08 acid-base contacts are formed per nm^2. The overestimation of $\Delta(G_m)_{AB}$ and underestimation of n_{AB} are likely due to the fact that the negative of the logarithm of the proton dissociation constant of toluene is very large [48]. Furthermore the acidic nature of toluene in presence of silica is questionable.

The acid-base contribution to the work of adhesion can also be expressed as [47]

$$W_{A,\,AB} = 2\sqrt{\gamma_+^L \, \gamma_-^S} + 2\sqrt{\gamma_-^L \, \gamma_+^S} \qquad (II.3)$$

with γ_-^L and γ_+^L are the electron donor component and the electron acceptor component of the interfacial tension of L respectively. Using the parameters given in Table I.1 the acid-base part of the work of adhesion for water on laboratory and commercial SiO$_2$ are 82.4 and 83.4 mJ/m^2 respecively, for toluene 5.1 and 1.2 mJ/m^2 respectively. The agreement with the experimentally found values for $W_{A,\,nLW}$ is not very good.

The different outcome of the various semi-empirical acid-base descriptions shows that the models describing acid-base interactions need further improvement. Furthermore, by setting $W_{A,\,AB} = W_{A,\,nLW}$, all molecular subtilities and long range electrostatic interactions are interpreted as acid-base interactions. This complicates (experimental) verification of acid-base models.

References

[1]   Wade, W. H. and Slutsky, L. J., *J. Chem. Phys.*, 40 (11), **1964**, p. 3394-3396.

[2]   Gee, L. M., Healy, T. W. and White, L. R., *J. Colloid Interface Sci.*, 131 (1), **1989**, p. 18.

[3]   Pashley, R. M. and Kitchener, J. A., *J. Colloid Interface Sci.*, 71 (3), **1979**, p. 491-500.

[4]   Beaglehole, D. and Christenson, H. K., *J. Phys. Chem.*, 96, **1992**, p. 3395.

[5]   Derjaguin, B. V., Churaev, N. V. and Muller, V. M., in *"Surface Forces"*; Consultants Bureau: New York, **1987**.

[6]   Levinson, P., Valignat, M. P., Fraysse, N., Cazabat, A. M. and Heslot, F., *Thin Solid Films*, 234 , **1993**, p. 482-485.

[7]   Hair, M. L. and Hertl, W., *J. Phys. Chem.*, 73 (12), **1969**, p. 4269-4276.

[8]   Fowkes, F. M., McCarthy, D. C. and Mostafa, M. A., *J. Colloid Interface Sci.*, 78 (1), **1980**, p. 200-206.

[9]   Armistead, C. G. and Hockey, J. A., *Trans. Faraday Soc.*, 67, **1964**, p. 2249-2556.

[10]   Hertl, W. and Hair, M. L., *J. Phys. Chem.*, 75 (14), **1971**, p. 2181-2185.

[11]   Nishioka, G. M. and Schramle, J. A., *J. Colloid Interface Sci.*, 105 (1), **1985**, p. 102-111.

[12]   Rouquerol, J. and Davy, L., *Thermochimica Acta*, 24, **1978**, p. 391-397.

[13]   Partyka, S. and Rouquerol, J., in *"Progress in Vacuum Microbalance Techniques"* (Vol. 3), Eyroud, C. and Escoubes, M. (Eds.), Heyden: London, **1975**: p. 83-92.

[14]   Gee, M. L., Healy, T. W. and White, L. R., *J. Colloid Interface Sci.*, 140 (2), **1990**, p. 450-465.

[15]   Whalen, J. W., *J. Phys. Chem*, 65, **1961**, p. 1676-1681.

[16]   Blake, T. D., Cayias, J. L., Wade, W. H. and Zerdecki, J. A., *J. Colloid Interface Sci.*, 37 (4), **1971**, p. 678-685.

[17]   Lyklema, J., in *"Fundamentals of Interface and Colloid Science"*; Academic Press Inc.: London, **1991**: Appendix 9.

[18]   Iler, R. K., in *"The Chemistry of Silica"*; John Wiley & Sons: New York, **1979**: p. 634.

[19]   Baker, F. S. and Sing, K. S. W., *J. Colloid Interface Sci.*, 55 (3), **1976**, p. 606-613.

[20]   Derjaguin, B. V., Zorin, Z. M., Churaev, N. V. and Shisin, V. A., in *"Wetting, Spreading and Adhesion"*, Padday, J. F. (Ed.), Academic Press: London, **1978**: p. 201-212.

[21]   Chibowski, E., Holysz, L., Kip, G. A. M., van Silfhout, A. and Busscher, H. J., *J. Colloid Interface Sci.*, 132 (1), **1989**, p. 54.

[22]   Gregg, S. J. and Sing, K. S. W., in *"Adsorption, Surface Area and Porosity"*; Academic Press Inc.: London, **1982**: p. 71.

[23]   Blake, T. D. and Wade, W. H., *J. Phys. Chem.*, 75 (12), **1971**, p. 1887-1892.

[24]   Fowkes, F. M., *J. Colloid Interface Sci.*, 28 (3/4), **1968**, p. 493-505.

[25]   Adamson, A. W., in *"Physical Chemistry of Surfaces"*; John Wiley & Sons: New York, **1976**: Chapter 14.

[26]   Scheutjens, J. M. H. M. and Fleer, G. J., *J. Phys. Chem.*, 83, **1979**, p. 1619-1635.

[27]   Zisman, W. A., in *"Contact Angle, Wettability, and Adhesion"*; Gould, R. F. (Ed.), Advances in Chemistry Series, Vol. 43: American Chemical Society, Washington, D. C., **1964**: p. 21.

[28]   Churaev, N. V. and Zorin, Z. M., *Adv. Coll. Int. Sci.*, 40, **1992**, p. 109-146.

[29]   Schlangen, L. J. M., Koopal, L. K., Cohen Stuart, M. A. and Lyklema, J., *Colloids Surfaces A*, 89, **1994**, p. 157-167; most of it is included as Chapter 2 in this thesis

[30]   Fowkes, F. M., *J. Adhesion Sci. Techn.*, 1 (1), **1987**, p. 7-27.

[31]   Mittal, K. L. (Ed.), *"Contact Angle, Wettability and Adhesion"*; VSP B.V., Utrecht, **1993**.

[32]   Fowkes, F. M., in *"Chemistry and Physics of Interfaces"*, Gushee, D. E. (Ed.), American Chemical Society: Washington, D. C., **1965**: p. 5-14.

[33]   Wojcik, W. and Bilinski, B., *Colloids Surfaces A*, 30, **1988**, p. 275-285.

[34]   Chibowski, E., in *"Contact Angle, Wettability and Adhesion"*, Mittal, K. L. (Ed.), VSP: Utrecht, **1993**: p. 641-662.

[35]   Wu, S., in *"Polymer Handbook"*, Brandrup, J. and Immergut, E. H. (Ed.), John Wiley & Sons: New York, **1989**: p. VI/411.

[36]   Fowkes, F. M., in *"Contact Angle, Wettability and Adhesion"*, Gould, R. F. (Ed.), American Chemical Society: Washington, D. C., **1964**: p. 99-111.

[37]   Churaev, N. V. and Derjaguin, B. V., *J. Colloid Interface Sci.*, 103 (2), **1985**, p. 542-553.

[38]   Fowkes, F. M., *J. Phys. Chem.*, 84 (5), **1980**, p. 510-512.

[39]   Adamson, A. W., *J. Colloid Interface Sci.*, 27 (2), **1968**, p. 180-187.

[40]   Adamson, A. W., *J. Colloid Interface Sci.*, 44 (2), **1973**, p. 273-281.

[41]   Hough, D. B. and White, L. R., *Adv. Colloid Int. Sci.*, 14, **1980**, p. 3-41.

[42]   Derjaguin, B. V., Churaev, N. V. and Rabinovich, Y. I., *Adv. Colloid Int. Sci.*, 28 , **1988**, p. 197-244.

[43]   Churaev, N. V., *Kolloidnyi Zhurnal*, 36 (2), **1974**, p. 323-327.

[44]   Gregg, S. J. and Sing, K. S. W., in *"Adsorption, Surface Area and Porosity"*; Academic press: London and New York, **1967**: p. 328.

[45]   Fowkes, F. M., in *"Adhesion and Adsorption of Polymers"*, Lee, L.-H. (Ed.), Plenum Publishing Corporation: New York, **1980**: p. 43-52.

[46]   Bolger, J. C. and Michaels, A. S., in *"Interfacial conversions"*, Weiss and Cheevers (Eds.), Elsevier: New York, **1969**.

[47]   van Oss, C. J., Chaudhury, M. K. and Good, R. J., *Adv. Colloid Interface Science*, 28, **1987**, p. 35-64.

[48]   Berg, J. C., in *"Wettability"*, Berg, J. C. (Ed.), Marcel Dekker Inc.: New York, **1993**: p. 101-107, 133-136.

[49]   Drago, R. S., Vogel, G. C. and Needham, T. E., *J. Am. Chem. Soc.*, 93, **1971**, p. 6014-6026.

[50]   Backstrom, K., Lindman, B. and Engstrom, S., *Langmuir*, 4 , **1988**, p. 872.

[51]   Fowkes, F. M., in *"Acid-Base Interactions"*, Mittal, K. L. and Andersom, H. R. (Eds.), VSP, The Netherlands: Utrecht, **1991**: p. 104.

[52]   Mc. Clellan, A. L. and Harnsberger, H. F., *J. Colloid Interface Sci.*, 23 (4), **1967**, p. 577-599.

[53]   Drago, R. S., Parr, L. B. and Chamberlain, C. S., *J. Am. Chem. Soc.*, 99 (10), **1977**, p. 3203-3209.

Chapter 5

A Lattice-Fluid Description of n-Alkanes: vapour-liquid properties, heat of vaporization, interfacial structure and surface tensions[*]

Abstract

A self-consistent-field (SCF) lattice theory for chain molecules in inhomogeneous systems is used to evaluate the physical and thermodynamic properties of fluids and fluid-fluid interfaces. The fluid is considered as a mixture of chain molecules and monomeric vacancies. Intermolecular interactions are described in terms of Flory-Huggins (FH) χ parameters. For the homologous series of linear alkanes, these parameters are assessed from a fit to vapour pressure data. Each carbon atom of the linear alkane is considered as a segment with a volume of 0.027 nm^3. The χ value of a segment-vacancy contact reflects the segment-segment interaction, for which χ equals zero by definition, and is taken inversely proportional to the temperature T in K according to 580/T. With these parameters n-alkane bulk properties such as vapour pressures, density and heat of vaporization can be obtained together with structural and thermodynamic properties of the liquid-vapour (LV) interface. The calculated volume fraction profiles of the LV interfacial region reveal that chain ends are the major constituents on the vapour side of the interface. For longer chains and lower temperatures the relative preference of the chain ends to protrude into the vapour phase is more pronounced. The calculated variation of the n-alkane LV interfacial tension (γ) with temperature agrees quantitatively with experimental data. At temperatures close to 0 K, the theory predicts the occurence of positive $d\gamma/dT$ values. The trend in the LV interfacial tension of n-alkanes with increasing molecular weight is also correctly predicted by the theory.

5.1. Introduction

A profound knowledge of the structure and thermodynamic properties of interfaces (e.g. surface and interfacial tensions) contributes to a better understanding and prediction of cohesion-, adhesion- and wetting phenomena. In many practical applications chain molecules are an important constituent of interfacial regions and there is a need for a theory capable of describing the properties of such interfaces. Lattice theories, demanding relatively low computational cost, are useful for this aim. They have been applied quite succesfully to investigate a wide variety of systems such as fluid mixtures

---

[*] This chapter has been submitted for publication in *J. Phys. Chem.*

and interfaces [1], polymeric melts, polymeric solutions and polymer adsorption [2], solid-fluid interfaces and polymeric brushes [3], lipid bilayers [4] and surfactant behaviour [5, 6]. This list of different applications indicates that lattice theories provide a versatile theoretical framework for the description of both bulk and interfacial properties of chain molecules.

A large part of lattice theory studies concentrates on polymer-containing solutions or polymer melts [3]. The description of gaseous phases by lattice theories has recieved less attention [7, 8]. Liquid-vapour interfaces are sometimes investigated while neglecting the presence of molecules in the vapour phase [9] but such approaches are not rigourous. A consistent description requires a theory in which both bulk-liquid and -vapour are taken into account.

The liquid-vapour (phase) behaviour of hydrocarbons is well studied as it is of particular importance to the petrochemical industry. Monte Carlo simulations of n-alkanes yield phase diagrams [10] and heats of vaporization [11] that are in good agreement with experimental data. Such simulations also provide a useful model for the determination of the critical properties of long chain alkanes [10, 12]. Monte Carlo (or molecular dynamics) simulations are also able to describe the molecular sturcture of polymer melt-gas interfaces [13]. However, they are less suited to investigate the interfacial thermodynamics of these systems.

In the present paper a self-consistent-field (SCF) theory, originally developed by Scheutjens and Fleer [14, 15] and generalized by Evers et al. [16] is used as a lattice fluid (LF) theory. This SCF-LF theory is capable to describe both the thermodynamic and structural properties of chain molecules at liquid-vapour (LV) interfaces. Furthermore, it also describes bulk liquid and vapour properties of chain molecules with the same set of input parameters.

In the SCF-LF theory, chain-molecular fluids are described as a binary mixure of chain-molecules (alkanes) and free volume entities, the vacancies. The parameters needed follow from the temperature dependence of the vapour pressure. The critical temperatures, fluid densities, heats of vaporization and interfacial tensions of chain molecules will be investigated with the theory. Furthermore, the temperature dependence of the heat of vaporization, the structure of the LV interface and its interfacial tension will be investigated and compared to experimental data.

The SCF-LF approach can be extended to investigate fluids of complicated molecular architecture (e.g., long, branched or cyclic hydrocarbons) and their mixtures. In addition, adsorption can be easily studied within the SCF-LF theory. Hence, the n-alkane description presented here is a first step on the way to investigate vapour adsorption and wetting on solid surfaces.

5.2. Self consistent field theory for chain molecules in inhomogeneous systems

General

The lattice theory of Scheutjens and Fleer [14, 15] was originally developed to describe the equilibrium adsorption of systems containing long flexible chain molecules. By restricting the molecules on a lattice the probabilities of all conformations can be evaluated relatively easily. Lattice theories can describe fluids as a mixture of empty sites, the vacancies, and the fluid molecules. In the theory, each molecule consists of a chain of segments. The individual segments experience a potential energy that depends on their average surrounding by other segments. Using Boltzmann statistics, the segment volume fractions can be calculated from the potential energies. However, the segment volume fractions, in turn, determine the segment potential energies. Therefore, numerical methods are applied to find the self-consistent potential energy field and the corresponding equilibrium segment density profiles. The final volume fraction profiles describe the set of conformations for every type of molecule that corresponds to the minimum Helmholtz energy of the system.

In the SCF theory of Scheutjens and Fleer there is always one component (often denoted solvent) that is considered to fill all lattice sites of the system that are not already occupied by the other component(s). The SCF theory can be used as a statistical thermodynamic lattice fluid theory in which vacancies may be included as the space filling component. Scheutjens and Kijlstra [17] were the first to include free volume in the SCF theory and explored the possibility of using the SCF theory as a lattice fluid theory.

Segment density distribution

In the SCF theory it is assumed that each segment exactly fills one lattice site. The lattice consists of M parallel lattice layers numbered $z = 1...M$ each with lattice spacing (i.e., the lattice layer thickness) l. Each lattice layer contains L lattice sites. The lattice boundary conditions of the system are of key importance. At a reflecting boundary, the distribution functions and volume fractions in the layers outside the system equal those of the layers inside the system if the layers are equidistant with respect to the reflecting boundary. If reflecting conditions are imposed on both lattice boundaries, fluid-fluid or gas-liquid interfaces, can be investigated. The system then has to be large enough so that bulk properties have been reached within the limits of the lattice boundaries.

The density (or volume fraction) of the segments is considered to be uniform within each lattice layer but variable in the z direction. A flexible chain molecule has an

71

integer number of segments of type(s) x and/or y. Each type of molecule present in the system (i.e., the molecular components) is denoted by an index i, vacancies are distinghuished by the index o. The total length of the chain molecule is detemined by the number (N_i) of segments it contains. The volume fraction of segment x in layer z is indicated as $\phi_x(z)$.

The various segments interact with each other, with the vacancies (or solvent) and with the adjoining phase (e.g. the surface, if present). The interaction of segment x with segment y is given by the Flory-Huggins contact interaction parameter χ_{xy} (expressed in units of kT). The potential energy (with respect to that in the bulk solution) of a free segment x in layer z, $u_x(z)$, is given by [18]

$$u_x(z) = u'(z) + kT \sum_y \chi_{xy} (< \phi_y(z) > - \phi_y^b) \tag{1}$$

The potential energy $u'(z)$ is independent of the segment type and accounts for the fact that the sum of all volume fractions in layer z should equal unity (i.e., the lattice is completely filled). The volume fraction of segment y in the bulk is denoted ϕ_y^b. The summation term in Eq. (1) accounts for the contact energies of segment x with its nearest neighbours. The number of contacts of a segment x, in layer z, with segment y are considered to be proportional to the volume fractions of y in the same and adjacent lattice layers (z, $z-1$ and $z+1$). The "contact-averaged" volume fraction $< \phi_y(z) >$ is given by

$$< \phi_y(z) > = \lambda_{-1} \phi_y(z-1) + \lambda_0 \phi_y(z) + \lambda_{+1} \phi_y(z+1) \tag{2}$$

where λ_0 is the fraction of contacts within the layer z, λ_{-1} and λ_{+1} denote the fractions of contacts in the layers $z-1$ and $z+1$ respectively. The values of λ_0, λ_{-1} and λ_{+1} depend on the type of lattice used. In general, the contact fractions only affect the results quantitatively, without affecting qualitative features. In the interfacial region, however, lattice artefacts may appear. These artefacts are minimal when λ_0, λ_{-1} and λ_{+1} in Eq. (2) are put equal to $1/3$.

The conformational statistics of the chain molecules in the lattice are evaluated using a weighted chain extension procedure that adds, one by one, segments to the chain. The probability of each chain extension with a segment x is weighted with a (Boltzmann-like) segment weighting factor $G_x(z)$ defined as

$$G_x(z) = exp (-u_x(z)/kT) \tag{3}$$

The product of the appropriate segment weighting factors of all the chain segments of a molecule determines the molecular volume fraction. In this multiplication the

connectivity of the chain molecule has to be taken into account. For this goal the chain statistics have to be evaluated.

Chain conformation: first order Markov statistics

A detailed and generalized derivation of the SCF theory for first-order-Markov statistics can be found in [16], here its main principles are resumed. Consider a flexible molecule i of chain length N, built of segments with ranking number s and end segments $s=1$ and $s=N$. In order to facilitate the counting of conformations of such a molecule, it is customary to divide the chain molecule into two chain fragments with their corresponding distribution functions.

The weighting factor of a chain molecule (fragment) i with segment s in layer z under the condition that segment s is linked by a chain of segments to segment s' somewhere in the system will be denoted as $G_i(z, s \mid s') = \sum_{z'} G_i(z, s \mid z', s')$, where the sum is over all possible starting positions z'. Likewise, $G_i(z, s \mid 1)$ is the weighting factor of an s-mer of which the position of the first segment is free and its last segment s localized in layer z, $G_i(z, s \mid N_i)$ is the distribution function for an $(N_i - s + 1)$-mer with its last segment s in layer z and its first segment N_i free. The distribution functions of these two end fragments of a free chain are generated by "growing" the chain fragments by means of recurrence relations. One chain is generated from segment 1 to s, Eq. (4a), the other from segment N_i to s, Eq. (4b).

$$G_i(z, s \mid 1) = G_i(z, s) < G_i(z, s - 1 \mid 1) > \tag{4a}$$

$$G_i(z, s \mid N_i) = G_i(z, s) < G_i(z, s + 1 \mid N_i) > \tag{4b}$$

The brackets $<>$ denote "contact-averaged" distribution functions for the three possible values of z, according to

$$< G_i(z, s - 1 \mid 1) > = \lambda_{-1} G_i(z - 1, s - 1 \mid 1) + \lambda_0 G_i(z, s - 1 \mid 1) + \lambda_{+1} G_i(z + 1, s - 1 \mid 1) \tag{5}$$

and likewise for $< G_i(z, s + 1 \mid N_i) >$. If segment s of molecule i is of type x then $G_i(z, s) = G_x(z)$.

The distribution functions of the chain fragments in Eqs. (4a) and (4b) are generated starting from free segments, $s=1$ and $s=N_i$ respectively, according to

$$\begin{aligned} G_i(z, 1 \mid 1) &= G_i(z, s) \\ G_i(z, N_i \mid N_i) &= G_i(z, s) \end{aligned} \qquad \forall z \tag{6}$$

The distribution functions (4a) and (4b) determine the distribution function $G_i(z, s \mid 1; N_i)$ of chain molecule segment s in layer z provided segment s is part of a chain molecule with the first segment and the last (N_ith) segment anywhere in the system. The segment volume fraction $\phi_i(z, s \mid 1; N_i)$ of s in z now follows from

$$\phi_i(z, s \mid 1; N_i) = C_i \, G_i(z, s \mid 1; N_i) = C_i \, \frac{G_i(z, s \mid 1) \, G_i(z, s \mid N_i)}{G_i(z, s)} \tag{7}$$

where C_i is a normalisation constant. In order to prevent double counting of the linking segment s (present in both chain end fragments), the product of both chain end point distribution functions is divided by the free segment weighting factor of s in layer z. The normalisation constant follows from the total amount of segments of component i θ_i in the system according to

$$\theta_i = \sum_{s=1}^{N} \sum_{z=1}^{M} \phi_i(z, s \mid 1; N_i) \tag{8}$$

For component i with chain length N_i, Eqs. (7) and (8) can be combined to

$$C_i = \frac{\theta_i}{N_i \sum_z G_i(z, N_i \mid 1)} = \frac{\theta_i}{N_i \, G_i(N_i \mid 1)} \tag{9}$$

If not θ_i, but the volume fraction in the bulk ϕ_i^b is kept constant the normalisation constant follows from

$$C_i = \frac{\phi_i^b}{N_i} \tag{10}$$

The segment density profiles in layer z follow from a summation over all possible values of s within a chain molecule of chain lenght N_i.

$$\phi_i(z) = \sum_{s=1}^{N} \phi_i(z, s \mid 1; N_i) \tag{11}$$

The SCF theory can also be applied to branched chains (i.e., chains with more than two chain fragments linked to one segment s) [4].

Once the self-consistent equilibrium volume fraction profile and the correponding potential energy field are found, the partition function can be evaluated so that the mechanical (e.g. pressure and energy) and thermodynamic properties (e.g. enthalpies, interfacial tensions and chemical potentials) of the system can be derived [4].

Thermodynamic relations and the SCF-LF theory

According to thermodynamics the differential of the Helmholtz energy F of a system consisting of two homogeneous bulk phases separated by a flat interface reads

$$dF = -S\,dT - p\,dV + \gamma\,dA + \sum_i \mu_i\,dn_i \tag{12}$$

where S is the entropy, T the temperature, p the pressure and V the volume of the system, γ and A are the interfacial tension and the area of the interface, respectively, μ_i is the chemical potential of molecule i and n_i denotes the number of molecules i present in the system. The index i runs over all types of molecules present in the system.

According to Eq. (12) the pressure is given by

$$p = -(\partial F/\partial V)_{T,\,A,\,\{n_i\}} \tag{13}$$

In a lattice fluid system, free volume is accounted for by means of vacancies. The volume in a lattice fluid system is given by the sum of the volumes of all lattice sites that are either occupied by molecule segments or monomeric vacancies according to

$$V = v \sum_k n_k N_k = M L \tag{14a}$$

where v is the volume of a lattice site and the index k runs over all components $\{k\}$ (i.e., the molecules $\{i\}$ and vacancies o) present in the system. The lattice site volume is defined by the lattice spacing and the type of lattice used. In the lattice fluid model v and N_k are constants and we have

$$dV = v \sum_k N_k\,dn_k \tag{14b}$$

The only way in which V of a lattice fluid system can change at constant T, A and $\{n_i\}$ is by adding or withdrawing vacancies, therefore, $(dV)_{T,\,A,\,\{n_i\}}$ is equal to $(dV)_{T,\,A,\,\{n_{k\neq o}\}} = v\,dn_o$. Hence, Eq. (13) can be rewritten as

$$p = -\frac{1}{v}(\partial F/\partial n_o)_{T,\,A,\,\{n_{k\neq o}\}} = -\tilde{\mu}_o/v \tag{15a}$$

where $\tilde{\mu}_k = (\partial F/\partial n_k)_{T,\,A,\,\{n_{k'\neq k}\}}$, or, alternatively,

$$-p\,dV = \tilde{\mu}_o\,dn_o \tag{15b}$$

This means that for a lattice fluid system, Eq. (12) reduces to

$$dF = -S\,dT + \gamma\,dA + (\partial F/\partial n_o)_{T, A, \{n_{k\neq o}\}}\,dn_o + \sum_{k\neq o}(\partial F/\partial n_k)_{T, A, \{n_{k'\neq k}\}}\,dn_k$$

$$= -S\,dT + \gamma\,dA + \sum_k \bar{\mu}_k\,dn_k \tag{16}$$

Note that the equality $\sum_{k\neq o} \bar{\mu}_k\,dn_k = \sum_i \mu_i\,dn_i$ following from Eqs. (12), (15b) and (16) does not neccessarily imply that $\bar{\mu}_k$ equals μ_i, see also Eq. (21).

According to statistical thermodynamics, the characteristic function of the grand canonical partition function $\Xi(\{\bar{\mu}_k\}, M, L, T)$ equals

$$-kT\;\ln\,\Xi(\{\bar{\mu}_k\}, M, L, T) = -kT\;\ln\,\Omega(\{n_k\}, M, L, \tilde{U}) + \tilde{U} - \sum_k \bar{\mu}_k\,n_k$$

$$= \gamma A \tag{17}$$

where $\Omega(\{n_k\}, M, L, \tilde{U})$ is the micro canonical partition function and the energy $\tilde{U} = TS + \gamma A + \sum_k \bar{\mu}_k\,n_k$. Within the SCF theory Eq. (17) can be evaluated according to [16]

$$\gamma a/kT = \gamma A/L\,kT$$

$$= -\sum_k \theta_k^{exc}/N_k - \sum_z u'(z)/kT - \frac{1}{2}\sum_z \sum_A \sum_B \chi_{AB}(\phi_A(z) < \phi_B(z) > - \phi_A^b\,\phi_B^b) \tag{18}$$

where a is the lattice cell area, $\theta_k^{exc} = \theta_k - M\,\phi_k^b$ and ϕ_k^b is the bulk volume fraction of the segment type (A or B) or component (k) denoted by the subscript.

According to Eq. (12), the chemical potential μ_j is defined as the change in Helmholtz energy upon the addition of one molecule j to a macroscopic system, without changing T, V, A and $\{n_{i\neq j}\}$ of the system

$$\mu_j \equiv (\partial F/\partial n_j)_{T, V, A, \{n_{i\neq j}\}} \tag{19}$$

In the lattice fluid theory (free) volume is treated as a component, and the condition of constant V in Eq. (19) has to be restated in terms of the composition of the system. According to the generalized chain rule we have

$$(\partial F/\partial n_j)_{T, A, V, \{n_{i\neq j}\}} = (\partial F/\partial n_j)_{T, A, \{n_{i\neq j}\}, n_o} + (\partial F/\partial n_o)_{T, A, \{n_i\}}\,(\partial n_o/\partial n_j)_{T, A, \{n_{i\neq j}\}, V} \tag{20}$$

The subsripts i and j are used to denote the type of the molecular component whereas the vacancies are denoted by o. In a lattice fluid system constant T, A, V and $\{n_{i\neq j}\}$ imply that $(\partial n_o/\partial n_j)_{T, A, \{n_{i\neq j}\}, V} = -N_j$. Hence, equation (20) can be rewritten as

$$\mu_j = \bar{\mu}_j - N_j\,\bar{\mu}_o \tag{21}$$

Note that Equation (21) only applies to molecular components j.

In a lattice fluid theory a liquid-vapour system is considered as a binary mixture of molecules i (containing segments A only) and monomeric vacancies o. In such a binary mixture the partial Helmholtz energy of a vacancy equals, according to FH theory (Ref. [2] p. 511),

$$\tilde{\mu}_o = kT \left(\ln \phi_o^b + (1 - 1/N_i) \phi_i^b + \chi_{Ao} (\phi_i^b)^2 \right) \tag{22}$$

Equations (22) and (15a) can be combined to find the expression for p

$$p = - \frac{kT}{v} \left(\ln \phi_o^b + (1 - 1/N_i) \phi_i^b + \chi_{Ao} (\phi_i^b)^2 \right) \tag{23}$$

The interactions in the lattice fluid are accounted for by FH contact interaction parameters χ_{xy}. The FH parameters are related to the the pair contact energies ε_{xy} (in J) between the segment types denoted by the subscipts according to

$$\chi_{xy} = Z (2\varepsilon_{xy} - \varepsilon_{xx} - \varepsilon_{yy}) / 2kT \tag{24}$$

where Z is the coordination number. According to Eq. (24), the FH interaction parameter for identical segments equals zero. In a binary mixture of aliphatic chain molecules (consisting of segments A) and vacancies (o) there is only one non-zero interaction parameter, χ_{Ao}. By definition, the contact energy for a contact in which a vacancy is involved equals zero. Hence, χ_{Ao} is directly related to the contact energy between two A segments as

$$\chi_{Ao} = - Z \varepsilon_{AA} / 2kT . \tag{25a}$$

As identical molecule segments attract each other ε_{AA} is negative and χ_{Ao} is positive. In the FH theory, χ is considered as purely enthalpic, i.e., its (absolute) magnitude is independent of temperature. Hence, one may write

$$\chi_{Ao} = c_2/T \tag{25b}$$

where c_2 (expressed in K) is a constant equal to $- Z \varepsilon_{AA} / 2 k$.

The above expressions for the bulk parameters illustrate how the SCF-LF theory can be used to assess fluid properties. When necessary, a further elaboration of the theory will be presented in the results section. To be able to describe the properties of n-alkanes, the values of the chain length, segment-vacancy interaction and lattice cell volume have to be determined. In the results section reliable estimates for these parameters will be obtained.

5.3. Results

SCF-LF parameters for n-alkanes

For the shorter n-alkanes, experimental data on the pressure at the critical point are available. Above the critical point phase separation is no longer possible. For a homopolymer in a binary mixture of chain molecules and monomers, the FH segment-vacancy interaction at the critical point equals (Ref. [2] p. 544)

$$(\chi_{AO})_c = \tfrac{1}{2}(1 + 1/\sqrt{N_i})^2 \tag{26}$$

and the bulk molecular volume fraction of the lattice fluid

$$(\phi_i^b)_c = 1/(1 + \sqrt{N_i}) \tag{27}$$

where the subscript c denotes the lattice fluid critical point. For $\chi_{AO} > (\chi_{AO})_c$ phase separation occurs. Substitution of $(\chi_{AO})_c$ and $(\phi_i^b)_c$ in Eq. (23) shows that the pressure at the critical point is solely determined by the chain length and the lattice cell volume. The critical temperature is found by combining Eqs. (26) and (25b).

As a first approximation v is estimated from the density $\rho_{L,i}$ and molar mass $M_{w,i}$ of liquid i according to $v \approx M_{w,i}/\rho_{L,i} N_A N_i$ where N_A stands for Avogadro's number. The chain length N_i of the lattice fluid molecules is related to the number of carbon atoms C_n of the n-alkane under consideration. According to Eqs. (25b) and (26) the value of c_2 can be calculated directly from the (experimental) critical temperature and $(\chi_{AO})_c$.

In Fig. 1 some lattice fluid results that match the experimental data fairly well are shown. The critical pressure decreases with increasing chain length of the n-alkane. The best agreement with the experimental critical pressures of the different n-alkanes is obtained for chain lengths N_i slightly larger than C_n. For chain lengths equal to or below C_n the critical pressure is overestimated. For larger chain lengths the agreement improves and for $N_i = C_n + 2$ the theoretical critical pressures matches the experimental values very well.

Figure 2 shows the c_2 values corresponding to five choices of the chain lengths N_i. For all choices of N_i, the magnitude of c_2 is alkane chain length dependent. In the lattice fluid theory the n-alkanes are modelled as chains consisting of one and the same type of segment. In the FH theory, identical segments have identical interaction parameters, and for a consistent description c_2 should be independent of the length of the n-alkane. Hence, the present choice for the chain length is not yet entirely satisfactory.
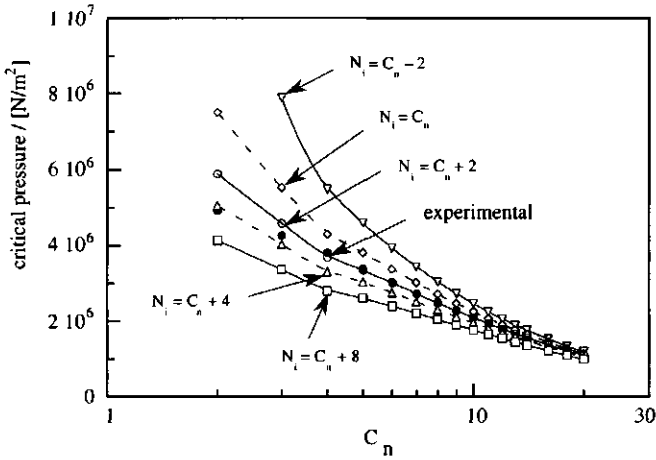
Figure 1. The critical pressure of various n-alkanes as a function of chain length, plotted on a semi-logarithmic scale. Lattice fluid results (curves through open points) compared to experimental data (solid circles) [19].
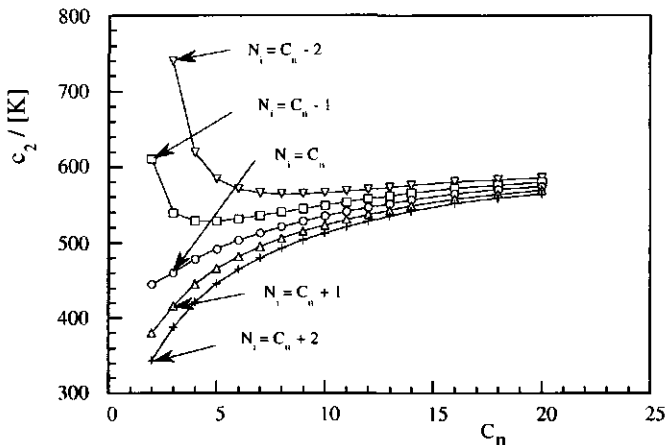

Figure 2. The molecule segment-vacancy contact interaction parameter c_2 that matches the experimental critical temperature [19] and Eq. (26) through Eq. (25b). Different choices of N_i are made to describe the n-alkanes.

79

An alternative way to assess a general set of lattice fluid parameters describing the n-alkanes is through the (saturated) vapour pressure as a function of temperature, see Refs. [20, 21] for experimental data. Equations (23) and (25b) define the temperature dependence of the lattice fluid pressure. The lattice cell volume follows from the molar mass M_i of component i, its density $\rho_i(T)$ and molecular bulk volume fraction $\phi_i^b(T)$ at temperature T according to

$$v = \frac{M_i \, \phi_i^b(T)}{N_i \, \rho_i(T) \, N_A} \tag{28}$$

According to Eqs. (25b) and (28) the lattice cell volume is defined by the volume fractions ϕ_i^b that, in turn, depend on χ_{Ao}. In order to assess χ_{Ao} or c_2 from experimental vapour pressure data, a numerical least square procedure is used. In this procedure, the lattice cell volume used is taken to be independent of temperature and determined by Eq. (28) and the liquid density at 293.15 K.

The outcome of the numerical procedure for each alkane depends on the chain lengths assigned to N_i. We substituted those values that agreed best with the critical pressures (see Fig. 1). The use of Eq. (28) in the numerical procedure resulted in lattice cell volumes that are n-alkane dependent. For a general lattice fluid description of the n-alkanes, the partial molecular volume of the latttice fluid should be defined by the chain length only. Therefore, it is preferable to set the lattice cell volume of all n-alkanes at a constant value. A volume of 0.027 nm^3 for a CH_2 group is a reasonable choice. Using this constant (n-alkane independent) v in the numerical procedure instead of Eq. (28), hardly affects the accuracy and c_2 values with which the experimental vapour pressures are described. For various relations between N_i and C_n, the resulting c_2 values of the n-alkanes up to $C_n=25$, are shown in Fig. 3. According to Fig. 3 the c_2 value (for $v = 0.027$ nm^3) approaches a rather constant value of about 580 if N_i equals C_n. The present choice of (general) n-alkane parameters is quite satisfactory and summarized in Table 1, in which a denotes the lattice cell area. The a value given in the Table corresponds to an (FCC) lattice cell volume of 0.027 nm^3. Also included in the Table are the lattice cell volume and the lattice-fluid critical temperature T_c, the latter is obtained by equating Eqs. (25b) and (26). In the next sections, the SCF-LF theory is used to predict several bulk and interfacial properties of the n-alkanes with the parameters shown in Table 1.
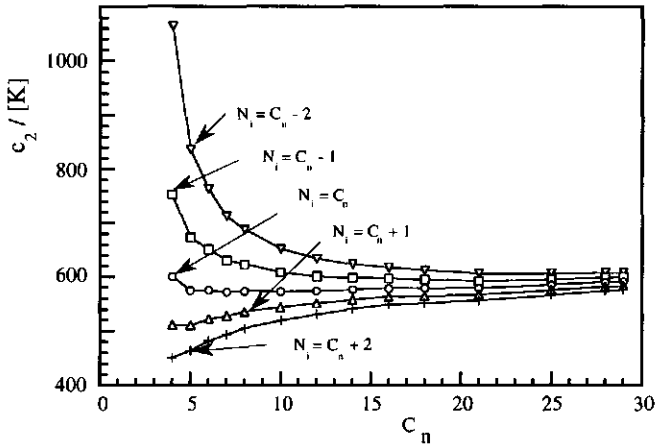
Figure 3. The molecule segment-vacancy contact interaction parameter c_2 obtained from the numerical procedure for $v = 0.027$ nm^3. Different choices of N_i are made to describe the n-alkanes.

Table 1. Parameter choice for the description of n-alkanes with the SCF lattice fluid theory. The critical temperature within the SCF-LF theory is also given.

χ_{AO}	[kT]	$580/T$
N_i		C_n
v	[nm^3]	0.027
a	[nm^2]	0.09
T_c	[K]	$\dfrac{1160}{(1 + 1/\sqrt{N_i})^2}$

81

Bulk properties of n-alkanes

Vapour pressures

For n-octane and n-hexadecane, the calculated vapour pressures (using the parameters in Table 1 are compared to the experimental data in Fig. 4.
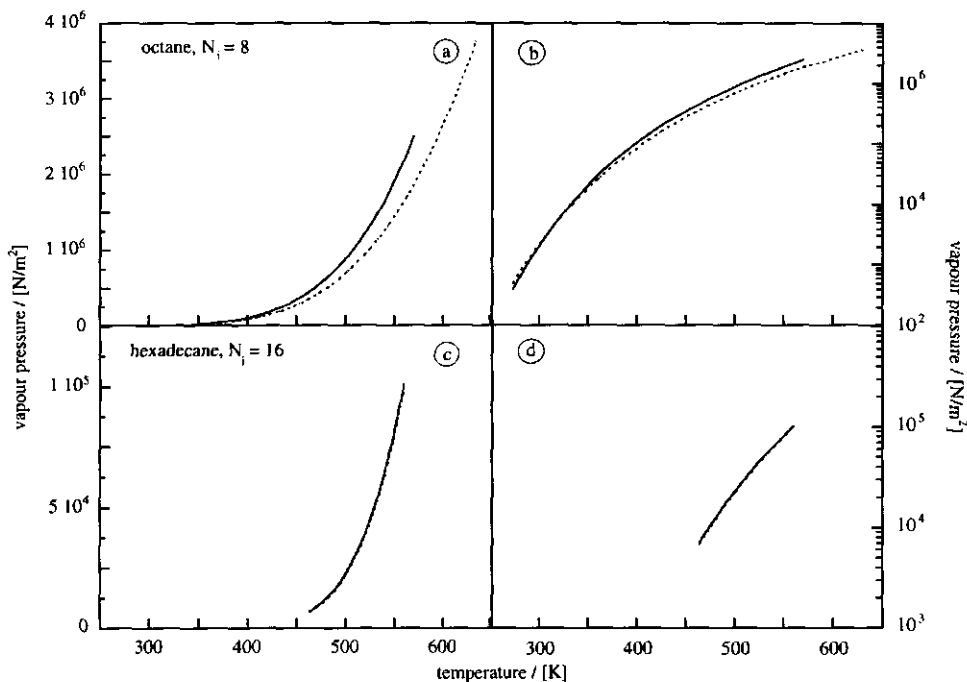
Figure 4. Saturated vapour pressures of n-octane (a and b) and n-hexadecane (c and d). The solid curves are experimental results [20, 21], dashed curves are calculated. In panels (a) and (c) the pressure is plotted on a linear scale; in panels (b) and (d) a logarithmic pressure scale is used.

Figure 4 demonstrates that the lattice fluid theory is able to reproduce, at least semiquatitatively, the temperature dependence of the n-alkane vapour pressures. For long n-alkanes the agreement is excellent. For short n-alkanes the lattice fluid theory underestimates the vapour pressure, especially at more elevated temperatures. For $N_i = 8$, the dotted curve covers a larger temperature range than the solid curve. This implies that the calculated critical temperature is slightly overestimated. For longer chains the agreement between the calculated and experimental pressures improves.
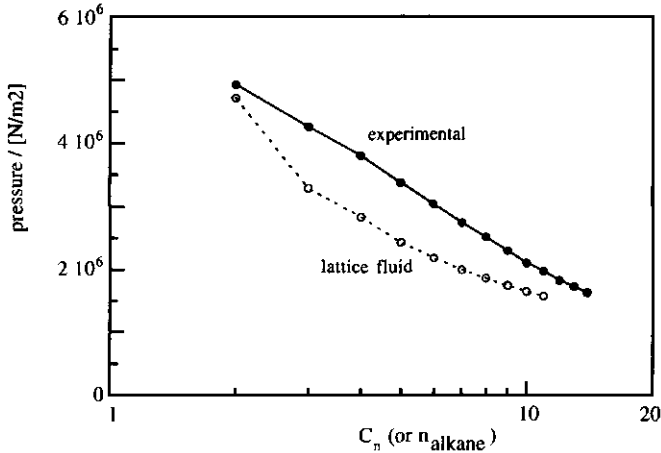
Figure 5. The lattice fluid pressures (the open circles) at the experimental critical temperature (calculated using the perameters shown in Table 1) compared to the experimental critical pressure (the solid circles) of various n-alkanes [19].

Critical point

In Fig. 5 the lattice fluid pressure (using the parameters in Table 1) at the experimental critical temperature of the different n-alkanes is calculated and compared to the critical pressure. At the (experimental) critical temperature the calculated pressure aproaches the experimental critical pressure. For chain lengths above 12 the theory is unable to calculate the volume fractions accurately (the value of χ_{Ao} according to Eq. (25b) approaches $(\chi_{Ao})_c$).

As noted in relation to Fig. 4, the critical temperature within the lattice fluid theory does not correspond precisely to the experimental value. In Fig. 6 the two are compared. For infinitely large chains, the critical temperature of the lattice fluid (using $c_2 = 580$) attains a plateau value of 1160 K. Especially for the shorter n-alkanes the critical temperatures are overestimated by the lattice fluid theory. For larger n-alkanes the agreement is again quite good. The extends of correspondence between theory and experiment indicate the over-all accuracy of the choices made with respect to the lattice theory and its parameter values.

Liquid and vapour densities

In the theory, both the liquid and vapour density as a function of temperature follow from the volume fractions of the coexisting phases according to Eq. (28). For n-octane volume fractions and densities are calculated functions of the temperature. The
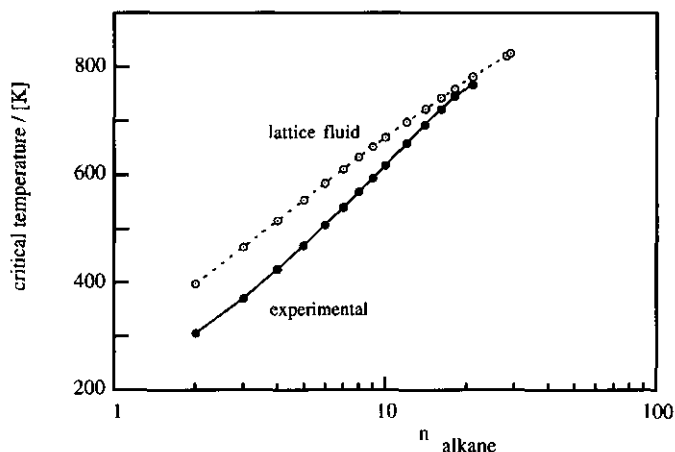
Figure 6. The critical temperatures of various n-alkanes. The experimental results [19] (solid circles) are compared to the values of the lattice fluid (dashed circles) obtained using the parameters shown in Table 1.

theoretical critical temperature of an octamer is 633 K, the experimental critical temperature of octane equals 569 K. In Fig. 7 the calculated densities of the octameric fluid are shown and compared to the experimental data of n-octane. In panel a), the density is plotted on a linear scale, in panel b) semi-logarithmically. Figure 7 shows that the lattice fluid theory adequately describes both the liquid and vapour densities. Close to the critical point the liquid density is underestimated by the lattice fluid theory; otherwise, the fluid density is somewhat overestimated by the theory.
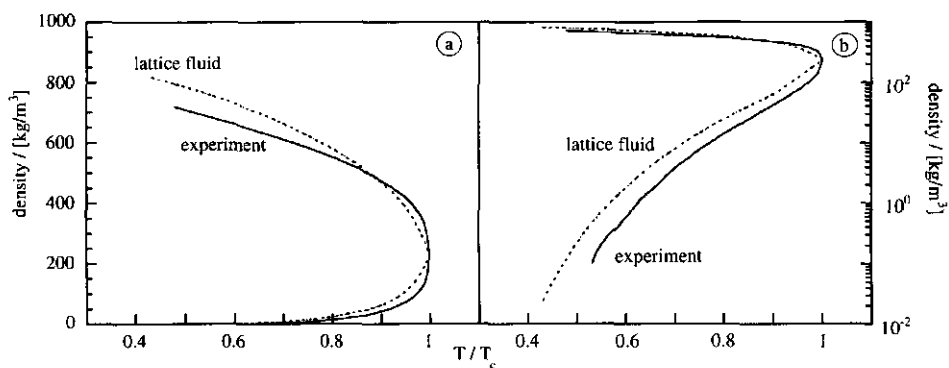
Figure 7. Binodal, orthobaric densities of n-octane, experimental data [20] (solid curve) are compared to lattice fluid results (dashed curve). In panel (a) the density is plotted on a linear scale, in panel (b) a logarithmic scale is used.

Heat of vaporization of n-alkanes

The heat of vaporization expresses the enthalpy difference between coexisting liquid and vapour phases. The enthalpy is defined as $H = U + pV$. Within the SCF-LF theory, the (configurational) energy U^b of a homogeneous binary mixture bulk phase, consisting of $N_x^{\#}$ segments x and $N_y^{\#}$ segments y, equals

$$U^b = \tfrac{1}{2}Z(\varepsilon_{xx} N_x^{\#} + \varepsilon_{yy} N_y^{\#}) + N_y^{\#} \phi_x^b \chi_{xy} kT \tag{29a}$$

The first term in Eq. (29a) represents the (perfect) configurational energy for random mixing, the second term is the mixing energy contribution due to interactions between the mixing segments.

For a mixture of molecule segments and vacancies $\varepsilon_{oo} = \varepsilon_{Ao} = 0$ (vacancies experience no interactions). Furthermore, χ_{Ao} can be related to ε_{AA} (Eq. 25a)) and Eq. (29a) reduces to

$$U^b = -\chi_{Ao} N_i n_i \phi_i^b kT \tag{29b}$$

where n_i is the number of molecules i in the system with energy U^b. The molecular energy u_i^b in bulk liquid or vapour of molecules i, defined as $u_i^b = U^b/n_i$, therefore equals $-N_i \chi_{AO} \phi_i^b kT$. The molecular enthalpy h_i^b, in bulk liquid or vapour follows from $h_i^b = (U^b + pV)/n_i$. Realizing that $V = n_i N_i v / \phi_i^b$, and making use of Eq. (15a), h_i^b can be calculated as

$$h_i^b = u_i^b - \tilde{\mu}_o N_i / \phi_i^b \tag{30}$$

The molecular enthalpy of vaporization $\Delta_{vap} h_i$ is defined as the enthalpy difference between the coexisting bulk vapour and liquid phases (denoted by the superscripts V and L, respectively):

$$\Delta_{vap} h_i = h_i^v - h_i^L \tag{31}$$

The molar heat (enthalpy) of vaporization is obtained as $\Delta_{vap} H_i = N_A \Delta_{vap} h_i$.

In Fig. 8, the computed molar heats of vaporization for the homologous series of n-alkanes are compared to experimental data [19], see Fig. 8. Panel a) shows the results at 298.15 K, panel b) shows the results at the normal (1 atm) boiling points. At room temperature, the calculated values tend to be too low. The discrepancy increases with N_i. The experimental and theoretical data both depend linearly on the chain length (Fig. 8a). At the normal boiling points the enthalpy of vaporization of the n-alkanes also increases with increasing chain length (see Fig. 8b), however, this increase is smaller than that at room temperature. At the normal boiling points, the calculated heats of

85
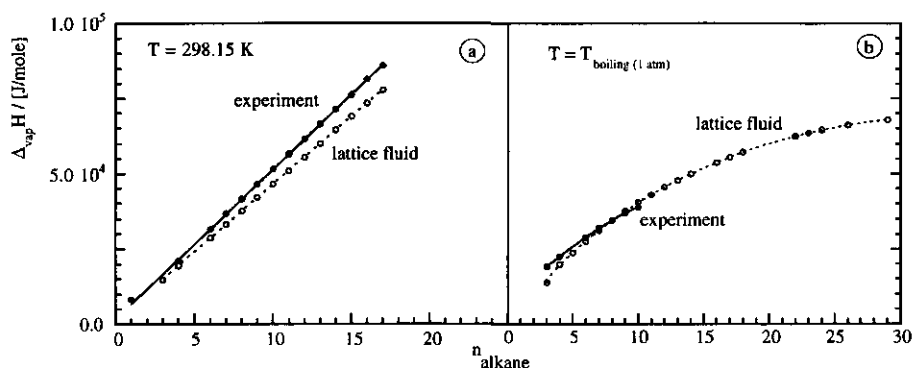
Figure 8. The molar enthalpy of vaporization of different n-alkanes. Experimental data [19] (solid points) are compared to lattice fluid results (open circles). In (a) the data at 298 K are plotted against the number of carbon atoms of the n-alkane, in (b) the SCF results at the normal boiling points of the n-alkanes are compared to (extrapolated) experimental data.

vaporization are in quite good agreement with the (extrapolated) experimental values [19].

The entropy of vaporization is related to the enthalpy of vaporization. In a binary mixture of vacancies and molecules i we have for the Gibbs energy $G = \mu_i\, n_i$ and $\Delta_{vap}g_i = g_i^v - g_i^L = \mu_i^v - \mu_i^L = 0$. This implies that the molar entropy of vaporization directly follows from $\Delta_{vap}S_i = \Delta_{vap}H_i\ /\ T$. The molar entropies of vaporization corresponding to the enthalpies of Fig. 8 are plotted in Fig. 9. At room temperature $\Delta_{vap}S_i$ increases with the chain length of the n-alkane. However, at the normal boiling points $\Delta_{vap}S_i$ is rather constant for the different chain lengths. Increasing the n-alkane chain length raises the boiling temperature and $\Delta_{vap}H_i$ similarly, consequently, $\Delta_{vap}S_i$ is hardly affected. For most fluids, molecules in the vapour phase interact minimally and are in a state of disorder. The differences in $\Delta_{vap}S_i$ of individual fluids may be associated with the internal order in the liquid. Obviously, for n-alkanes, the molecular stucture at the normal boiling point is rather independent of the alkane chain length.

Summarizing we conclude that the parameters shown in Table 1 are reasonable choices for the description of the bulk properties of n-alkanes with the SCF-LF theory. Figures 4 to 9 show that, with these parameters, the theory is able to reproduce the trends in bulk properties as a function of chain length and temperature and that even a reasonable quantitative agreement between calculated and experimental data is achieved, especially for longer n-alkanes. Therefore, the present parameter choice will be maintained when describing the interfacial properties of different n-alkanes with the SCF-LF theory.
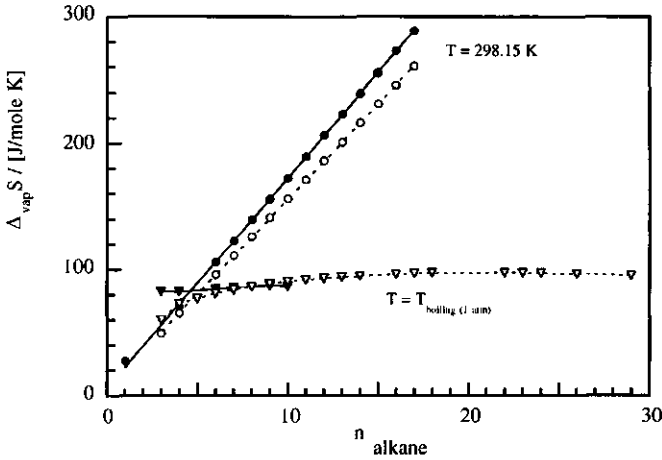
Figure 9. The entropy of vaporization for the homologous series of n-alkanes corresponding to Fig. 8. Calculated values (open points) are compared to experimental data (solid points) at room temperature (circles) and at the normal boiling temperature (triangles).

Interfacial properties of n-alkanes at the liquid-vapour interface

Volume fraction profiles

With the SCF-LF theory the structure of the liquid-vapour (LV) interface can be investigated. The segments of a chain molecule are numbered from $s = 1$ to $s = N_i$. Segments with ranking numbers $s = 1+x$ and $s = N_i-x$ have identical volume fraction profiles $\phi_i(z,s)$. The total volume fraction in layer z ($\sum_s \phi_i(z,s)$) is further investigated by expressing the contribution of a segment with ranking number s to $\sum_s \phi_i(z,s)$ in a relative volume fraction according to $\phi_i(z,s) N_i / \sum_s \phi_i(z,s)$. If a lattice layer is part of an isotropic phase, the relative volume fractions are unity for any segment. The density profiles at the boundary of the coexisting liquid and vapour phases are plotted in Fig. 10 for two temperatures and for chain molecules with $N_i = 4$ and $N_i = 8$. Both the absolute (left) and the corresponding relative (right) volume fraction profiles are shown. In each panel, the liquid phase is positioned at the left hand side, the vapour phase on the right hand side. The shaded regions in the plots indicate the highest segment and vacancy density gradients between two adjacent lattice layers. The volume fraction profiles are symmetrical with respect to exchanging molecules and vacancies.

87

With decreasing temperature the thickness of the interfacial region (with densities differing from those in the coexisting bulk phases) decreases. At $T = 0$ K any interface becomes dead sharp. The relative volume fraction profiles (panels b, d and f) reveal that the chain end segments have a (relative) preference for the vapour side of the interface whereas the middle segments avoid this region. In a molecular dynamics simulation study [22] and other lattice fluid studies [9] this feature has also been observed. With increasing temperature this behaviour becomes less pronounced (compare panels b and d). Increasing the chain length enhances the (relative) preference of the chain ends for the vapour phase boundary side of the interface (compare panels d and f).

The reason for the difference in interfacial behaviour of chain end and -middle segments is twofold. Firstly, middle segments drag two neighbouring segments to the interfacial region whereas end segments only have one neighbouring segment. Thus, when chain ends are exposed to the vapour boundary side of the interface, the number of unfavourable segment-vacancy contacts is smaller. Secondly, the conformational entropy of a chain molecule in the interfacial region is larger when a chain end is pushed out of the interface instead of a train of segments. These two effects become more pronounced upon decreasing the temperature and increasing the chain length.

LV interfacial tension

The interfacial tension γ follows from the density profiles according to Eq. (18). To investigate a liquid-vapour interface within the SCF-LF theory, the amount of molecules in the system is chosen such that two homogeneous bulk phases coexist. The densities of these coexisting phases follow directly from the Flory theory [2]. In the SCF-LF calculations of the interfacial tension, lattice artefacts are elimated by adjusting the amount of molecules until the volume fractions of the coexisting bulk phases equal those calculated with the Flory theory [23]. The interfacial tension of the lattice fluid is expressed per area of a lattice-site. For conversion to units of J/m^2 this value has to be multiplied with the lattice cell area (a). This area is assigned the value corresponding to the lattice cell volume in the FCC lattice used, i.e., $a = v^{\frac{2}{3}} = 0.09$ nm^2.

The interfacial tensions for different temperatures and chain lengths are calculated and compared with experimental data. Usually, experimental data are obtained under an atmosphere of hydrocarbon vapour and dry nitrogen. In the temperature range of the comparison (i.e., above 0°C) nitrogen is assumed an inert gas with a negligible influence on the measured interfacial tensions.
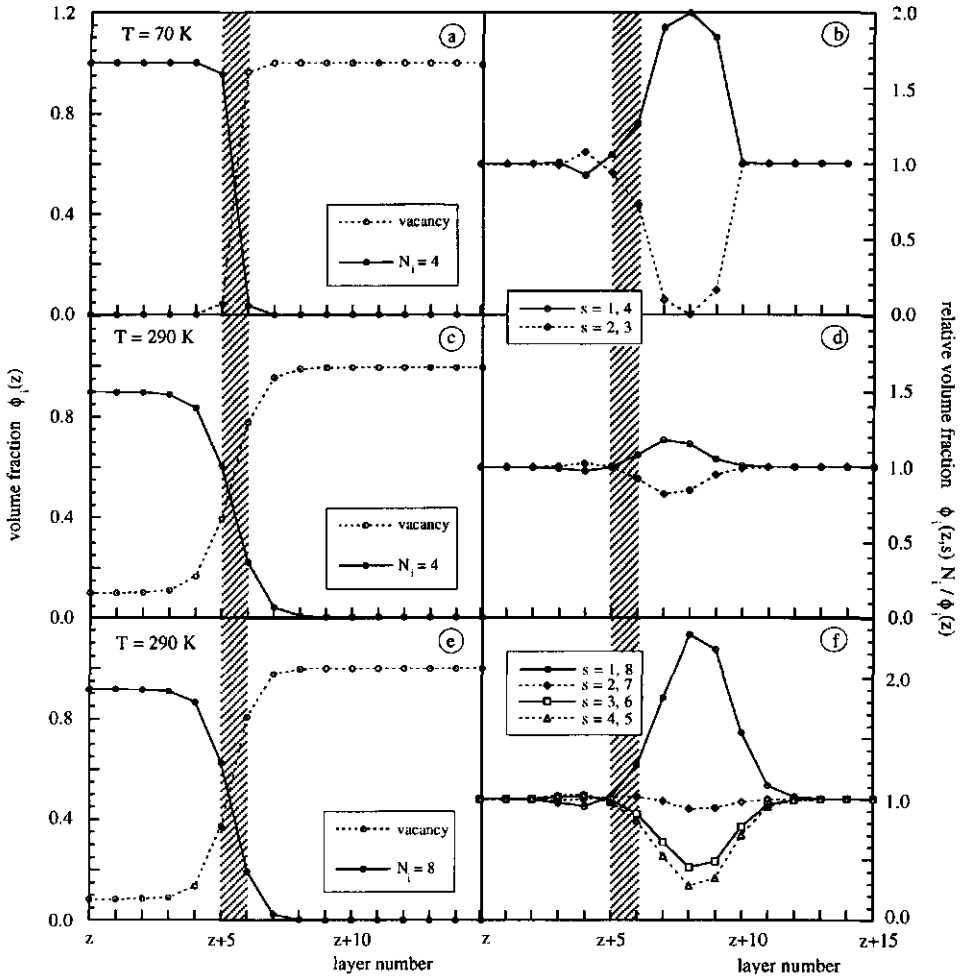
Figure 10. Absolute (left) and correponding relative (right) volume fraction profiles of the liquid-vapour interfacial region for various temperatures and chain lengths. The steepest decay in the absolute volume fraction profiles between two adjacent lattice layers is shaded.

Temperature dependence

According to general thermodynamics (Eq. (12)) the interfacial tension γ is related to the Helmholtz energy as

$$\gamma = (\partial F/\partial A)_{T, V, \{n_i\}} = (\partial U/\partial A)_{T, V, \{n_i\}} - T (\partial S/\partial A)_{T, V, \{n_i\}} \tag{32}$$

the second term on the right hand side accounts for the excess interfacial entropy $S^\sigma \equiv (\partial S/\partial A)_{T,V,\{n_i\}}$ and equals $-(\partial \gamma/\partial T)_{V,\{n_i\}}$. According to Eq. (32), the interfacial tension at the absolute zero point equals $(\partial U/\partial A)_{T, V, \{n_i\}}$.

Figure 11a shows the calculated temperature dependence of the interfacial tension for (alkane) molecules of various lengths. Upon decreasing the temperature any fluid will eventually freeze. As application of the SCF-LF theory may not be justified for frozen states, the curves are only drawn for temperatures above the freezing temperatures of the n-alkanes. The frozen states will be briefly discussed at the end of this section. The calculated $\gamma(T)$ curves above the melting point (see solid curves in Fig. 11a) show that $(\partial \gamma/\partial T)_{V,\{n_i\}} < 0$, both for monomers and chain molecules, hence S^σ is positive. According to the theory S^σ decreases with increasing chain length. Upon increasing the temperature (for a certain chain length) the magnitude of S^σ increases until it reaches a maximum (at the inflection point of the $\gamma(T)$ curve). After the maximum S^σ decreases with increasing temperature to vanish (together with the phase boundary) at the critical temperature.

The interfacial excess entropy has two (main) contributions: the excess conformational entropy of the chains at the interface and the excess entropy of mixing vacancies and molecules. For monomeric fluids the conformational contribution at the interface is absent and S^σ is solely determined by the mixing term. Thus, the maximum in $S^\sigma(T)$ for the monomeric fluid is a reflection of the temperature dependency of the interfacial excess mixing entropy. The $\gamma(T)$ curves suggest that this conclusion also applies to chain molecular fluids.

In Fig. 11b the results of the lattice fluid calculations for n-alkanes in the liquid state (i.e., for $T/T_c > 0.35$) are plotted against the reduced temperature T/T_c. The calculated $\gamma(T/T_c)$ curves are virtually independent of the chain length. When experimental data on the temperature dependency of the interfacial tension for different individual n-alkanes [24] are plotted against the reduced temperature T/T_c an almost linear mastercurve results (see Fig 11b). The quantitative agreement between the lattice fluid results and experimental data is satisfactory, the calculated values are somewhat lower than the experimental data.
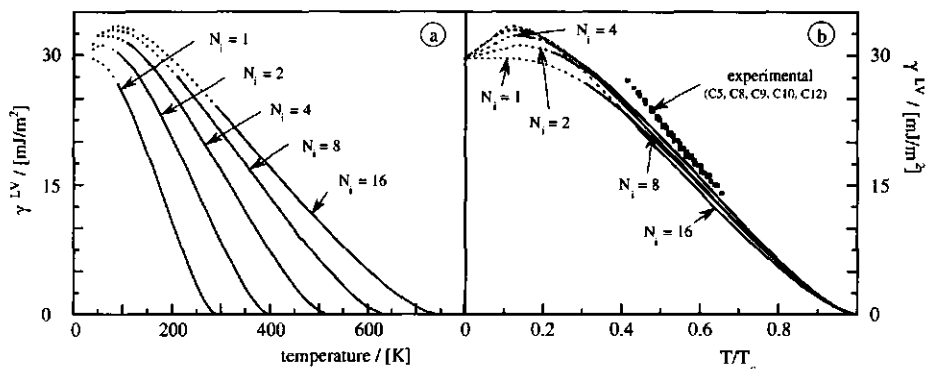
Figure 11. The liquid-vapour interfacial tension for liquids of varying chain length as a function of temperature (calculated using the parameters in Table 1). The drawn curves are the results calculated for temperatures above the melting temperature of the n-alkane with $C_n = N_i$. Below the melting point only calculated points are shown. In panel (b) the calculated interfacial tensions are plotted against the reduced temperature. Below the melting temperature the curves are dashed. The experimental interfacial tensions for several n-alkanes [24] (C5, C8, C9, C10 and C12) are also shown.

As indicated above, the SCF-LF theory may not be suited to describe highly ordered frozen phases. In the theory molecules are considered to be randomly distributed, i.e. at low temperatures it describes a supercooled fluid. Yet it may be interesting to discuss the initial (low temperature) part of the $\gamma(T/T_c)$ plots as the calculated trends may be useful to improve our understanding of surface freezing (occuring a few degrees above the bulk freezing temperature) of longer ($C_n > 14$) n-alkanes [25, 26].

At 0 K, interfaces are dead sharp (i.e., $\phi_i^V = 0$ and $\phi_i^S = 1$). In the SCF-LF theory the interfacial tension is given by the contact fraction with the next layer λ_{+1} together with the segment-vacancy interaction according to $\gamma = \lambda_{+1} c_2 k / a$ (as $\chi_{Ao} = c_2 k$, see Eq. (25b)), independent of the chain length. Very close to the absolute zero point S^σ vanishes and $(\partial \gamma / \partial T)_{V,\{n_i\}}$ has to become 0, irrespective of the chain length. Calculations of this region are hampered by numerical problems associated with the high χ_{Ao} values. Figure 11b shows that for monomers γ only decreases with temperature whereas for chain molecules a maximum interfacial tension is found at $T/T_c \approx 0.12$, rather independent of the chain length. The maximum in the $\gamma(T/T_c)$ curves, if real, would imply the occurence of negative $(\partial S/\partial A)_{T,V,\{n_i\}}$ values around $T/T_c \approx 0.12$. For n-alkanes just above their bulk freezing temperature, the occurence of negative S^σ values has also been observed experimentally [25, 26]. A negative S^σ

91

means that the entropy of the interfacial region is lower than in the bulk, i.e. the interfacial region has a higher degree of organisation than the high density bulk phase. A physical argument could be that at a sharp interface, the conformational entropy of the molecules in the interface is restricted as compared to that in the (high density) bulk phase. This restriction will be more serious for longer chains than for shorter ones.

In our calculations the maximum in the $\gamma(T/T_c)$ curve not only occurs for longer n-alkanes, it is also found for very short n-alkanes for which surface freezing has not been observed. Furthermore, the γ maximum occurs at temperatures below the experimentally established n-alkane surface freezing temperatures [25, 26]. These discrepancies propably have to do with the weakness of the current SCF-LF theory to describe frozen phases. However, it is worthwhile trying to improve the SCF-LF description of frozen n-alkane surface films by f.i. application of the Self-Consistent Anisotropic Field Scheme[27] in which the tendency of densily packed chain molecules to line up is accounted for.

Chain length dependence

The calculated chain length dependence of n-alkane LV interfacial tension is compared with experimental data [24] (at $T = 293.15$ K, under 1 bar of hydrocarbon vapour and dry nitrogen) in Fig. 12a. Another way of comparing is to plot the SCF-LF results directly against the experimental values, this is done in Fig. 12b. The experimental surface tensions of the homologous series of n-alkanes scale with the molecular weight to the power $-2/3$ [28]. The drawn and dotted curves in Fig. 12a are described by the relation

$$\gamma_n = \gamma_{n \to \infty} - k_{alk} / C_n^{2/3} \tag{33}$$

The constants $\gamma_{n \to \infty}$ and k_{alk} (in mJ/m^2) corresponding to these curves are 37.3 and 62.5 for the experimental data and 27.9 and 25.4 for the SCF-LF results, respectively. This implies that the scaling of the calculated LV interfacial tension with the number of carbon atoms of the n-alkane is correcly reproduced but not the absolute value.

For the shorter n-alkanes, the generalized lattice fluid parameters (see Table 1) overestimate the interfacial tension. This overestimation can be traced back to the fact that the lattice cell volume determines the area of a lattice site. According to the liquid density at 293.15 K and Eq. (28), the lattice cel volume of the shorter n-alkanes (especially for $C_n < 8$) is higher than the 0.027 nm^3 used in the calculations. This means that lattice cell area is underestimated and that the calculated value of the interfacial tension will be too high. For $C_n > 8$ the lattice cell volume is close to 0.027
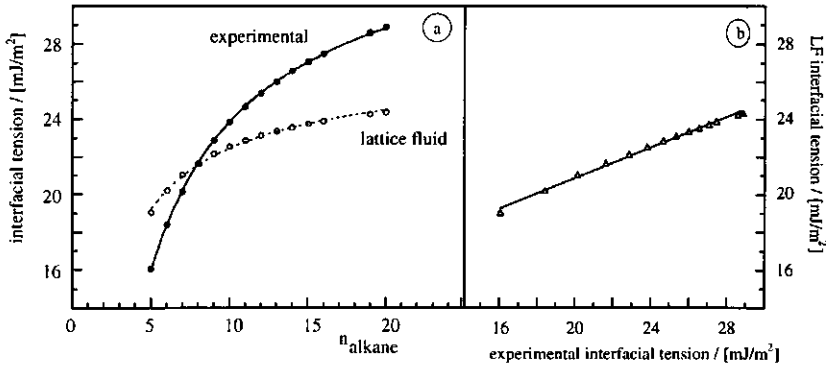
Figure 12. The lattice fluid (LF) interfacial tensions (open circles) of the liquid-vapour interface of various n-alkanes at 293.15 K (calculated using the parameters shown in Table 1) compared to experimental data [24] (solid points). In (a) the curves through the points are drawn according to Eq. (33). In (b) the calculated interfacial tensions are plotted against the experimental ones.

nm^3 and the a value of 0.09 nm^2 is correct, Yet, the lattice fluid theory slightly underestimates the interfacial tension of the n-alkanes. This underestimation increases with increasing chain length and eventually, according to the $\gamma_{n\to\infty}$ values, the theory underestimates the interfacial tension of infinitely long chains by 32%. According to Fig. 11b, the SCF-LF theory increasingly underestimates the LV interfacial tension for lower reduced temperatures. With increasing chain length of the n-alkane, the critical temperature increases (see Fig. 6) and T/T_c at 293.15 K decreases so that γ at 293.15 K will be increasingly underestimated by the theory.

General remark on the interfacial tension calculations

The nearest neighbour interactions of Table 1 in combination with $N_i = C_n$ correctly describe the (infinite range) Lifshits-van der Waals interactions in n-alkane bulk fluids. However, for inhomogeneous and anisotropic systems such as a LV interface, such a parameter choice results in an underestimation of the n-alkane interfacial tension. As we are mainly interested in trends in the behaviour and properties of chain molecules at interfaces, we did not attempt to improve the quantitative agreement between the calculated and experimental LV interfacial tensions. However, the linear relationship between the experimental and lattice fluid interfacial tensions (see Fig. 12b) can be used to predict the actual interfacial tensions of the n-alkanes. It is expected that the

93

calculated and experimental interfacial tensions of chain molecules will ameliorate if the chain flexibility is reduced by, for instance, the RIS scheme [4].

The current lattice fluid calculations are an important improvement compared to previous efforts to model the chain length dependence of the interfacial tension of the n-alkanes [9]. In these previous calculations the volatility of the liquid has been neglected. Including vapour molecules in the lattice fluid theory description of the LV interface results in rather good quantitative and qualitative agreement between calculated and experimental n-alkane interfacial tensions.

5.4. Conclusions

The SCF-LF theory (semi)quantitatively reproduces various bulk and interfacial properties of normal-alkanes. The description of the temperature dependence of the vapour pressure of the homologous series of n-alkanes is optimal if the n-alkane molecules are considered as chain molecules with a chain length equal to the number of carbon atoms. In the SCF-LF theory the segment-segment interactions (for which the FH parameter is zero by definition) are reflected in the non zero FH interaction parameter for a chain segment-vacancy contact $\chi_{A\theta}$. Under the conditions mentioned $\chi_{A\theta}$ is independent of the (n-alkane) chain length and equals $580/T$ (T in K) for all n-alkanes. Using these parameters n-alkane (liquid-vapour) bulk properties such as saturated vapour pressure, densitiy and heat of vaporization are calculated for different temperatures. The qualititative and quantative agreement between the calculated results and experimental data is satisfactory.

Density profiles of the LV interfacial region reveal that chain end segments, protruding into the vapour, are the major constituent of vapour side of the interface. At the liquid side of the interface, chain middle and end segments are equally distributed. The theory is able to reproduce the chain length dependence and temperature dependence of the n-alkane interfacial tensions rather accurately. For $0.4 < T/T_c < 0.8$, the calculated interfacial tension of chain molecule fluids rises linearly with decreasing T/T_c. This has also been established experimentally. For the moment experimental data on the interfacial tension of n-alkanes for T/T_c values below 0.4 are lacking. The theoretical predictions can be verified experimentally by measuring the LV interfacial tension of shorter n-alkanes, which are still liquids below $T/T_c = 0.4$.

If the theory is applied for temperatures below the n-alkane freezing temperatures, positive $d\gamma/dT$ values occur and a maximum in the LV interfacial tension is found at $T/T_c \approx 0.12$, irrespective of the chain length of the molecule.

The lattice fluid theory description of the n-alkane interfacial properties may be improved by considering flexibility contraints, for instance trans-gauche conformations. Furthermore, it is rather straightforward to extend the present theory to more complex systems such as fluid mixtures, or fluids (vapour and liquid) at solid surfaces with or without grafted groups. As the present theory allows the computation of interfacial tensions of these interfaces the work of adhesion and contact angles as a function of temperature and chain length of the (wetting) liquid can be investigated. The same can be done for grafted solids as a function of grafting-density and -chain length. Some of these aspects will be elaborated a forthcoming publication.

References

[1]   Guggenheim, E. A., in *"Mixtures"*; Clarendon : Oxford, **1952**.

[2]   Flory, P. J., in *"Principles of Polymer Chemistry"*; Cornell University Press: Ithaca (N. Y.), **1953**.

[3]   Fleer, G. J., Cohen Stuart, M. A., Scheutjens, J. M. H. M., Cosgrove, T. and Vincent, B., in *"Polymers at Interfaces"*; Chapman & Hall.: Cambridge, **1993**.

[4]   Leermakers, F. A. M. and Scheutjens, J. M. H. M., *J. Phys. Chem.*, 89 (5), **1988**, p. 3264-3274.

[5]   Böhmer, M. R., Koopal, L. K. and Lyklema, J., *J. Phys. Chem.*, 95 (23), **1991**, p. 9569-9578.

[6]   Böhmer, M. R. and Koopal, L. K., *Langmuir*, 8 (11), **1992**, p. 2660-2665.

[7]   Sanchez, I. C. and Lacombe, R. H., *J. Phys. Chem.*, 80 (21), **1976**, p. 2353-2362.

[8]   Poser, C. I. and Sanchez, I. C., *J. Colloid Interface Sci.*, 69 (3), **1979**, p. 539-548.

[9]   Theodorou, D. N., *Macromolecules*, 22 (12), **1989**, p. 4578-4589.

[10]   Siepmann, J. I., Karaborni, S. and Smit, B., *Nature*, 365 (23 Sept.), **1993**, p. 330-332.

[11]   Kaminski, G., Duffy, E. M., Matsui, T. and Jorgensen, W. L., *J. Phys. Chem.*, 98 (49), **1994**, p. 13077-13082.

[12]   Smit, B., Karaborni, S. and Siepmann, J. I., *J. Chem. Phys.*, 102 (5), **1995**, p. in press.

[13]   Madden, W. G., *J. Chem. Phys.*, 87 (2), **1987**, p. 1405-1422.

[14]   Scheutjens, J. M. H. M. and Fleer, G. J., *J. Phys. Chem.*, 83, **1979**, p. 1619-1635.

[15]   Scheutjens, J. M. H. M. and Fleer, G. J., *J. Phys. Chem.*, 84, **1980**, p. 178-190.

[16]   Evers, O. A., Scheutjens, J. M. H. M. and Fleer, G. J., *Macromolecules*, 23, **1990**, p. 5221-5232.

[17]   Kijlstra, J. and Scheutjens, J. M. H. M., *"Vacancies in the Lattice Model"*, **1986**, MSc thesis Dept. Physical and Colloid Science, Wageningen Agricultural University, The Netherlands.

[18]   van Lent, B. and Scheutjens, J. M. H. M., *Macromolecules*, 22, **1989**, p. 1931-1937.

[19]   Lide, D. R. (Ed.) , in *"CRC Handbook of Chemistry and Physics"*; CRC Press Inc.: Boca Raton, U.S.A., **1992-1993**.

[20]   Timmermans, J., in *"Physico-Chemical Constants of Pure Organic Compounds"*; American Elsevier.: New York, **1950** (Vol. I) and **1965** (Vol. II).

[21]   Boublink, T., Fried, V. and Hala, E., in *"The vapour Pressures of Pure Substances"*; Physical Sciences Data 17; Elsevier: **1984**.

[22]   Weber, T. A., *J. Chem. Phys.*, 72 (7), **1980**, p. 4014-4018.

[23]   Barneveld, P. A., Scheutjens, J. M. H. M. and Lyklema, J., *Langmuir*, 8, **1992**, p. 3122-3130.

[24]   Jasper, J. J. and Kring, E. V., *J. Phys. Chem*, 59, **1955**, p. 1019-1021.

[25]   Earnshaw, J. C. and Hughes, C. J., *Phys. Rev. A.*, 46 (8), **1992**, p. R4494-R4496.

[26]   Wu, X. Z., Ocko, B. M., Sirota, E. B., Sinha, S. K. and Deutsch, M., *Physica A*, 200 , **1993**, p. 751-758.

[27]   Meijer, L. A., Leermakers, F. A. M. and Nelson, A., *Langmuir*, 10 (4), **1994**, p. 1199-1206.

[28]   Legrand, D. G. and Gaines, G. L., *J. Colloid Interface Sci.*, 31 (2), **1969**, p. 162-167.

Chapter 6

Vapour Adsorption and Wetting of Alkanes on Bare and Alkylated Solids: a statistical thermodynamic approach

Abstract

The adsorption, structure and thermodynamics of aliphatic chain molecular fluids at rigid solids and at solids with terminally grafted aliphatic chains are investigated with a lattice-fluid theory. Vapour adsorption isotherms, including the meta- and unstable regions, are calculated for both types of substrates. The effect of adsorption energy differences between end and middle segments on the adsorption isotherm of an octamer on a rigid solid is investigated together with the influence of the chain flexibility. Furthermore, contact angles are calculated on rigid solids and on solids with terminally grafted chains. On a poorly wetted rigid solid, the contact angle decreases with increasing chain length of the wetting liquid and increasing temperature. This is mainly due to the influence of the temperature on the liquid-vapour and solid-liquid interfacial tensions. Grafting of aliphatic chains to a very poorly wetted (bare) solid decreases the contact angle of the octameric liquid. Moreover, the contact angle as a function of the grafting density passes through a minimum. The rise beyond the minimum has an entropic origin. When chains are grafted on a completely wetting solid this eventually results in a finite contact angle; higher grafting densities give higher contact angles. With increasing chain length of the grafted molecules lower contact angles are found on both solid substrates. With the theory both the thermodynamics and molecular aspects of chain molecular fluids at solid substrates are described. This reveals that contact angles on grafted solids mainly result from the absorption of middle segments (of the wetting molecules) within the grafted layer.

6.1. Introduction

Adhesion and wetting are technologically interesting phenomena and have many practical applications including printing, painting, coating, oil recovery and polymer melt processing. For such applications control over the adhesion and wetting properties of materials is extremely relevant. This requires a profound understanding of the thermodynamics and structures of the interfaces involved.

Vapour adsorption and contact angle measurements are useful tools to study the behaviour of fluids at solid interfaces. In general the vapour adsorption gradually rises with increasing vapour pressure. If the fluid completely wets the substrate, the vapour adsorption isotherm rises very steeply to infinity as saturation is approached (i.e., a

macroscopic liquid layer is formed). A partial wetting adsorption isotherm has two stable states at saturation; a finite adsorbed amount (thin film) and a macroscopic liquid layer. If enough liquid is present, these two states can coexist through the curved interface of a droplet with a finite contact angle.

Hydrocarbons are major constituents of fuels, oils, lubricants and polymers. Because of their (industrial) importance both the bulk and interfacial properties of hydrocarbons are extensively studied. Their properties are also important with respect to the behaviour of biological molecules (such as lipids) of which hydrocarbon chains are important building units. In wetting and adhesion studies alkanes are often used as standards [1]. Furthermore, in many scientific and technological applications the hydrophobicity of solids is controlled by grafting aliphatic chains to the solid surface.

Usually alkanes completely wet oxide surfaces. On alkylated substrates short n-alkanes completely wet whereas longer n-alkanes partially wet [2]. In various independent gravimetric and ellipsometric vapour adsorption studies, isotherms with a large linear part have been reported for alkanes adsorbing onto silica surfaces [3, 4]. Up to close to saturation the adsorption is lower than the coverage that corresponds to a monolayer of perpendicularly adsorbed n-alkanes. At saturation the isotherm diverges to infinity (complete wetting). Vapour adsorption isotherms of alkanes on alkylated surfaces show low adsorbed amounts [3, 5]. The adsorbed amounts are lower than the adsorption corresponding to a monolayer of n-alkanes oriented parallel to the surface. This persists until close to saturation.

Bulk fluid properties of n-alkanes have been described succesfully by means of Monte Carlo simulations [6, 7]. Until now, the simulation of chain molecular fluids at interfaces has recieved less attention [8, 9]. Furthermore, usually such simulations concentrate on the molecular structure and not on the adsorbed amounts or the interfacial thermodynamics. Modelling approaches leading to adsorption isotherm equations for spherical molecules (such as BET, Volmer and Langmuir [10]), are inadequate to describe n-alkane adsorption isotherms; they do not take into account the chain nature of the molecules. However, the self-consistent-field (SCF) theory, originally developed by Scheutjens and Fleer [11, 12], is very well suited for the description chain molecules and their (interfacial) behaviour and provides an excellent alternative for the classical adsorption theories.

In the previous Chapter a self-consistent-field lattice fluid (SCF-LF) theory has been outlined and applied to describe both the stucture and the thermodynamics of n-alkane bulk fluids and their liquid-vapour (LV) interfaces. Here, the theory will be applied to describe n-alkane adsorption on solid surfaces. Vapour adsorption isotherms (including the meta- and unstable regions) of chain molecules on rigid solids and on solids with grafted chains will be calculated. For rigid solids, the influence of differences in

adsorption energy between chain end and middle segments will be investigated together with the effect of chain flexibility. Moreover, the interfacial tensions of the solid-vapour and solid-liquid interfaces of aliphatic fluids on hard solids and "soft" alkylated substrates (i.e., a solid with terminally grafted aliphatic chains) are calculated and used to obtain contact angles [13]. On a hard solid, the contact angles of aliphatic liquids are calculated for different chain lengths and temperatures. The contact angle of an octameric liquid on "soft" alkylated substrates is calculated as a function of the grafting density and the grafted chain length.

The theory describes both the thermodynamics and structural aspects of chain molecular fluids at solid substrates. It offers a united approach of wetting and adsorption in which thermodynamics and molecular aspects are included. This allows one to relate the wettability in a system to the structure of the interfaces involved in the wetting process.

6.2. Self-consistent field lattice fluid theory for adsorption of chain molecules

SCF theory for adsorption

The main principles of the Self Consistent Field (SCF) theory for adsorption of chain molecules are shortly summarized in this section; for a detailed description of the theory we refer to Chapter 5 and Refs. [11, 12, 14, 15].

In the SCF theory a chain molecule i is considered as a series of N_i segments numbered $s=1... N_i$. Examples of chain molecules with $N_i = 8$ that can be built from segment types x and y are x_8 or y-x_6-y, when we whish to to take the difference between end and middle segments into account. The segments are placed on a lattice consisting of layers parallel to the surface and numbered from $z=1$ to $z=M$. The segments in a lattice layer experience a potential energy field that depends on their average surrounding by other segments and (nearest-neighbour) segment-segment interactions. The latter are quantified by Flory-Huggins χ parameters. With a mean field approximation in every lattice layer (only inhomogeneities in the direction prependicular to the surface are considered), the weighted probability $G_i(z,s)$ of finding an arbitrary free segment s of molecule i in an arbitrary layer z, is evaluated using Boltzmann statistics. The probabilities of all possible conformations of the chain molecules are calculated by means of Markov statistics. This allows one to obtain the equilibrium volume fraction $\phi_x(z)$ for all segment types x in all lattice layers z. As the segment volume fraction profiles both determine and depend on the potential energy field, the equilibrium field and volume fraction profile are determined numerically. From these self consistent volume fraction profiles the partition function can be

101

calculated and the thermodynamic and mechanic properties of the system can be derived.

Adsorption on solids can be studied with the SCF theory by placing an adsorbing, impenetrable boundary (a solid wall) on one side of the system. At the other boundary of the system, reflecting conditions are assumed [11]. The interaction of a segment (x) in the lattice layer directly adjacent to the solid wall S, with the solid is described by the χ_{xs} interaction parameter. If two impenetrable walls are placed on both system boundaries, adsorption in slits can be investigated.

The excess adsorbed amount of component i, θ_i^{exc} (expressed as the number of segments adsorbed on top of one surface site) follows from the equilibrium density profiles according to

$$\theta_i^{exc} = \sum_{z=1}^{M}(\phi_i(z) - \phi_i^b)$$ (1)

where ϕ_i^b is the volume fraction of molecule i in the bulk. The (excess) number of adsorbed molecules per surface site n_i^{exc} is related to θ_i^{exc} according to

$$n_i^{exc} = \frac{\theta_i^{exc}}{N_i}$$ (2)

In the SCF theory different kind (c.q. order) of Markov statistics can be used [14]. If first order Markov statistics are applied, two consecutive bonds of a chain may overlap each other (i.e., backfolding of segment $s+1$ on $s-1$ can occur). When dealing with short chains, it is, in principle, possible to store the whole chain conformation so that backfolding within a chain can be excluded. However, due to the mean field approximation made within the SCF theory, it is impossible to prevent a segment of one chain molecule from entering a lattice site that is already occupied by a segment belonging to another chain molecule. Therefore it is not very utile to implement full self-avoidance in the theory. However, within the SCF theory, a rotational isomeric state (RIS) scheme (i.e., a third order Markov approximation) has been developed [14]. This scheme reduces the chain flexibility and distinghuishes between gauche and trans conformations of the chain.

Rotational isomeric state scheme

The RIS scheme excludes direct backfolding of a chain and takes the semi-flexibility of the chain configurations into account. Each sequence of three C-C bonds has two secondary minima and one primary minimum in the configurational energy. These minima correspond to the two gauche configurations and the trans configuration,

respectively. The energy of the trans configuration is about 1 kT lower than that of the gauche configuration [16]. In the RIS scheme a three propagation choice lattice (a tetrahedral lattice) is used in order to describe the probability of the trans and gauche configurations.

A typical chain molecule segment has two bond directions with the rest of the chain, denoted by the superscripts α, β and γ or α', β' and γ' depending on the type of site it occupies [14]. The weighting factor of a free segment s is independent of the bond directions α and β and given by

$$G_i(z, s^{\alpha\beta}) = G_i(z, s) \qquad \text{if } \alpha \neq \beta$$
$$G_i(z, s^{\alpha\beta}) = 0 \qquad \text{if } \alpha = \beta \tag{3}$$

The second equality expresses that segment s cannot form two bonds in the same direction, i.e., it excludes direct backfolding within one chain. The probabilities of the different conformations of a chain molecule are counted by splitting the chain in fragments with their corresponding fragment weighting factors. The weighting factor of a chain extending from segment 1, anywhere in the system, to segment s, in layer z, with orientation $\alpha\beta$, is denoted by $G_i(z, s^{\alpha\beta} \mid 1)$. The subscript i denotes that the fragment is part of chain (molecule) i. Note that that for all segments s, $G_i(z, s^{\alpha\beta} \mid s)$ equals the free segment weighting factor $G_i(z, s^{\alpha\beta})$. The chain (fragment) weighting factors are generated, starting from the monomeric weighting factors for $s = 1$ or $s = N_i$ (Eq. (3)), by adding segments one by one according to

$$G_i(z, s^{\alpha\beta} \mid 1) = G_i(z, s^{\alpha\beta}) \sum_{\gamma''} \lambda^{\gamma''-\alpha''-\beta''} G_i(z', s - 1^{\gamma'\alpha'} \mid 1)$$
$$G_i(z, s^{\alpha\beta} \mid N_i) = G_i(z, s^{\alpha\beta}) \sum_{\gamma''} \lambda^{\alpha''-\beta''-\gamma''} G_i(z', s + 1^{\beta'\gamma'} \mid N_i) \tag{4}$$

The superscripts α'', β'' and γ'' denote the bond orientation as determined by the two bond directions of the bonds linking two segments (e.g. for α'' these bond directions are α and α') and $\lambda^{\gamma''-\alpha''-\beta''}$ and $\lambda^{\alpha''-\beta''-\gamma''}$ are the probabilities of such a set of successive bond orientations. In order to prevent overlapping of two consecutive bonds $\lambda^{\alpha''-\beta''-\gamma''} = 0$ when $\alpha'' = \beta''$ or $\beta'' = \gamma''$. Depending on the bond direction, z' can be $z-1$, z or $z+1$.

In the first extension step according to Eq. (4) (i.e., when growing monomers to dimers), the trans or gauche configurational energy of the chain does not play a role; the second segments $s = 2$ and $s = N_i-1$ of the chain fragments may choose from four, equally probable, propagation directions; in this case, $\lambda^{\alpha''-\beta''-\gamma''}$ equals 0.25. During the second and further extensions, the $\alpha''-\beta''-\gamma''$ configuration of each three consecutive bonds is reflected in $\lambda^{\alpha''-\beta''-\gamma''}$. The configuration is trans if the bond orientations α''

and γ'' are identical, otherwise the configuration is gauche. For a trans configuration the value of $\lambda^{\alpha''-\beta''-\gamma''}$ equals $\lambda^t = 1/C^{tg}$, for a gauche configuration $\lambda^g = exp(-U^{tg}/kT)/C^{tg}$, where U^{tg} is the gauche configuration energy minus the trans configuration energy and C^{tg} is a normalisation constant. For each trans configuration of a linear chain two gauche configurations are possible hence, $\lambda^t + 2\lambda^g = 1$ so that $C^{tg} = 1 + 2 exp(-U^{tg}/kT)$ must be obeyed.

The volume fractions of segment s, with orientation $\alpha\beta$ of chain molecule i can be calculated from the two chain fragment distribution functions according to

$$\phi_i(z, s^{\alpha\beta} \mid i; N_i) = C_i G_i(z, s^{\alpha\beta} \mid i; N_i)$$
$$= C_i \lambda^{\alpha\beta} \frac{G_i(z, s^{\alpha\beta} \mid i) G_i(z, s^{\alpha\beta} \mid N_i)}{G_i(z, s^{\alpha\beta})} \qquad (5)$$

On a tetrahedral lattice two alternating types of sites can be distinghuished, on each type a segment may assume 12 different orientations $\alpha\beta$, therefore $\lambda^{\alpha\beta}$ equals 1/24 [14]. The volume fraction of segment s in layer z is obtained by summation of Eq. (5) over all possible bond orientations $\alpha\beta$.

If studying isotropic systems (e.g., a bulk phase), application of the RIS scheme in the SCF theory does not affect the calculated volume fractions and thermodynamic quantities. Only when anisotropic systems (e.g. interfaces) are studied does application of the RIS scheme affect the SCF results.

SCF-lattice fluid theory

The Self Consistent Field theory can be used as a lattice fluid (LF) theory, capable of describing bulk fluid and liquid-vapour interfacial behaviour of chain molecules. Hereto free volume is accounted for by introducing vacancies as one of the components in the system. Due to the presence of these vacancies the expressions for the chemical potential μ_j of molecular component j and the pressure p in the SCF-LF theory read (see previous Chapter)

$$\mu_j = (\partial F/\partial n_j)_{T, A, \{n_{i \neq j}\}, n_o} - N_j (\partial F/\partial n_o)_{T, A, \{n_i\}} = \tilde{\mu}_j - N_j \tilde{\mu}_o \qquad (6a)$$

$$p = -\frac{1}{v}(\partial F/\partial n_o)_{T, A, \{n_i\}} = -\tilde{\mu}_o/v \qquad (6b)$$

where F represents the Helmholtz energy of a system of temperature T, area A, n_j molecules j, with chain length N_j, and n_o (monomeric) vacancies, v is a constant that represents the volume of one lattice cell, $\tilde{\mu}_{k'}$ is defined as $(\partial F/\partial n_{k'})_{T, A, \{n_{k \neq k'}\}}$, where

the index k runs over all components in the system, hence it also includes the vacancies.

In order to calculate the relative vapour pressure of a lattice fluid the saturated vapour pressure p_0 is needed. At p_0 two homogeneous phases (liquid and vapour) may coexist. In the lattice fluid theory phase separation can only occur if the binodal is reached. The binodal position can be found by equating the pressures and chemical potentials μ_j in the two coexisting phases. The relative vapour pressure of a lattice fluid p/p_0 directly follows from the the partial of the Helmholtz energy of a vacancy in a sytem with pressure p and molecular composition n_i (Eq. 6b) divided by the value of this partial at the binodal

$$\frac{p}{p_0} = \frac{\tilde{\mu}_o}{(\tilde{\mu}_o)_0} \tag{7}$$

with $(\tilde{\mu}_o)_0 = (\partial F/\partial n_o)_{T, A, \{n_{k\neq o}\}_0}$, where $\{n_{k\neq o}\}_0$ is the molecular composition of the system at the binodal.

According to Eq. (6b), varying the molecular composition of a binary SCF-LF system changes the vapour pressure of the system and allows us to calculate vapour adsorption isotherms.

SCF-LF theory and wetting

Vapour adsorption isotherms can be used to characterize the wettability of the fluid-solid pair considered. In the case of complete wetting the adsorbed amount (expressed in moles/m^2 and denoted by Γ) at saturation approaches the value for a macroscpic layer with properties of bulk liquid ($\Gamma \rightarrow \Gamma_\infty$). In the case of partial wetting the isotherm intersects the saturation axis with a finite adsorbed amount ($\Gamma_\ddagger$), only after supersaturating the vapour does the isotherm rise to infinity (condensation). If enough vapour is present at saturation, both adsorbed states $\Gamma_\ddagger$ and Γ_∞ can coexist through the curved interface of a droplet with a finite contact angle θ. The larger the contact angle the poorer the wetting. In the case of complete wetting, the notion of contact angle looses its meaning ($\theta = 0$).

The magnitude of the equilibrium contact angle in a liquid (L)-vapour (V)-solid (S) system can be related to the interfacial tensions involved in the contact angle formation according to [13]

$$\gamma^{LV} (\cos\theta - 1) = \gamma^{SV} - (\gamma^{SL} + \gamma^{LV}) \tag{8}$$

where γ^{SV} is the interfacial tension of the solid with the thin adsorbed film ($\Gamma_\ddagger$) that is formed at the saturated vapour pressure and $\gamma^{SL} + \gamma^{LV}$ is the interfacial excess free energy of the same solid, covered by a macroscopically thick adsorbed layer with

properties of bulk liquid. The value of the contact angle in a liquid-vapour-solid system can be assessed from an integration of the meta- and unstable region of the (semi-logarithmically plotted) vapour adsorption isotherm. With help of Gibbs' adsorption law we have derived [17]

$$\gamma^{LV} (\cos \theta - 1) = RT \int_{\Gamma_+}^{\Gamma_\infty} \Gamma(\tfrac{p}{p_0}) \, d \ln \tfrac{p}{p_0} \tag{9}$$

where R is the gas constant.

According to general thermodynamics, the interfacial excess free energy is related to the Helmholtz energy F of the system:

$$F = -pV + \gamma A + \sum_i \mu_i \, n_i \tag{10}$$

where V is the volume of the system, A denotes the interfacial area and the index i runs over all types of molecules present in the system. Within the SCF-LF theory this expression reduces to (see Chapter 5)

$$F = \gamma A + \sum_k \tilde{\mu}_k \, n_k \tag{11}$$

where the index k runs over all components in the system, inclusive the vacancies as they account for the free volume contribution ($-pV$) to F in the system. According to standard statistical thermodynamics, the Helmholtz energy of a system follows from the canonical partition function Q as $F = -kT \ln Q$. In the SCF theory Q can be evaluated from the volume fraction profiles [15] and γ can be calculated by rewriting Eq. (11) as

$$(\gamma - \gamma^*) A = -kT \ln Q - \sum_k \tilde{\mu}_k \, n_k \tag{12}$$

where γ^* denotes the interfacial tension of the reference state. Its appearance in Eq. (12) is due to the fact that, in the SCF theory, the term on the right hand side of Eq. (12) gives the excess interfacial free energy per unit surface with respect to a reference state in which the pristine interface (i.e, the interface without adsorbed and/or grafted chains) is included. For liquid-vapour systems, the reference state is the homogeneous bulk fluid without any interface and $\gamma^* = 0$. For solid-fluid systems, the reference state is defined by the homogeneous bulk fluid and the pristine solid surface with interfacial tension γ^{s*}.

In the SCF theory the surface tension γ can also be evaluated directly from the grand canonical partition function and the segment density distribution according to [15]

$$(\gamma - \gamma^*) A = L\,kT\left(-\sum_k \theta_k^{exc}/N_k - \sum_z u'(z)/kT \right.$$
$$\left. - \frac{1}{2}\sum_z \sum_{A'} \sum_{B'} \chi_{A'B'}(\phi_{A'}(z) <\phi_{B'}(z)> - \phi_{A'}^b \phi_{B'}^b) \right)$$
(13)

where L is the number of lattice sites per lattice layer. The potential energy $u'(z)$ accounts for the fact that the sum of all volume fractions in layer z should equal unity (i.e., the lattice should be completely filled). The counters A' and B' in Eq. (13) run over all segments (including the vacancies) in the system except for the segments of the solid surface (S), the brackets $<>$ denote a contact averaged volume fraction [15]. For the derivation of Eq. (13) use is made of the following expression for the normalisation constant

$$C_i = \phi_i^b /N_i$$
(14)

For ungrafted solids Eqs. (12) and (13) both yield correct, identical values of γ. However, for chains that are grafted to a solid, Eq. (14) does not apply as such chains cannot leave the system. In this case Eq. (13) becomes more complicated and its correct version has not yet been implemented. Therefore, the interfacial tensions of grafted solids are calculated by means of Eq. (12). In Eq. (12), the contribution of the grafted chains is included in Q whereas the index k runs over all components in the system except for the grafted molecules (for which $\bar{\mu}$ is not defined).

The theory expresses the interfacial tensions of the thin adsorbed film ($\Gamma_{\ddagger}$) and the macroscopic liquid layer (Γ_{∞}), both formed at the saturated vapour pressure, with respect to the same reference state (γ^{s^*}). The first, $\gamma^{sv}(\Gamma_{\ddagger})$, equals $\gamma^{sv} - \gamma^{s^*}$, the latter, $\gamma^{sv}(\Gamma_{\infty})$ equals $\gamma^{sL} + \gamma^{Lv} - \gamma^{s^*}$. Once $\gamma^{sv}(\Gamma_{\ddagger})$, $\gamma^{sv}(\Gamma_{\infty})$ and γ^{Lv} are calculated, the contact angle can be predicted by rewriting Eq. (8) to

$$\gamma^{Lv}(\cos\theta - 1) = \gamma^{sv}(\Gamma_{\ddagger}) - \gamma^{sv}(\Gamma_{\infty})$$
(15)

For the calculation of the contact angle the reference state γ^{s^*} is irrelevant as it cancels in Eq. (15).

Calculating the contact angle, either by means of Eq. (15) or by means of Eq. (9), yields the same results. However, Eq. (15) is quicker and more accurate than Eq. (9) as the latter requires calculation and numerical integration of the adsorption isotherm. Therefore we will use Eq. (15) for our contact angle predictions.

Parameter choice

The properties of chain molecules at solid sufaces are studied using the same parameters as those that successfully described bulk fluid poperties of hydrocarbons (see Chapter 5). This means that n-alkanes will be described as flexible chains of n segments (A_n), in which each segment A represents one carbon atom. Furthermore, the segment (and lattice cell) volume equals 27 nm^3 and the interaction between two A segments is described by a FH segment (A)-vacancy (o) interaction parameter χ_{Ao} equal to 580/T (as $\chi_{xx} \equiv 0$ for all segment types X). In this description, differences between the n-alkane CH$_3$- and -CH$_2$- groups (the chain end and middle segments, respectively) are averaged over all segments of the chain molecule.

Aliphatic chains are anisotropic in their polarizability [18, 19]. In the present theory this anisotopy can be incorporated in a primitive way by differentiating between the interactions of the end and middle segments of an n-alkane with the other segments in the system. In homogeneous (isotropic) bulk phases, differences between chain end and middle segments are averaged out and making a distinction does not affect the results. At interfaces preferential structuring may occur and it is important to make a distinction between end and middle segments, especially at solid-fluid interfaces as the solid may have a substantially different interaction with a CH$_3$ segment than with a CH$_2$ segment. Therefore, the adsorption of aliphatic chains is investigated by modelling n-alkanes as B–A_{n-2}–B chains with end segments of type B and middle segments of type A. The A and B segments have different interactions with the solid substrate S only; several values ($\sim 1/T$) will be chosen. The segment-vacancy interaction parameters of the A and B segments are kept the same, i.e. $\chi_{Bo} = \chi_{Ao} = 580/T$ and $\chi_{AB} = 0$, so that the description of the n-alkane bulk and LV interfacial properties as given in Chapter 5 remains the same.

The effect of the chain flexibility on the adsorption isotherms is investigated by comparing SCF calculations for flexible chains (first order Markov chain statistics) to calculations for semi-flexible chains using the RIS scheme. The trans-gauche energy in units of kT (U^{tg}/kT) in the RIS scheme is assigned a value of 290/T. The trans-gauche energies segments A and B within a certain bond are identical.

For many applications the hydrophobicity of solid surfaces is controlled by grafting aliphatic chains to the surface. In our calculations, the simplest model of a hydrophobic solid is a hard wall consisting of aliphatic segments. The interactions of A and B segments with such a solid are described by $\chi_{AS} = \chi_{BS} = 0$ and $\chi_{oS} = \chi_{oA} = 580/T$. We will refer to such a solid as a rigid alkylated surface. With the theory also a more sophisticated description of an alkylated solid is possible, e.g. by considering such a

substrate as a hard solid S with terminally grafted (or chemisorbed) chains. For this purpose, one end of the grafted chain is restricted to the first lattice layer adjacent to the solid surface. The adsorption energy of the restricted end segment is effectively $-\infty$. Except for this difference, the segments of the grafted chains are identical to those of the free (adsorbing) chains. The grafting density σ_g equals the number n_g of grafted chains per lattice layer of L lattice sites according to

$$\sigma_g = n_g / L \tag{16}$$

For the investigation of alkane adsorption and contact angles on soft alkylated surfaces we do not discriminate between the adsorption energies of end and middle segments. Furthermore we will, for these systems, restrict ourselves to first order Markov statistics. Hence, for this part of the study the n-alkanes and the grafted n-alkyl chains are exclusively described as homo-oligomers A_n.

6.3. Vapour adsorption isotherms

The different kinds of experimentally measured hydrocarbon adsorption isotherms are interpreted with the SCF-LFA theory. Before starting the more detailed presentation and discussion of the adsorption isotherms we wish to make a general remark concerning the (small) oscillations occurring in our calculated vapour adsorption isotherms around the condensation axis. These oscillations are lattice-layer condensation steps, artefacts resulting from the lattice and the mean field approximation used. Each lattice layer has a uniform density (mean field), and condenses at a specific chemical potential. When a layer condenses, the amount of material and the chemical potential of the bulk phase suddenly decrease. This results in the (artificial) oscillating behaviour of the chemical potential upon each successive layer condensation. In the lattice layers near the interface, the segment adsorption energy of the surface and the chain length of the molecules dominate the layer-filling. Therefore, at lower adsorbed amounts the oscillations in the adsorption isotherm are much less pronounced or absent. Chain flexibility reduction (or a temperature decrease) results in larger density differences between the vapour and the adsorbed phase. In this case lattice layer condensation steps require more vapour molecules. This increases the oscillation of the chemical potential upon a layer condensation step.

When interpreting the calculated results it should be realized that χ_{AS} is not the standard adsorption energy. It is appropriate to consider the standard adsorption energy of segment A as the energy change upon displacing a vacancy in layer $z=1$ by an A segment: $\chi^d_{AS(o)} = \lambda_{-1} (\chi_{AS} + \chi_{OO} - \chi_{OS} - \chi_{AO})$, where λ_{-1} is the contact fraction between the surface and the first adsorbate (lattice) layer, see also previous Chapter.

Ia: Bare rigid solids without grafted chains

First we consider adsorption of a homo-oligomer (A_8) on a hard impenetrable interface. In Fig. 1 some calculated results are presented for four values of χ_{AS}. In general, a chain molecule adsorbing onto a solid substrate is restricted in its number of conformations. The adsorption energy has to compensate for the entropy loss upon adsorption. If the adsorption energy is not sufficiently negative the molecules do not adsorb. When the chemical potential of the adsorbate (the A_8 vapour pressure) is increased more molecules adsorb. Low adsorption energies are unable to compensate for the entropy loss upon adsorption (see Fig. 1 for $\chi_{AS} \geq -2$), and noticable adsorption only occurs upon supersaturating the vapour. Once the whole supersaturation part of the isotherm has been passed, all layers do fill up and the adsorption diverges to infinity at $p/p_0 = 1$ (condensation). When the adsorption energy becomes more favourable, adsorption occurs at low vapour pressures (see $\chi_{AS} \leq -4$). In order to maximize their configurational entropy the adsorbed molecules stick out from the first lattice layer to the adjacent layers. This means that after some adsorption has occurred at fairly low vapour pressure, the lateral interactions in the first lattice layers adjacent to the solid surface become significant. Therefore, the adsorption proceeds rather strongly when the vapour pressure is further increased and a step in the isotherm occurs. After this step, the vapour boundary side of the adsorbed layer becomes less diffuse. This decreases the lateral interactions and the adsorption rises gradually with the vapour pressure until condensation occurs. For very favourable adsorption energies (see f.i. $\chi_{AS} = -6$), the "step" occurs at much lower vapour pressures and becomes more gradual.

Semi-flexible chains loose less configuration entropy upon adsorption, therefore, they already adsorb at lower pressures than flexible ones. For low adsorption energies this reduces the size of the supersaturation loops. For high adsorption energies semi-flexible chains have a smaller step in the isotherm than flexible ones. Moreover, at higher vapour pressures they adsorb less than flexible ones. An adsorbed semi-flexible chain can increase its number of favourable segment-surface contacts at a lower entropic cost. Therefore, semi-flexible chains adsorb more flat to the surface than flexible ones. Therefore, the molecular volume fractions and the lateral attraction in the lattice layers near the solid will be lower than for flexible chains. This reduces the size of the initial step in the isotherm and the further adsorption (compare panels a and b with c and d in Fig. 1 for $\chi_{AS} \leq -4$ kT).

As a second case we consider the adsorption of aliphatic chains $B\text{-}A_6\text{-}B$ while differentiating between the adsorption energies of chain end segments B (the CH_3 groups) and chain middle segments A (the CH_2 groups). In Figs. 2 and 3 some
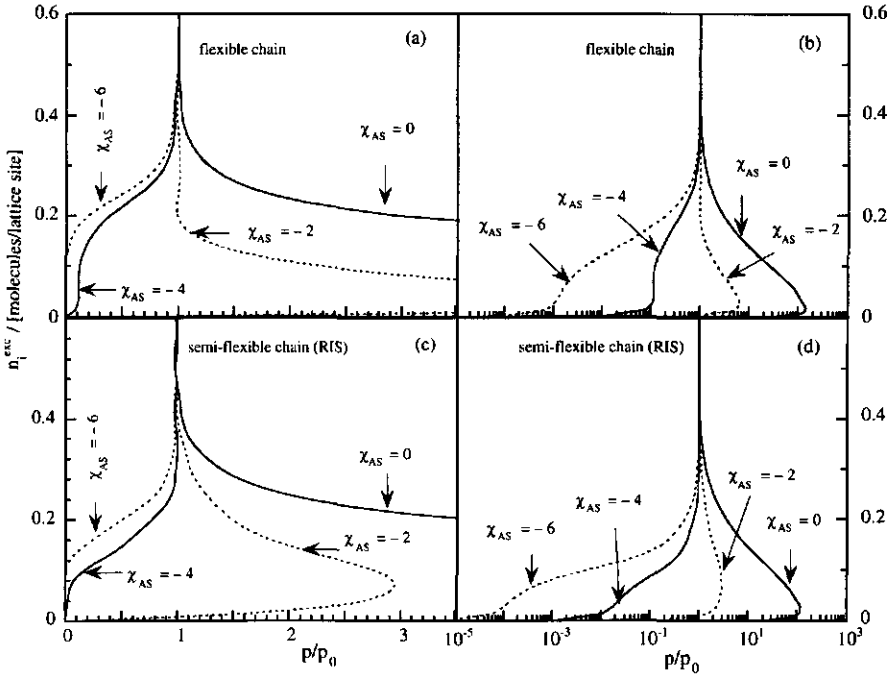
Figure 1. The surface excess amount (at T = 290 K) of a homo-oligomer (A_8) as a function of its relative pressure for different χ_{AS} values as indicated in the figure, $\chi_{OS} = 0$ and $\chi_{AO} = 2$. In a) and b) the results for first order Markov chain statistics are shown on a linear and logarithmic axis, respectively. Figures c) and d) are identical plots obtained by applying the RIS scheme with $U^{tg}/kT = 1$.

calculated vapour adsorption isotherms of the octamer $B\text{-}A_6\text{-}B$ are plotted against the relative vapour pressure for different adsorption energies χ_{AS} and χ_{BS}.

First we discuss the isotherms of a flexible chain with a low middle segment-surface interaction parameter, $\chi_{AS} = -2$ (Fig. 2a and b) using the homogeneous chain with $\chi_{BS} = \chi_{AS} = -2$ as standard. If χ_{BS} is less favourable than χ_{AS} this decreases adsorption and increases the supersaturation loop in the isotherm. When χ_{BS} is decreased below χ_{AS}, the size of the supersaturation loop decreases and the isotherm has an initial step/loop after which the adsorption significantly increases with the vapour pressure. Decreasing χ_{BS} implies that adsorbed chains will stick out more strongly from the interface. The lateral attractions are effective over more lattice layers and, especially at higher adsorption values, end on adsorption becomes more favourable. When $\chi_{BS} < \chi_{AS}$, after the initial step in the isotherm, higher adsorbed amounts occur for $B\text{-}A_6\text{-}B$ than for A_8.
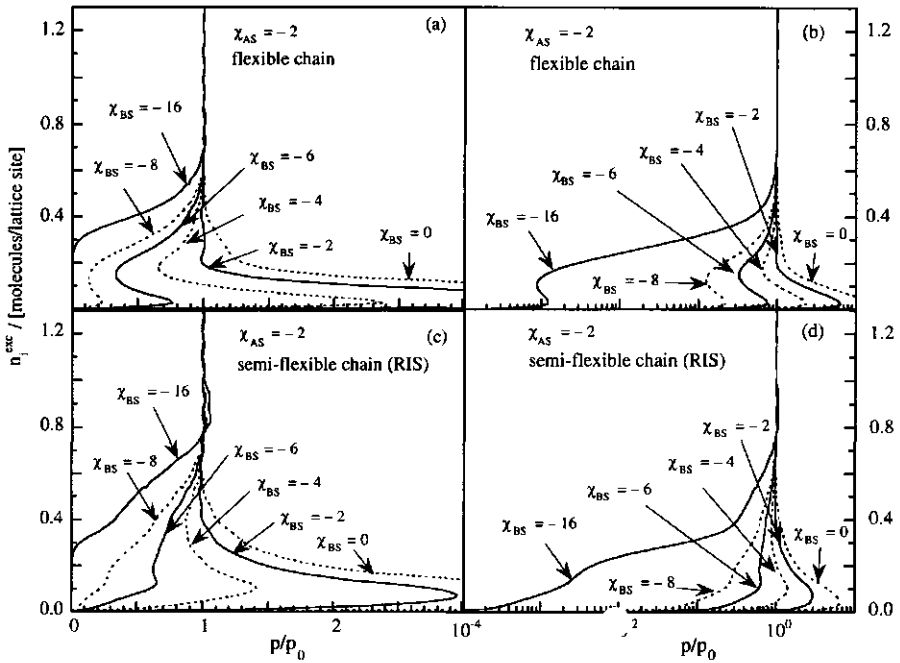
Figure 2. The excess adsorbed amount of B-A$_6$-B plotted against the vapour pressure for $\chi_{AO} = \chi_{BO} = 2$, $\chi_{AB} = 0$, $\chi_{OS} = 0$ and $\chi_{AS} = -2$, the χ_{BS} values are denoted in the figures. In panels (a) and (b) the results for first order Markov statistics are shown. Panels (c) and (d) show the results obtained upon applying the RIS scheme with $U^{tg}/kT = 1$.

Now consider adsorption of semi-flexible chains (Fig. 2c and d). As explained previously, the initial adsorption of semi-flexible chains is higher than that of flexible ones (compare panels a and b with c and d in Fig. 2); this also reduces the supersaturation loops in the isotherms. For $\chi_{BS} > \chi_{AS}$ (weak end segment-surface interactions), semi-flexible chains initally adsorb more strongly to the interface than flexible ones as their entropic penalty for flat adsorption is less than for flexible chains. At higher vapour pressures semi-flexible and flexible chain behave rather alike. For $\chi_{BS} < \chi_{AS}$ (strong end segment-surface interaction), semi-flexible chains initially adsorb more strongly to the interface than flexible ones. At higher surface coverages this effect is inversed. In this case the adsorbed semi-flexible chains extend further from the interface than flexible ones. This raises the volume fractions and lateral interactions in the lattice layers near the solid and enhances adsorption. For $\chi_{BS} = -16$ the chains have a strong preference to adsorb with their end segments. Close to the saturated vapour pressure only one end segment per chain is adsorbed and the semi-flexible chains form a densely packed layer of end-on adsorbed molecules. The vapour boundary side of this layer is rather sharp. Therefore, adsorption onto this layer is entropically
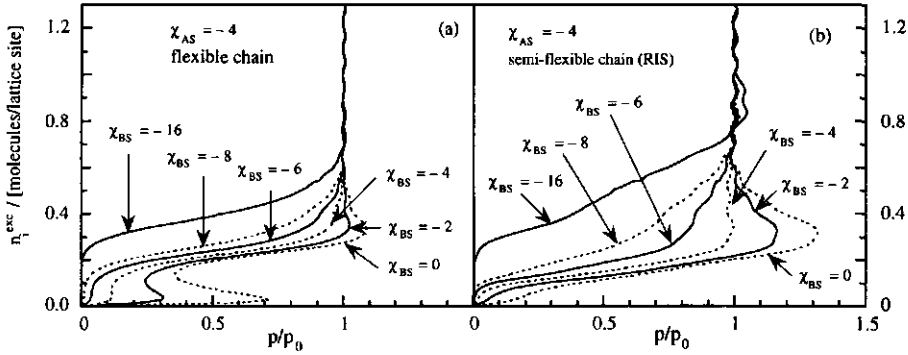
Figure 3. The excess adsorbed amount of the octameric molecules (B-A$_6$-B) plotted against the vapour pressure for $\chi_{AO} = \chi_{BO} = 2$, $\chi_{AB} = 0$, $\chi_{OS} = 0$ and $\chi_{AS} = -4$, the χ_{BS} values are denoted in the figures. In panel (a) the results for first order Markov statistics are shown. Panel (b) shows results obtained using the RIS scheme with $U^{1g}/kT = 1$.

unfavourable and a slight supersaturation is required before molecular multilayer condensation occurs (see Fig. 2c and d for $\chi_{BS} = -16$). Flexible chains with $\chi_{BS} = -16$ have a higher fraction of molecules with both end segments adsorbed than semi-flexible chains. Therefore, their alignment in the adsorbed layer is more difficult and less perfect than for semi-flexible chains and no supersaturation loop occurs (see Fig. 2a and b).

Next we discuss adsorption of B-A_6-B with $\chi_{AS} = -4$ (Fig. 3). These isotherms resemble the ones in Fig. 2. For $\chi_{BS} \geq \chi_{AS}$, the isotherms in Fig. 3 are higher than those of Fig. 2, at low pressures more molecules adsorb in the first layer due to the lower χ_{AS} value. At somewhat higher pressures, these higher adsorbed amounts enhance the lateral atttractions so that the initial step in the isotherm in Fig. 3 occurs at much lower pressures than in Fig. 2. For $\chi_{BS} < \chi_{AS}$, the high middle segment adsorption energy makes the initial adsorption in Fig. 3 higher than of Fig. 2. Furthermore, the intial step in the isotherm is shifted to lower vapour pressures. However, once beyond the initial step, the isotherms with $\chi_{BS} < \chi_{AS}$ of Fig. 3 are lower than the ones in Fig. 2. In Fig. 3 the chains adsorb in a more flat configuration than in Fig. 2. This decreases the segmental volume fractions and lateral attractions in the lattice layers further away from the surface and results in lower adsorbed amounts. When the flexibility of the chains in Fig. 3a is reduced this results in an flatter adsorption and in lower adsorbed amounts (compare Figs. 3a and 3b). For the lower values of χ_{BS} and higher relative vapour pressures, the chains tend to be end-on adsorbed, leading to relatively high adsorption values. For $\chi_{BS} = -16$, the end segment adsorption energy is so large that it dominates the adsorption and the isotherms in Figs. 2 and 3 are very similar.

Ib: Rigid surfaces; solids completely grafted with chains

In the SCF-LFA theory, the simplest case of an alkylated solid is a flat solid covered with a completely filled monolayer of end-grafted aliphatic chains (σ_g=1). Adsorption onto such a substrate does not alter the structure of the grafted layer and is independent of the grafted chain length or the underlying solid. A flexible homo-octamer A_8, adsorbing on a rigid alkylated solid grafted with chains of segments A, with $\chi_{oA} = 2$, yields an identical adsorption isotherm as the one shown in Fig. 1a and b with $\chi_{AS} = -2$, $\chi_{OS} = 0$, $\chi_{Ao} = 2$. In both cases the displacement energy $\chi_{AS(o)}^d$ equals -4.

Ic: Volume fraction profiles of octamer films on rigid substrates

For the discussion and understanding of the adsorption behaviour of chain molecules at rigid substrates it is instructive to compare the structures of the adsorbed layers fromed on the different substrates. With the SCF-LFA theory these structures can be easily investigated by means of segment density profiles. In Fig. 4 the segment density profiles of the adsorbed octamer films ($\Gamma_{\ddagger}$) formed at p/p_0=1 on two rigid solids (χ_{AS} = 0 and $\chi_{AS} = -4$), investigated in the section Ia, are plotted semilogarithmically. Also the octamer profile on a completely alkylated surface (σ_g=1) is included. Both the end and middle segment density profiles of the adsorbate chains are plotted. The end segments are indicated as "CH$_3$" the middle segments as "C H$_2$". Despite the different nomenclature of the chain end and middle segments, no distinction is made between their interactions; in the calculations both are represented by the same segment type A. In the figures, the solid surface is positioned in layer 0, for σ_g= 1, layer z=1 is the first lattice layer adjacent to the (fully occupied) grafted layer. The lattice layers $z \geq 13$ are part of the homogeneous bulk vapour phase.

In an isotropic octameric bulk the CH$_3$:CH$_2$ density ratio equals 1:3. In Fig. 4 this 1:3 ratio corresponds to the difference (in cm) between the "CH$_3$" and "C H$_2$" segment volume fractions in the vapour phase (i.e., for $z \geq 13$). When this difference is below the bulk value, this means that the CH$_3$:CH$_2$ density ratio in that layer is above that in bulk vapour, i.e., in such a layer the end segments are preferred over the middle segments.

The thickness of the adsorbed layer in Fig. 4 increases with increasing affinity of the segments for the surface (i.e., with decreasing $\chi_{AS(o)}^d$). For all (rigid) substrates shown in Fig. 4 the decay of the volume fraction in the adsorbed layer extends over about 5
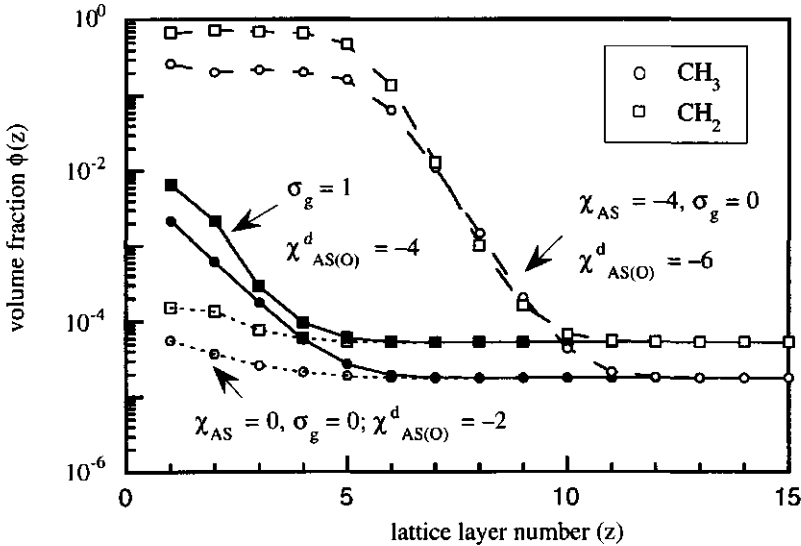
Figure 4. *Volume fractions of the end ("CH₃") and middle ("CH₂") segments of an octamer A₈ on rigid substrates for each lattice layer z. The profiles shown correspond to the adsorbed octamer films ($\Gamma_{\downarrow}$) formed at p/p₀=1 on the substrates with σ_g =0 and σ_g =1 of with $\chi_{AS} = 0$ or $\chi_{AS} = -4$, $\chi_{os} = 0$ and $\chi_{A_0} = 2$. The solid surface is positioned in layer 0, lattice layers z ≥ 13 are part of the homogeneous bulk vapour phase. For σ_g =1 the volume fractions within the grafted layer are not shown, here layer z=1 is the first lattice layer adjacent to the (fully occupied) grafted layer.*

lattice layers. For the substrate with $\chi_{AS} = -4$, the CH_3:CH_2 density ratio in the layers z=2 to z=4 virtually equals that in the bulk. This implies that the adsorbed layer has properties of bulk liquid. The CH_3:CH_2 ratio in the first lattice layer near the solid exceeds that in isotropic bulk. For entropic reasons the end segments have a slight preference for the surface over the middle segments. In the decay regions of Fig. 4, the "CH_3" and "CH_2" segment profiles approach each other. For $\chi_{AS} = 0$ this effect is minimal, for more favourable adsorption energies this effect becomes more pronounced. It displays the rather strong preference of the end segments to stick out from the substrate. When chain ends are exposed to the vapour boundary side of the adsorbed layer this optimizes the configuration entropy of the adsorbed chains. Finally we wish to remark that for a substrate with $\chi_{AS} = -4$ with a thicker adsorbed layer than the one shown in Fig. 4, the same density profile is expected but than with the decay region shifted to the right.

115

IIa: Soft surfaces: solids partially grafted with chains

Molecules adsorbing on substrates that are partially grafted with chains are able to penetrate the grafted layer and alter its structure. Therefore, we will refer to such a substrate as a "soft surface". On a soft surface, both adsorbing and grafted chains occur in the lattice layers adjacent to the surface. This affects the volume fractions, lateral interactions and entropy in these layers. The adsorption of an octameric fluid A_8 onto soft surfaces with grafted chains A_n is investigated for different grafting densities and grafting chain lengths n. This is done for two different interactions (χ_{AS}) between the bare surface S and the A segments. In Fig. 5 χ_{AS} equals 0, in Fig. 6 χ_{AS} equals -4.

When a solid with $\chi_{AS} = 0$ (Fig. 5) is grafted, the interactions of the adsorbate segments with segments of the grafted chains are more favourable than with the (bare) solid itself. Grafting monomers onto such a solid hardly imposes extra conformation restrictions on the adsorbing molecules with respect to their adsorption on the bare solid. The main effect of monomer-grafting is the increased affinity of the adsorbing molecules for the substrate; the adsorption continuously increases with increasing monomer grafting density (see Fig. 5a). For low grafting densities ($\sigma_g \leq 0.25$) of tetramers (Fig. 5b) and octamers (Fig. 5c) the adsorption also increases with σ_g. However, by further increasing the tetramer or octamer grafting density, the order in the grafted layer increases together with the (configuration) entropy loss upon adsorption. Adsorption of chains within the grafted layer now leads to considerable entropy losses and hardly occurs. Therefore, the adsorption (eventually) decreases with increasing σ_g and a maximum occurs in the adsorbed amount as a function of σ_g (see Fig. 5 panels b and c). Longer grafted chains affect the configurational entropy in the lattice layers adjacent to the surface more strongly than shorter ones. Hence, the maximum adsorption for the first occurs at lower σ_g values than for the latter, compare panels (b) and (c) in Fig. 5.

On the solid with a high adsorption energy (Fig. 6) the interactions of the adsorbate segments with the solid itself are more favourable than those with the grafted chains. In general, increasing the grafting density on such a solid decreases the adsorbed amounts. An exception to this trend occurs for low grafting densities and low vapour pressures. In this case grafted chains increase the adsorption compared to the bare solid (see Figs. 6a and b for $\sigma_g = 0.25$). For low vapour pressures and $\sigma_g = 0.25$, the adsorption energy gain due to the formation of adsorbate segment - solid contacts is still considerable. In addition to this adsorption energy, the adsorbate also has favourable lateral interactions with the grafted chains so that the adsorption is increased. The segments of the grafted chain also adsorb on the high affinity solid ($\chi_{AS} = -4$). This decreases the lateral interactions in the outer part of the grafted layer. Moreover, at low grafting densities

Figure. 5. Octamer (A_8) adsorption isotherms on alkylated substrates with 4 different grafting densities (0, 0.25, 0.5, 0.75 and 1), $\chi_{AS} = 0$, $\chi_{OS} = 0$ and $\chi_{AO} = 2$. Different homogeneous grafted chains A_n are examined; (a) n = 1, (b) n = 4 and (c) n = 8.
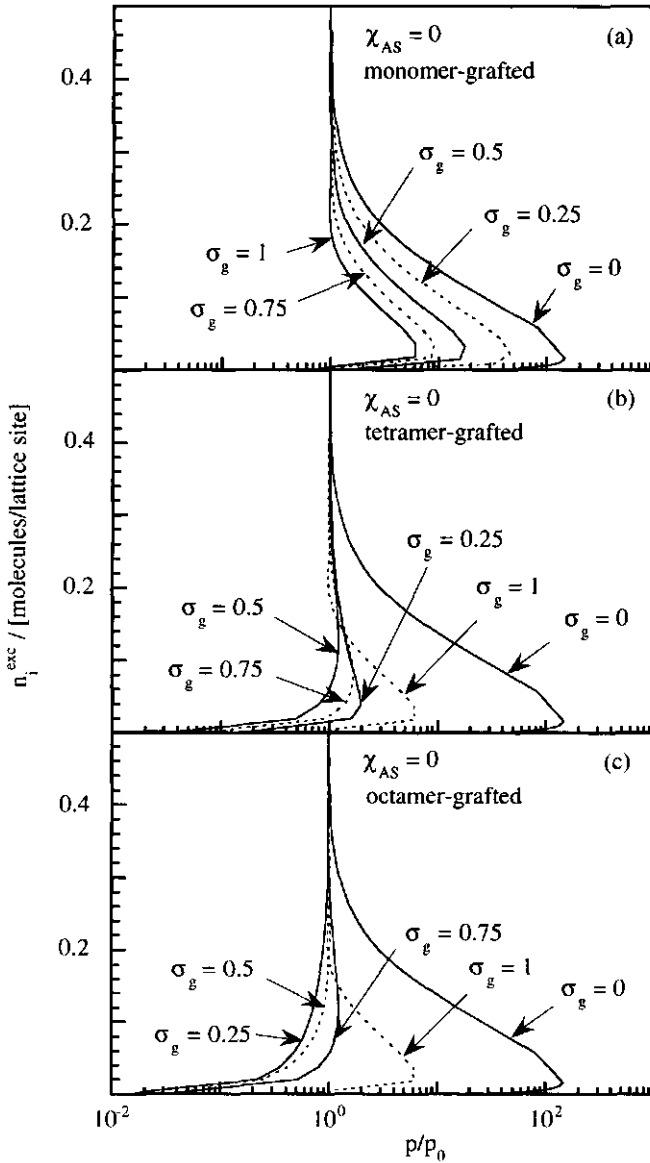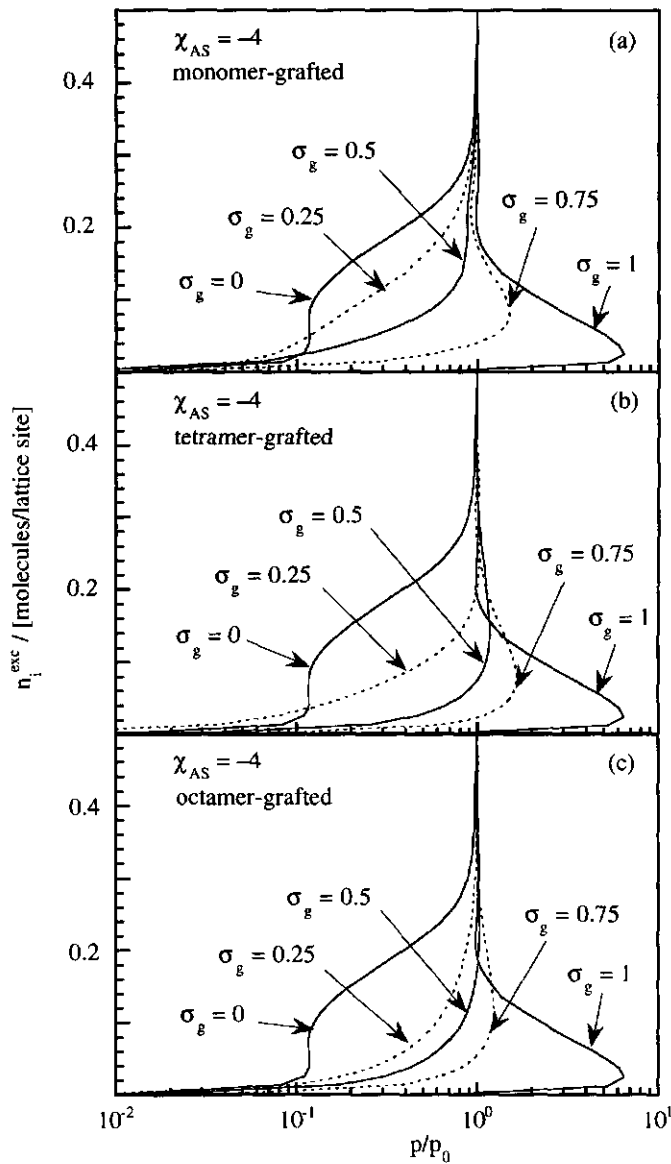
117

Figure 6. Octamer (A₈) adsorption isotherms on alkylated substrates with 4 different grafting densities (0, 0.25, 0.5, 0.75 and 1), $\chi_{AS} = -4$, $\chi_{OS} = 0$ and $\chi_{AO} = 2$. *Different homogeneous grafted chains A$_n$ are examined; (a) n = 1, (b) n = 4 and (c) n = 8.*

(for $\sigma_g \leq 0.25$) longer grafted chains screen the underlying solid more effectively than shorter ones and the initial part of the isotherms with $\sigma_g=0.25$ in Fig. 6 is lower for substrates with longer grafted chains than for substrates with shorter grafted chains.

IIb: Volume fraction profiles of octamer films on soft surfaces

In Figs. 7 and 8 the respective volume faction profiles on the substrates of Figs. 5 and 6 with $\sigma_g=0.25$ and $\sigma_g=0.75$ are considered. The end and middle segment density profiles of both the grafted and adsorbing chains are shown. The end and middle segments of the adsorbate are indicated as "CH$_3$ octane" and "CH$_2$ octane", respectively. The end segment of a grafted chain which is restricted to the solid is denoted as "S-CH$_2$ grafted". The middle segments of the grafted chains are denoted by "CH$_2$ grafted", the free end segment of the grafted chain is denoted as "CH$_3$ grafted". The nomenclature used only serves to distinghuish the end and middle segments of the chains. No distinction is made between the interactions of the CH$_3$ and CH$_2$ groups; both are represented by the same segment type A.

The volume fraction profiles in Figs. 7 and 8 reveal that at the vapour side of the adsorbed layer end segments are preferred over middle segments. With increasing grafting density the grafted layer extends further from the solid. Moreover, the preference of the free, unrestricted end segment of the grafted chain to be far from the solid surface is enhanced. Increasing σ_g renders the grafted layer less diffuse, and its profile more stepwise. From Monte Carlo simulations of grafted chains in a poor solvent [20] similar conclusions are drawn. Our calculations also show that the vapour boundary of the grafted layer becomes more diffuse when the chain length of the grafted molecules is increased. A more diffure boundary of the grafted layer increases the lateral interactions between the adsorbate and grafted chains in the outer part of the grafted layer. This enhances adsorption.

Within the grafted layer close to the solid, adsorbate end segments are, for entropic reasons, preferred over adsorbate middle segments, see panels (d) and (f) in Figs. 7 and 8. In the outer part of the grafted layer (e.g. for octamer-grafted solids in lattice layers $z=6$, $z=7$ and $z=8$) the highest volume fractions of adsorbing segments are found. Moreover, the CH$_3$:CH$_2$ ratio of the adsorbate in these layers is below that in bulk. This implies that adsorption on soft alkylated surfaces is largely due to the accumulation of adsorbate chain middle segments in the outer part of the grafted layer.

At high(er) grafting densities and long(er) grafted chains, the lattice layers close to the solid become increasingly filled with segments of the grafted chains. This expels the adsorbate segments from the lattice layers near the surface to the layers where the volume fractions of the grafted segments are lower, see Figs. 7 and 8.
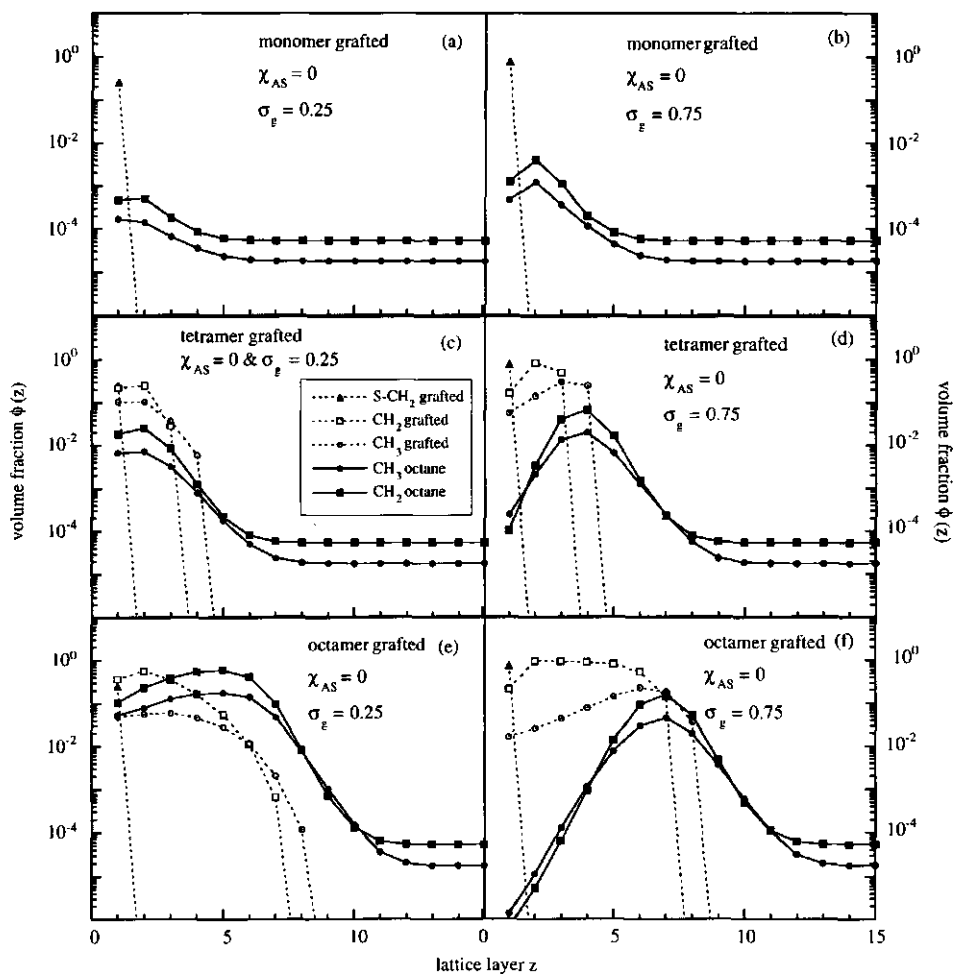
Figure 7. Volume fractions of the end ("CH3") and middle ("CH2") segments in each lattice layer z. The profiles shown correspond to the adsorbed octamer films ($\Gamma_\pm$) formed at $p/p_0=1$ on the substrates with $\sigma_g=0.25$ and 0.75 for which the adsorption isotherms are shown Fig. 5. The grafted segments are denoted by open symbols and dashed curves, the adsorbate segments correspond to the closed symbols and drawn curves. The solid surface is positioned in layer 0, lattice layers $z \geq 15$ are part of the homogeneous bulk vapour phase.

120
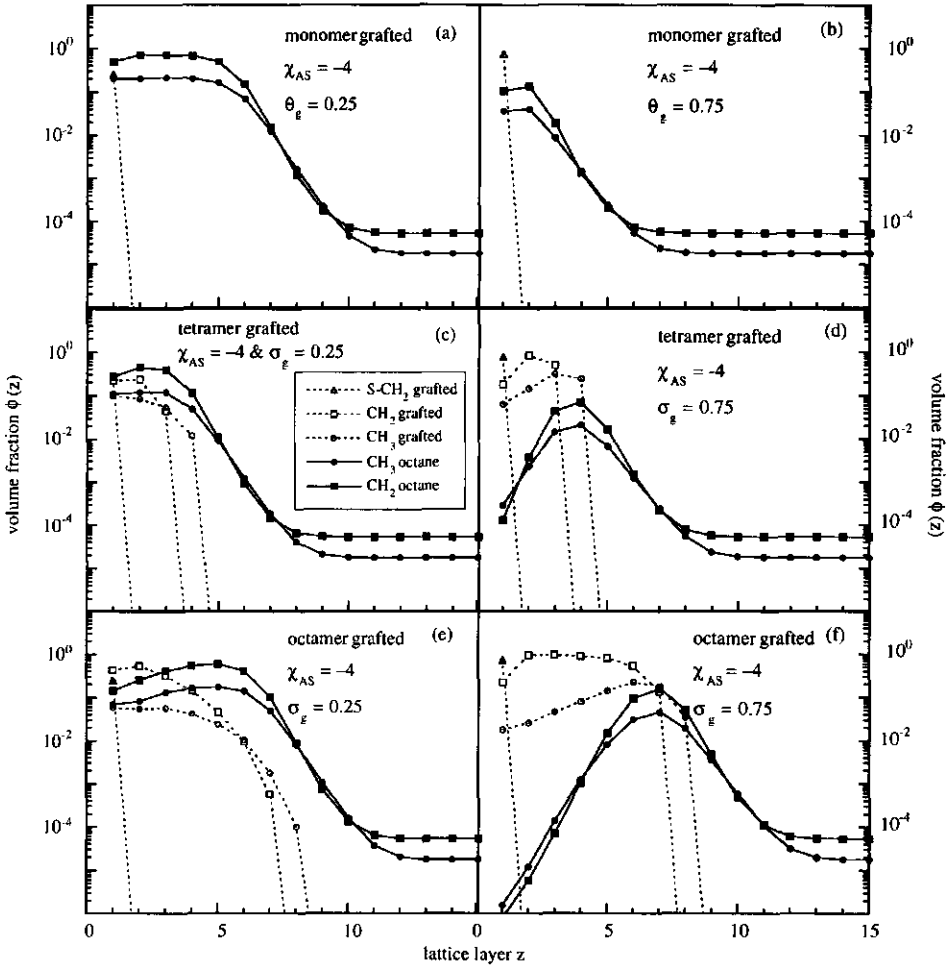
Figure 8. Volume fractions of the end ("CH₃") and middle ("CH₂") segments in each lattice layer z. The profiles shown correspond to the adsorbed octamer films ($\Gamma_{\ddagger}$) formed at p/p₀=1 on the substrates with σ_g =0.25 and 0.75 for which the adsorption isotherms are shown Fig. 6. The grafted segments are denoted by open symbols and dashed curves, the adsorbate segments correspond to the closed symbols and drawn curves. The solid surface is positioned in layer 0, lattice layers z ≥ 15 are part of the homogeneous bulk vapour phase.

When comparing the volume fraction profiles on the low affinity substrates (Fig. 7) to the ones on the high affinity substrates (Fig. 8), the grafted chains on the latter have a lower preference to stretch from the substrate. In Fig. 8 the segments are more strongly attracted by the solid than in Fig. 7. At high grafting densities of tetramers and octamers, the first lattice layers near the solid are almost exclusively filled by segments of the grafted chains, see Figs. 7 and 8. The solid is now practically screened by the grafted molecules and adsorption is mainly due to the adsorbate - grafted chain interactions. In this case the adsorption hardly depends on the adsorption energy of the solid, see also Figs. 5 and 6.

For very long grafted chains, the adsorption will almost entirely be determined by the interactions between the adsorbate and the grafted chains. For substrates with very long grafted chains, the volume fractions profiles and adsorption of the adsorbate segments will not be affected when changing the chain length of the grafted molecules. The density profile and the adsorption will only shift to lattice layers further away from the solid surface. This is not yet the case in Figs. 7 and 8 for which the changes in volume fraction profiles are still significant when grafting octamers instead of tetramers.

III: Comparison with measured alkane adsorption on bare and methylated silica

The calculated isotherm of a semi-flexible B-A_6-B chain with $\chi_{BS} = -8$ and $\chi_{AS} = -2$ (see Fig. 2c) resembles the experimentally observed linear adsorption isotherm of normal octane on silica (see Chapter 4). With increasing surface coverage the adsorbed molecules line up in a direction perpendicular to the surface, due to the favourable end segment adsorption energy. This increases the lateral interactions in the lattice layers adjacent to the solid but also decreases the configurational entropy of the adsorbed chains. These two opposing effects make that the vapour adsorption increases approximately linearly with the vapour pressure. This is in good agreement with the experimental results. Experimental studies showed that the adsorbed amount near $p/p_0 = 0.9$, was about the value corresponding to a monolayer of perpendicularly oriented alkanes (see Chapter 4). Our calculations yield lower adsorbed amounts. Probably, the chain flexibility is overestimated in the model so that the chains do not stretch up to 8 lattice layers from the surface. This results in an underestimation of the lateral attractions and of the adsorption in these layers. The quantitative agreement could be improved when chain end segments are assigned a different, more unfavourable, interaction with the vacancies than the chain middle segments. This will

increase the tendency of the chains to adsorb end on and also promote (further) adsorption at the vapour boundary of the end on adsorbed layer. The flexibility of the chains can be affected by assigning different values to the trans-gauche energies of the chain end and middle segments. If chain end segments have higher trans-gauche energies than middle segments they will adsorb more strongly than the middle ones, this will improve the quantitative agreement. For a more quantitative explanation of the measured linear isotherms these aspects require further investigation.

Experimental alkane adsorption isotherms on alkylated substrates are below the monolayer coverage for parallel adsorbed molecules until close to saturation (see Chapter 4). This behaviour can be reproduced by describing alkanes, adsorbing on a rigid alkylated solid, as semi-flexible chains A_8 with modest segment adsorption energies ($\chi_{AS} \geq -2$) or as B-A_6-B chains with a high middle segment adsorption energy ($\chi_{AS} = -4$) and a low end segment adsorption energies ($\chi_{BS} \geq -2$).

The calculations show that, in general, grafting of (alkyl) chains onto a solid with a high affinity for the chain-like adsorbate considerably reduces the adsorption at all grafting densities (see Fig. 6). The theoretical isotherms on such soft alkykated solids also agree qualitatively with experminetally measured ones (see Chapter 4). For all the cases in which qualitative agreement with experimental alkane adsorption isotherms on alkylated solids is found, adsorption of the adsorbate middle segments is more favourable than adsorption of the end segments of the adsorbate. Such behaviour can be due to different segment-surface interaction parameters of the chain end and middle segments. Moreover, this behaviour may also result from entropic effects that lead to preferential adsorption of middle segments within the grafted layer. By simulaneously considering both effects in our description of alkane adsorption on alkylated solids, a better quantitative agreement between theory and experiment can be obtained. However, this remains a task for the future.

6.4. Wettability of aliphatic fluids at solid substrates

Temperature dependence of alkane contact angles on rigid/fully alkylated surfaces

As explained in section 6.2. the SCF theory allows to calculate the wetting behaviour. For the calculation of the contact angle two ways are open: (i) substituting the (calculated) adsorption isotherm data in Eq. (9) or (ii) inserting the interfacial tensions calculated from Eq. (12) in Eq. (15). In general, the wettability in a solid-liquid-vapour system depends on the temperature. With increasing temperature, the wetting behaviour can change from partial to complete wetting.
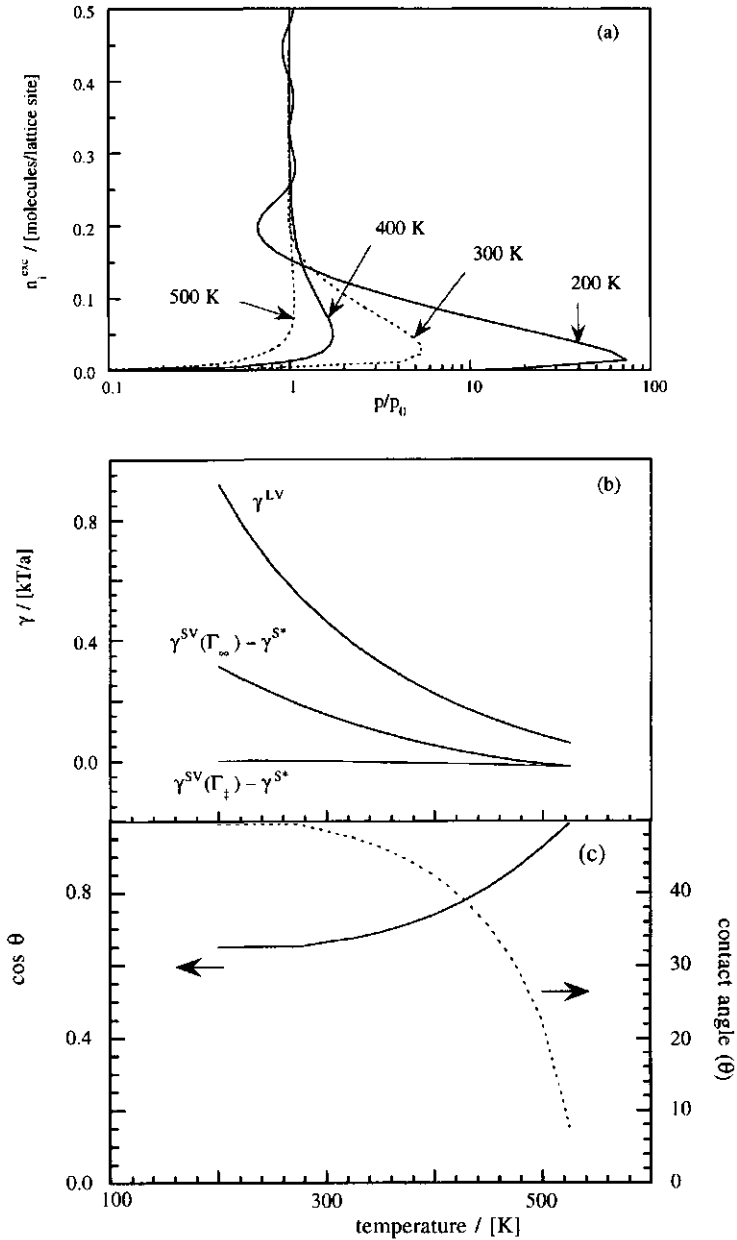
Figure 9. (a) Semilogarthmic adsorption isotherms of an aliphatic octameric fluid (A₈) on a rigid alkylated surface (S) at different temperatures T. Interactions used are $\chi_{AS} = 0$, $\chi_{aS} = 580/T$ and $\chi_{AO} = 580/T$. (b) Calculated $\gamma^{sv}(\Gamma_{\ddagger}) - \gamma^{s*}$, $\gamma^{sv}(\Gamma_{\infty}) - \gamma^{s*}$, and γ^{LV} values for an octamer on the rigid alkylated solid specified in (a). (c) Cosines of the contact angle (solid) and contact angle (dashed) at different temperatures T calculated using Eq. (15) and the data plotted in Fig. 9b.

In Fig. 9a some calculated adsorption isotherms of an octameric fluid (A_8) on a rigid alkylated surface are plotted for several temperatures. The interaction parameters used are $\chi_{AS} = 0$, $\chi_{OS} = 580/T$, $\chi_{AO} = 580/T$. All isotherms have very low adsorbed amounts and intersect the saturation axis ($p/p_0 = 1$) with a finite adsorption. With increasing temperature the size of the supersaturation loop decreases. At 500 K the supersaturation loop has practically disappeared.

With the SCF theory also $\gamma^{sv}(\Gamma_{\ddagger}) - \gamma^{s^*}$, $\gamma^{sv}(\Gamma_{\infty}) - \gamma^{s^*}$, and γ^{LV} of an octameric fluid at the rigid alkylated surface of Fig. 9a are calculated as a function of temperature. The results are plotted in Fig. 9b. The calculated interfacial tensions are expressed in units of kT per lattice site area. In our model the lattice area equals 0.09 nm^2, hence in order to transform the calculated values to units of J/m^2 we have to multiply with $kT/0.09 \cdot 10^{-18}$. Figure 9b shows that γ^{LV} strongly depends on the temperature, for a discussion of γ^{LV} and its temperature dependence we refer to Chapter 5. Figure 9b also shows that on the rigid substrate $\gamma^{sv}(\Gamma_{\ddagger}) - \gamma^{s^*}$ hardly depends on the temperature.

From the interfacial tensions in Fig. 9b the contact angle is calculated as a function of temperature by means of Eq. (15). The results are shown in Fig. 9c. Figures 9a and 9c clearly show that the contact angle decreases with the area of the supersaturation loop (from $\Gamma_{\ddagger}$ to Γ_{∞} in the isotherm, see Eq. 9); both decrease when the temperature is increased.

The results shown in Fig. 9 are in agreement with the Cahn prediction that for temperatures sufficiently close to the critical point (for our octamer 622 K) complete wetting occurs [21]. Moreover, Fig. 9 shows that the temperature dependence of the contact angle on the rigid alkylated surface is mainly due to the temperature dependencies of $\gamma^{sv}(\Gamma_{\infty}) - \gamma^{s^*}$ and γ^{LV}.

Alkane contact angles on soft/partially alkylated surfaces

Contact angles of an octameric liquid on two different solids with terminally grafted chains are calculated for different grafting densities and grafting chain lengths. The two solids differ with respect to the affinity of the bare, ungrafted surface for the aliphatic segments and have been previously considered in Figs. 4-8. The parameter choice in Fig 10a is identical to the one in Figs. 5 and 7, the parameters in Fig. 10b are the same as those used in Figs. 6 and 8. In order to display the trend more clearly also a grafted chain length of 16 is included in Fig. 10b.

On the bare solid with $\chi_{AS} = 0$ (Fig. 10a) the affinity of the solid for the aliphatic segments is low and the wettability is poor. In general, grafting aliphatic chains to the low affinity solid increases the wettability and decreases the contact angle. When
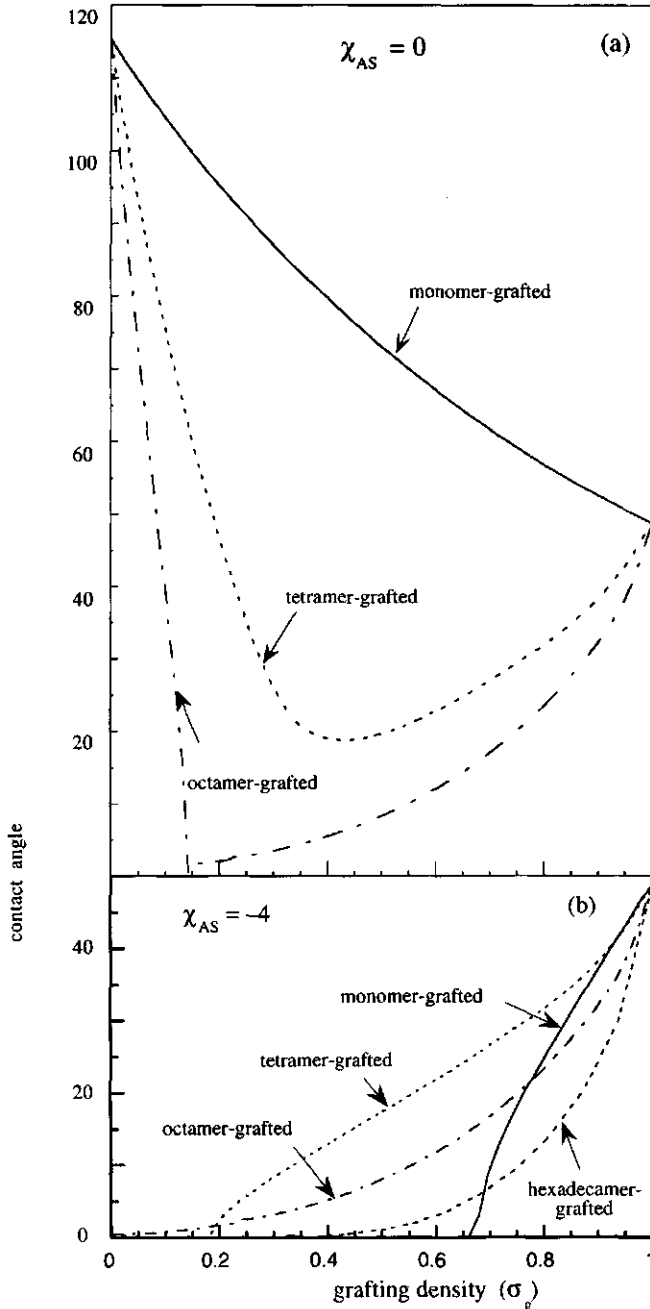
Figure 10. Contact angles of an octameric (A_8) liquid on two different solids as a function of the grafting density. Four different grafted chains A_n with $n=1$, 4 and 8 are examined. Panel (a): low affinity solid ($\chi_{AS} = 0$, $\chi_{OS} = 0$ and $\chi_{AO} = 2$). Panel (b): high affinity solid, $\chi_{AS} = -4$, $\chi_{OS} = 0$ and $\chi_{AO} = 2$, in order to display the trend more clearly we also included a hexadecamer-grafted surface (n=16).

monomers are grafted to the solid, the effective affinity of the liquid molecules for the substrate increases (see also Figs. 5 and 7 and their discussion) and the contact angle gradually decreases with increasing σ_g. In the present case the grafted segments are placed on top of the surface. Adsorption of adsorbate segments onto the grafted monomers is more favourable than adsorption on the bare solid. This largely accounts for the contact angle decrease with increasing σ_g. Moreover, monomer grafting with $\sigma_g < 0.5$ creates adsorption sites inbetween the grafted monomers with a rather favourable adsorption energy (due to the lateral attractions). Hence, initially the contact angle on the low affinity solid decreases rather strongly with increasing σ_g. When the first lattice layer becomes predominantly filled by grafted monomers, adsorbate molecules loose more configurational entropy when they adsorb into this layer and the contact angle decrease becomes more gradual. For a monomer-grafted substrate, the maximal number of high energy contacts possible within the first lattice layer (inbetween the grafted monomers) is reached at $\sigma_g = 0.5$ and for $\sigma_g > 0.5$, the number of high energy sites within the grafted layer diminishes. This also contributes to the more gradual contact angle decrease when increasing σ_g beyond 0.5.

When longer chains are grafted to the surface a pronounced minimum in the θ vs. σ_g plot occurs. With increasing grafted chain length this minimum decreases, moreover, the initial slope of the θ vs. σ_g plot becomes more negative. As a consequence, the minimum in the θ vs. σ_g plot shifts to lower grafting densities and lower contact angle values. The grafted chain-adsorbate contacts are more favourable than the adsorbate-(bare) solid contacts. Therefore, the adsorption increases (and the contact angle decreases) with the grafted chain length and/or with σ_g as long as this is not opposed by entropy effects within the grafted layer. At higher grafting densities of teramers and octamers entropy effects within the grafted layer become more important and begin to oppose adsorption; the contact angle starts to increase with increasing grafting density. For longer grafted chains this already occurs at lower grafting densities than for shorter chains.

For high affinity solids ($\chi_{AS} = -4$, Fig. 10b), increasing the grafting density (eventually) increases the contact angle as the grafted chains decrease the adsorption free energy. When the substrate is grafted with monomers the octameric liquid remains completely wetting (zero contact angle) up to grafting densities of 0.67. For σ_g above 0.67 the contact angle sharply increases with the grafting density. On a tetramer-grafted surface an octameric liquid becomes partially wetting at grafting densities of 0.17. When octamers (or even hexadecamers) are grafted on the solid, the contact angle already increases at grafting densities close to zero. Furthermore, increasing the chain length of the grafted molecules results in a more gradual transition from complete ($\theta = 0$) to partial wetting.

127

Grafting of a solid changes the volume fractions and lateral interactions in the adsorbed layer. Furthermore, the presence of grafted chains affects the configurational entropy of the adsorbed layer. When increasing the grafted chain length and/or σ_g, the screening of the solid underlying the grafted layer increases. On the low affinity solid (with $\chi_{AS}=0$, Fig. 10a) the grafted chains prefer to stretch from the surface for entropic reasons. This also occurs on the high affinity solid with rather high σ_g ($\chi_{AS}=-4$, Fig. 10b). Stretching of the grafted chains increases the adsorbate-surface interactions by means of the increased lateral attractions. Therefore, in general, longer grafted chains result in lower contact angles than shorter ones. The minimum in the θ vs. σ_g curve in Fig. 10a occurs due to the optimum in the number of configurations of the grafted and adsorbed chains as a function of σ_g: when the grafted layer gets more dense, it becomes increasingly difficult for the adsorbate to penetrate into the grafted layer. On a high affinity solid ($\chi_{AS}=-4$, Fig. 10b) the segments of the grafted chains adsorb onto the solid. Hence, at low grafting densities, the grafted molecules ly rather parallel to the solid surface. Therefore, shorter grafted chains are less capable to screen the high affinity solid than longer ones and require higher grafting densities in order to obtain a finite contact angle. As explained previously, at rather high σ_g, longer grafted molecules stretch further and more easily from the solid than shorter ones. On the high affinity solid this not only decreases the contact angle but also renders the transition from complete to partial wetting more gradual. In general, for very high σ_g and long grafted chains (larger than tetramers), the solid is completely screened by the grafted layer and the contact angle becomes virtually independent of the solid underlying the grafted layer (compare f.i. the tetramer and octamer grafted substrates with $\sigma_g > 0.5$ in Figs. 10a and b).

Chain length dependency of the contact angle and critical surface tension

The equilibrium contact angles of (aliphatic) chain-molecular liquids on a hard alkylated surface are calculated for different chain lengths of the wetting liquid. These calculations are performed for several temperatures. In Fig. 11 the resulting $\cos\theta$ values are plotted against the LV interfacial tension of the chain molecular liquid. In the figure the lowest $\cos\theta$ value at a certain temperature always corresponds to A_{20}, the shortest partially wetting liquid is also indicated.

A linear relation between $\cos\theta$ and γ^{LV} is found for each temperature. The contact angle decreases with decreasing the chain length of the wetting liquid. At high temperatures only the long n-alkanes partially wet an alkylated surface, at lower temperatures also relatively short n-alkanes partially wet the solid. Decreasing the temperature also renders the slopes of the curves less negative. Zisman [2] defined the
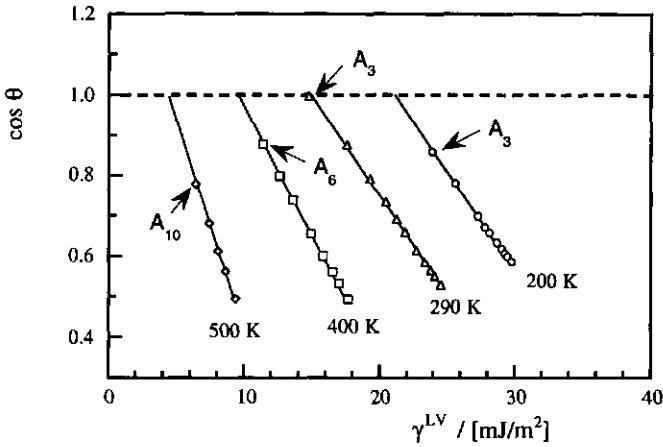
Figure. 11. Calculated contact angles of linear-chain-aliphatic liquids (A_n with n=3, 4, 5, 6, 7, 8, 10, 12, 14, 16, 20) on a rigid alkylated surface (S) as a function of the interfacial tension of the LV interface. The calculations are performed at various temperatures which are indicated in the figure. The interaction parameters used are $\chi_{AS} = 0$, $\chi_{OS} = 580/T$, $\chi_{AO} = 580/T$. For each temperature the shortest partial wetting liquid is indicated in the figure, for shorter n-alkanes cos $\theta = 1$.

critical surface tension as the intercept of the horizontal line $\cos\theta = 1$ with the straight line through $\cos\theta$. The intercept marks the transition from complete to partial wetting. With increasing temperature this intercept shifts to lower γ^{LV} values, i.e., the critical surface tension decreases. This shows that complete wetting becomes more favourable when the temperature is increased. For the n-alkanes it is predicted that the critical surface tension decreases by about 5 mJ/m^2 for each 100 K temperature increase.

With the theory plots like Fig. 11 can be calculated for different adsorbate-surface interactions. In Table 1 some of the contact angles of A_8 on the rigid substrates already presented in Fig. 10 are summarized. At T=290 K $\chi_{AS(O)}^d$ in Fig. 11 equals –4 and cos θ of A_8 equals 0.67. According to Table 1, cos θ of an A_8 droplet increases with increasing affinity (i.e., with decreasing $\chi_{AS(O)}^d$) of the substrate. Hence, the curves in Fig. 11 will shift to the right when increasing the adsorbate-substrate interactions (i.e., when decreasing $\chi_{AS(O)}^d$).

Table 1. Contact angles θ at T = 290 K of the octameric fluid A_8 on the different rigid substrates S of Fig. 10, $\chi_{OS} = 0$, $\chi_{AO} = 2$.

substrate		θ	$\cos \theta$
$\chi_{AS} = 0$, $\sigma_g = 0$	$\chi_{AS(O)}^d = -2$	115	– 0.42
$\sigma_g = 1$	$\chi_{AS(O)}^d = -4$	48	0.67
$\chi_{AS} = -4$, $\sigma_g = 0$	$\chi_{AS(O)}^d = -6$	0	1

129

Comparison with experimental contact angles

A detailed comparison of theoretical contact angle predictions with experimental studies is hampered by the microscopic heterogeneity of the surface (resulting from a number of complications including active sites, surface roughness or adsorbing molecules). Nevertheless, for the wetting of n-alkanes on low afffinity (alkylated) solids a reasonable agreement between the calculated contact angles and experimental data is obtained; Zisman plots for a series of homologous n-alkanes on various low affinity substrates [2] show a linear relation comparable to the one found in Fig. 11.

6.5. Conclusions

Vapour adsorption isotherms (including the meta- and unstable regions) of an octameric fluid on various solids are calculated. When the adsorption is mainly driven by a high end-segment (B) adsorption energy (f.i. $\chi_{BS} = -8$ and $\chi_{AS} \approx -2$), a linear isotherm results for semi-flexible chains B-A_6-B adsorbing on a rigid solid. The shape of this isotherm is qualitatively agrees with n-alkane isotherms measured on bare silica. With the theory also adsorption isotherms resembling the ones measured for n-alkanes on methylated silica can be obtained. Hereto interaction parameters are needed that favour a rather parallel adsorption of the chain-molecules with respect to the surface (f.i. $\chi_{BS} \geq -2$ and $\chi_{AS} = -4$).

A chain flexibility reduction (by applying the RIS scheme) increases the tendency of adsorbed chains to line up. In general, this increases the adsorbed amounts when the interaction parameters favour end-on adsorption, whereas this reduces the adsorbed amounts when the interaction parameters are in favour of adsorption parallel to the substrate.

On a poorly wetted rigid (allkylated) surface, an increasing contact angle has been calculated for increasing chain length of the wetting n-alkane A_n. The contact angles and the (Zisman) critical surface tension for wetting decrease with increasing temperature. When the temperature approaches the critical temperature of the wetting fluid, complete wetting occurs. Furthermore, it is established that the temperature dependence of the contact angle is largely due to the influence of the temperature on the liquid-vapour and solid-liquid interfacial tensions.

On solids with terminally grafted chains, octamer (A_8) adsorption isotherms and contact angles are calculated for different grafting densities and grafted chain lengths. Grafting of aliphatic chains to a very poorly wetted (bare) solid surface decreases the contact angle of the octameric liquid. On a such a solid, the contact angle as a function

of the grafting density passes through a minimum. Before the minimum the contact angle decreases due to the increasing number of contacts between the grafted chains and the adsorbate. The rise beyond the minimum is has an entropic origin. On a completely wetting (bare) solid grafting of chains eventually results in a finite contact angle and higher grafting densities give higher contact angles. In general, the contact angle on both substrates decreases with increasing grafted chain length.

On grafted solids adsorption mainly occurs in the outer parts of the grafted layer. The adsorption in this region is largely due to the penetration of adsorbate middle segments within the grafted layer. This implies that vapour adsorption and wettability of A_8 on alkylated substrates are largely determined by the sharpness of the vapour-boundary side of the grafted layer. When this boundary becomes more diffuse the lateral interactions between the adsorbate and the grafted chains are more favourable. This enhances the adsorption and decreases the contact angle.

The wettability of liquid-vapour-solid systems is, to a large extend, determined by the structure of the thinnest adsorbed layer/film that can form at saturation. When the solid-vapour interfacial structure of this layer resembles that of the bulk liquid-vapour interface, a liquid droplet will spread over its (thin) adsorbed film. When the structure differs considerably from that of the bulk liquid-vapour interface, the liquid will not spread on its adsorbed layer (autophobicity) and a finite contact angle occurs.

In this Chapter it has been shown that the thermodynamic and molecular aspects of wetting and adsorption can be described and related within the SCF-LFA theory. In principle, the theory is also suitable for the description of fluids of, or substrates grafted with, chains of a more complicated molecular architecture (e.g. branched or cyclic molecules) and their interfaces. Moreover, the work of adhesion of chain molecular liquids on various substrates can be calculated and compared to current theories of adhesion forces and (Lifshits-van der Waals) interfacial tension contributions. With the SCF-LFA theory also random heterogeneous surfaces [22] and rough substrates [23] can be described so that liquid contact angles on such substrates can be calculated and compared with the results obtained with e.g. the classical theories for heterogeneous (Cassie [22]) and rough (Wenzel [23]) surfaces.

It is also possible to extend the present theory to a two dimensional (2D) SCF approximation instead of the one dimension we used in this work. This allows one to calculate a contour plot of the droplet. From this plot the contact angle can be inferred. By comparing the contact angle obtained from this contour plot with the (1D calculated) equilibrium contact angle, the effect of the drop size and its curvature (and line tension) on the contact angle can, in principle, be studied.

Currently a "dynamic" version of the SCF theory is being developed in the department of Physical and Colloid Chemistry. In the future, this theory will allow investigation of the dynamics of evaporation of chain molecular liquids. Moreover, it will enable to study the dynamics of adsorption and wetting on solid substrates.

References

[1]   Mittal, L. K. (Ed.), *"Contact Angle, Wettability and Adhesion"*; VSP BV.: Utrecht, **1993**.

[2]   Zisman, W. A., in *"Contact Angle, Wettability, and Adhesion"*; Advances in Chemistry Series 43; Gould, R. F. (Ed.), American Chemical Society: Washington, D. C., **1964**: p. 1-52.

[3]   Schlangen, L. J. M., Koopal, L. K., Cohen Stuart, M. A., Lyklema, J., Robin, M. and Toulhoat, H., *Langmuir*, in press , **1995**; included as Chapter 4 in this thesis.

[4]   Levinson, P., Valignat, M. P., Fraysse, N., Cazabat, A. M. and Heslot, F., *Thin Solid Films*, 234 , **1993**, p. 482-485.

[5]   Blake, T. D., Cayias, J. L. and Zerdecki, J. A., *J. Colloid Interface Sci.*, 37 (4), **1971**, p. 678-685.

[6]   Kaminski, G., Duffy, E. M., Matsui, T. and Jorgensen, W. L., *J. Phys. Chem.*, 98 (49), **1994**, p. 13077-13082.

[7]   Smit, B., Karaborni, S. and Siepmann, J. I., *J. Chem. Phys.*, 102 (5), **1995**.

[8]   Madden, W. G., *J. Chem. Phys.*, 87 (2), **1987**, p. 1405-1422.

[9]   Xia, T. K., Ouyang, J., Ribarsky, M. W. and Landman, U., *Phys. Rev. Let.*, 69 (13), **1992**, p. 1967-1970.

[10] Adamson, A. W., in *"Physical Chemistry of Surfaces"*; John Wiley & Sons: New York, **1976**: Chapter 14 and references therein.

[11] Scheutjens, J. M. H. M. and Fleer, G. J., *J. Phys. Chem.*, 83, **1979**, p. 1619-1635.

[12] Scheutjens, J. M. H. M. and Fleer, G. J., *J. Phys. Chem.*, 84, **1980**, p. 178-190.

[13] Young, T., *Trans. Roy. Soc. London*, 95, **1805**, p. 65.

[14] Leermakers, F. A. M. and Scheutjens, J. M. H. M., *J. Phys. Chem.*, 89 (5), **1988**, p. 3264-3274.

[15] Evers, O. A., Scheutjens, J. M. H. M. and Fleer, G. J., *Macromolecules*, 23, **1990**, p. 5221-5232.

[16] Di Marzio, E. A. and Rubin, R. J., *J. Chem. Phys.*, 55, **1971**, p. 4318.

[17] Schlangen, L. J. M., Koopal, L. K., Cohen Stuart, M. A. and Lyklema, J., *Colloids Surfaces A*, 89, **1994**, p. 157-167; most of it is included in Chapter 2 of this thesis.

[18] Fowkes, F. M., *J. Colloid Interface Sci.*, 28 (3/4), **1968**, p. 493-505.

[19] Fowkes, F. M., *J. Phys. Chem.*, 84 (5), **1980**, p. 510-512.

[20] Weinhold, J. D. and Kumar, S. K., *J. Chem. Phys.*, 101 (5), **1994**, p. 4312-4323.

[21] Cahn, J. W., *J. Chem. Phys.*, 66 (8), **1977**, p. 3667-3672.

[22] Cassie, A. B. D., *Discussions Farad. Soc.*, 3, **1948**, p. 11.

[23] Wenzel, R. N., *Ind. Eng. Chem.*, 28, **1936**, p. 988.

Summary

Adsorption and wetting are related phenomena. In order to improve knowledge of both and their relations, experiments, thermodynamics and a theoretical interpretation have been connected, starring n-alkanes.

Starting from the Gibbs adsorption equation thermodynamic relations between vapour adsorption and wetting are derived. The surface pressure of a film, formed by vapour adsorption on a solid surface, is calculated by integrating the vapour adsorption isotherm. The surface pressure at the saturated vapour pressure determines, together with the interfacial tension of the liquid, the difference between the interfacial tension of a clean solid and a solid-liquid interface. Moreover, the surface pressure is related to the spreading tension and contact angle in a solid-liquid-vapour system. The thermodynamic equations derived are generally valid and the approach covers wetting on both flat and powdered solids. From the individual surface pressure values of two immiscible liquids, wetting and displacement in a solid-liquid-liquid system can be assessed. The procedure is illustrated for a silica-water-octane system. Silica is one of the most abundant minerals on earth and the oil/water wettability of silica can be considered a model for oil displacement in reservoir rocks.

By combining the Young equation with the Gibbs adsorption equation, the contact angle and the work of adhesion of an aqueous electrolyte solution on a charged solid is investigated as a function of the solid surface charge density or the electrolyte concentration. In the case of partial wetting, the solid-solution-vapour contact angle is a maximum at the point of zero charge of the solid. The contact angle decreases and the work of adhesion increases with increasing absolute value of the surface charge. The derived equations are used to study the wettability of silica under changing electrolyte conditions. The surface charge density of silica Aerosil OX-50 at a number of indifferent KCl concentrations, ranging from 0.01 M to 1M, is determined as a function of pH by potentiometric titrations. The silica surface charge increases with increasing ionic strength and increasing pH. At its point of zero charge ($pH^o \approx 3$) silica is already completely wetted by water. Charging of the surface results in an even better water wettability although this can not be observed experimentally. At $pH = 9$ and 1 M KCl the silica surface charge equals -0.25 C/m^2. Compared to the uncharged silica, this surface

135

charge decreases the silica-water interfacial tension by 22 mJ/m². Under usual conditions the electrolyte adsorption at the solid-vapour interface will be less than at the solid-water interface. With respect to an uncharged silica (*pH*=3), the silica surface charge of –0.25 C/m² decreases the silica-(water)vapour interfacial tension by maximally 22 mJ/m² whereas it increases the work of adhesion by maximally 22 mJ/m². By combining the present approach with theoretical equations describing the adsorption of charge determining ions on solids with different kinds and amounts of chargable groups the wettabililty of such solids as a function of their charging behaviour can be described theoretically. This remains a task for the future.

The vapour adsorption of different n-alkanes, cyclohexane, toluene and water on bare and methylated pyrogenic silica (Aerosil OX-50) has been studied gravimetrically. Linear adsorption isotherms of the n-alkanes and of cyclohexane on both substrates are found until high relative vapour pressures. The same holds for toluene on methylated silica. The linearity of the isotherms indicates relatively weak lateral interactions between adsorbed molecules. On bare silica, the adsorption of the n-alkanes studied (C7-C9) is, expressed in moles/m², independent of the chain length. The adsorption strongly increases after the coverage corresponding to a monolayer of alkanes, oriented perpendicular to the surface, has been reached (at $p/p_0 \approx 0.8$). Methylation of the silica decreases the adsorption of all adsorptives studied. Until just before saturation the octane adsorption on methylated silica is below that of a monolayer parallel to the surface. The shape of these adsorption isotherms indicates that on bare silica n-alkanes predominantly adsorb end-on, perpendicular to the surface, whereas on methylated silica, the adsorption is rather parallel. From the adsorption data surface pressure isotherms are constructed and the work of adhesion is obtained. The work of adhesion reveals that the Lifshits-van der Waals part of the silica surface tension is reduced from 44 mJ/m² for bare (pyrogenic) silica to 30 mJ/m² for methylated silica. The adsorption data are also converted to disjoining pressure isotherms. At low film thicknesses, these can be described by an exponential short-range interaction. The classical macroscopic models are not very suited for the description of such thin films for which the molecular organization and the discrete character of the adsorbed layer are extremely important. However, thin adsorbed layers can be described on the basis of microscopic models for adsorption. Also surface pressures of simple systems can be obtained from classical adsorption equations (e.g., Langmuir, Volmer, BET, Polyani). However, for chain molecules like n-alkanes these models are inadequate as they are unable to describe the structure of the molecules and their adsorbed layers. This problem can be overcome by

136

using, for instance, a more recent self-consistent-field (SCF) theory, orginially developed by Scheutjens and Fleer and extended by Leermakers and others.

The SCF theory is applied for the description of chain molecular fluids and their interfaces. Hereto a fluid is considered as a mixture of chains and monomeric vacancies. The latter account for the free volume in the system. Intermolecular interactions are described in terms of Flory-Huggins (FH) parameters. For the homologous series of linear alkanes, these parameters are generalized and assessed from a fit to vapour pressure data. In the SCF lattice-fluid theory, each alkane is described as a chain of segments with a volume of 0.027 nm^3 each. The segment-segment interactions (for which the FH parameter is zero by definition) are reflected in a non-zero FH interaction parameter for a chain segment-vacancy contact χ_{Ao}. Under the conditions mentioned χ_{Ao} equals $580/T$ (T in K) for all n-alkanes. With these parameters n-alkane bulk properties such as the vapour pressure, density, critical point and heat of vaporization can be obtained together with structural and thermodynamic properties of the liquid-vapour (LV) interface. The calculations reveal that chain ends are the major constituents on the vapour side of the (alkane) LV interface. For longer chains and lower temperatures the (relative) preference of the chain ends to protrude into the vapour phase is more pronounced. The calculated variation of the n-alkane LV interfacial tension (γ) with temperature and chain length agrees quantitatively with experimental data. If the theory is applied for temperatures below the (experimental) n-alkane freezing points, positive $d\gamma/dT$ values occur and a maximum in the LV interfacial tension is found at $T/T_c \approx 0.12$, irrespective of the chain length of the molecule. In experimental studies close to the n-alkane freezing points similar observations have been made. However, a comparion of these experimental observations with our theoretical predictions should be performed with some reservation as the theory describes a frozen phase as an isotropic supercooled fluid.

The lattice fluid theory description of the n-alkane interfacial properties may be improved by considering chain-flexibility constraints, such as trans-gauche conformations and/or by distinghuishing (the parameters of the) CH_3 and CH_2 segments. It is rather straightforward to extend the present theory to more complex systems such as fluid mixtures, or fluids (vapour and liquid) at solid surfaces. The interfacial tensions of such interfaces can be inferred from the theory so that the work of adhesion and contact angles on these interfaces can be investigated as a function of temperature and chain length of the (wetting) liquid. Some of these aspects are elaborated in the last Chapter.

137

The adsorption, structure and thermodynamics of (aliphatic) chain molecular fluids at rigid surfaces and at solids with thermally grafted (aliphatic) chains is also investigated. Vapour adsorption isotherms, inclusive the meta- and unstable regions, of an octameric fluid on various substrates are calculated. The octameric molecules are modelled as $B\text{-}A_6\text{-}B$ chains where A represents a CH_2 segment and B a CH_3 segment. On a bare solid, the influence of adsorption energy differences between the A and B segments of the chain molecule is investigated together with the influence of the chain flexibility. For semi-flexible chains with high chain end-adsorption energies the shape of the calculated isotherm qualitatively agrees with the linear vapour adsorption isotherms measured for n-alkanes on bare silica. With the theory adsorption isotherms resembling the ones measured for n-alkanes on methylated silica can be obtained. This requires semi-flexible chains with interaction parameters that favour a rather parallel adsorption of the chain-molecules with respect to the surface. A reduction of the chain flexibility, for instance by applying the RIS scheme, increases the tendency of the adsorbed molecules to line up. In general, this increases the adsorbed amounts when the interaction parameters favour end-on adsorption whereas this reduces the adsorbed amounts when the interaction parameters are in favour of parallel adsorption. On a poorly wetted rigid solid, a decreasing contact angle was calculated for increasing chain length of the (aliphatic) wetting liquid A_n. The contact angles and the (Zisman) critical surface tension for wetting decrease with increasing temperature. When the temperature approaches the critical temperature of the wetting fluid, complete wetting occurs. Furthermore, it is established that the temperature dependence of the contact angle mainly results from the influence of the temperature on the liquid-vapour and solid-liquid interfacial tensions.

On solids with grafted chains, octamer (A_8) adsorption isotherms and contact angles are calculated for different grafting densities and grafted chain lengths. Grafting aliphatic chains on a very poorly wetted (bare) solid decreases the contact angle of the octameric liquid. On such a solid, the contact angle as a function of the grafting density passes through a minimum. The rise beyond the minimum has an entropic origin. Grafting of chains on a completely wetting (bare) solid eventually results in a finite contact angle; higher grafting densities give rise to higher contact angles. When longer chains are grafted, lower contact angles result for both substrates. The calculations provide insight into the wettability of a substrate by chain-molecular fluids on a molecular level. Partial wetting of chain molecules can be explained from an autophobic effect: due to the ordering (anisotropy) of the molecules present in the thinnest adsorbed layer that can form at saturation, molecules of the isotropic liquid are repelled. The liquid does not spread on the thin film and droplet formation results. The calculations reveal that the partial wetting of

chain molecular liquids on grafted solids is largely due to the enrichment of the grafted layer by middle segments of the liquid molecules.

In this thesis the thermodynamics and molecular aspects of adsorption and wetting have been investigated and coupled by means of vapour adsorption isotherms and a lattice fluid theory. At present a reasonable (semi) quantitative agreement between theory and experiments has been achieved. For the (near) future, some other investigations based on the present theory are challenging. Firstly, a better quantitative agreement with experimental data is feasible by optimizing the description of the aliphatic molecules, for instance by incorporating differences between end and middle segments and their mutual interactions, or, in our case, their interactions with a vacancy. Secondly, the theory is able to describe random, heterogeneous surfaces and rough substrates so that contact angles of chain molecular liquids on such substrates can be inferred and compared to theories such as developed by Cassie and Wenzel. Moreover, the theory can be extended to a two-dimensional SCF approximation instead of the one dimension we used in this work. This renders calculation of the (density) contour plot of a droplet feasible. By comparing the contact angle of this contour plot with the equilibrium contact angle, calculated in one-dimensional SCF, the effect of the drop size, its curvature and line tension on the contact angle can be studied. Finally, a "dynamic" version of the SCF theory is currently being developed in the department of Physical and Colloid Chemistry. In the future, this theory will be suited to investigate the dynamics of evaporation of chain molecular liquids as well as the dynamics of their adsorption, spreading and contact angles on solid substrates.

Samenvatting

Bevochtiging heeft betrekking op het gedrag van een vloeistof aan een oppervlak. Wanneer een oppervlak volledig wordt bevochtigd dan spreidt de vloeistof over het oppervlak. Indien een oppervlak onvolledig of slecht wordt bevochtigd dan spreidt de vloeistof niet over het oppervlak maar vormt een druppel. Een alledaags voorbeeld van bevochtiging zijn de regendruppels op ruiten in huizen en auto's. Wanneer het water goed zou spreiden over de ruit dan zou dat op een regenachtige dag het zicht van een automobilist sterk verbeteren. Een ander voorbeeld: eenden vetten hun veren in om ze sterk waterafstotend te maken. Hierdoor kunnen ze makkelijker blijven drijven.

De bevochtiging van een oppervlak wordt beheerst door de stoffen die op dat oppervlak aanwezig zijn. Dit is relevant voor bijvoorbeeld de aardolie-, verf- en coatingindustrie. Teflon (polytetrafluorethyleen) bijvoorbeeld is een veel toegepaste oppervlaktecoating. Vergeleken met andere materialen is de hechting van allerlei stoffen op een teflon oppervlak relatief zwak. Teflon wordt dan ook vaak aangebracht in koekepannen om aanbakken te voorkomen. De lage affiniteit van teflon voor allerlei andere stoffen wordt direct zichtbaar wanneer een waterdruppel in een teflon gecoate koekepan wordt gelegd: de druppel probeert zo weinig mogelijk contact te maken met de pan en de vloeistof blijft als een klein bolletje op het oppervlak staan.

De affiniteit van een vast oppervlak voor andere moleculen komt tot uitdrukking in de oppervlaktespanning. Als ruwe vuistregel geldt: des te hoger de oppervlaktespanning van een vast oppervlak des te makkelijker de hechting (adsorptie) van moleculen aan dat oppervlak en des te beter de bevochtiging door een vloeistof. Adsorptie aan een oppervlak verlaagt normaal gesproken de oppervlaktespanning. Dit verklaart waarom water wel spreidt over goed schoon gemaakte ruiten maar niet over ongewassen (vette) ruiten. Op ongewassen ruiten maken geadsorbeerde "vettige" stoffen de oppervlakte-spanning van het glas zo laag dat waterdruppels blijven liggen.

Lineaire (n-)alkanen zijn moleculen met de chemische structuur $CH_3-(CH_2)_{n-2}-CH_3$. Alkanen zijn belangrijke bestanddelen van fossiele brandstoffen, olie, smeermiddelen en polymeren. In bevochtiging- en adhesieonderzoeken worden alkanen vaak gebruikt als model ("ijk") stoffen. In dit proefschrift worden daarom met name de adsorptie en bevochtiging van alkanen op vaste oppervlakken bestudeerd.

Adsorptie en bevochtiging staan nauw met elkaar in verband. Dit verband is het duidelijkst wanneer de damp van een vloeistof adsorbeert op een vast oppervlak. Met toenemende dampdruk hopen meer dampmoleculen zich op aan het oppervlak. Indien
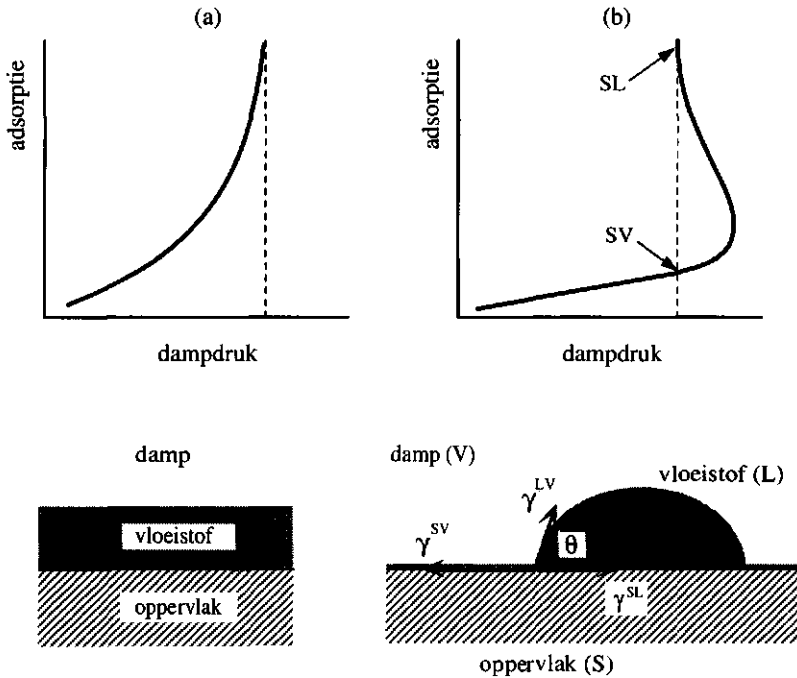
Figuur 1. Verschillende bevochtigingstoestanden en hun adsorptie als functie van de dampdruk in geval van volledige (a) en onvolledige (b) bevochtiging. Bovenaan zijn de twee adsorptie-isothermen getekend. De gestippelde lijn is de verzadigde dampdruk. Bij deze druk zal (uiteindelijk) een dikke laag vloeistof gevormd worden door condensatie van de damp. De twee schetsen eronder corresponderen met de situatie op de gestippelde lijn in de isotherm erboven. Voor situatie (a) is dit een macroscopische laag vloeistof op het oppervlak. In situatie (b) zijn twee geadsorbeerde fasen, aangegeven door de pijlen, met elkaar in evenwicht. Dit komt overeen met een druppel vloeistof L op S, waarbij de rest van S bedekt is met een zeer dunne film (het SV grensvlak) . De pijlen in schets (b) geven de oppervlakte-spanningen van de drie verschillende oppervlakken weer.

er genoeg dampmoleculen aanwezig zijn ontstaat bij de verzadigde dampdruk een dikke vloeistoflaag op het oppervlak. Wanneer deze laag gevormd kan worden zonder de verzadigde dampdruk te passeren is er sprake van volledige bevochtiging. Zo'n situatie is weergegeven in Fig 1a. In Fig. 1b is er sprake van onvolledige bevochtiging; bij de verzadigde dampspanning onstaat eerst een stabiele, maar zeer dunne film (aangegeven met sv) op het oppervlak. Pas na oververzadiging van de damp treedt condensatie op, maar dan wel in de vorm van druppels. Dit betekent dat de bevochtiging van een vloeistof op een oppervlak onderzocht kan worden door dampadsorptie als functie van

142

de dampdruk te meten. Een dergelijke dampadsorptie-curve, gemeten bij constante temperatuur, wordt een adsorptie-isotherm genoemd.

In een onvolledig bevochtigend vloeistof-damp-vast (oppervlak) systeem wordt de hoek die de druppel maakt met het oppervlak de randhoek genoemd. De grootte van de randhoek (θ) wordt gegeven door het mechanisch evenwicht tussen de grensvlak-spanningen, zie ook de schets in Fig. 1b. De randhoek karakteriseert de bevochtiging: hoe groter de randhoek des te slechter de bevochtiging.

Allereerst is dampadsorptie gekoppeld aan bevochtiging binnen een algemeen thermodynamisch kader. Met deze koppeling kan ook de verdringing van een vloeistof aan een oppervlak door een andere vloeistof beschreven worden. Het algemene kader verklaart ook waarom de randhoek van een waterdruppel op een oplaadbaar oppervlak maximaal is wanneer de oppervlaktelading nul is. Door het oppervlak op te laden (positief of negatief) neemt de randhoek af, dat wil zeggen, het oppervlak wordt beter bevochtigd door water.

De dampadsorptie van n-alkanen op silica (een van de meest voorkomende mineralen in de aardkorst) is, met een heel precieze balans, tot op één miljoenste gram nauwkeurig gemeten als functie van de dampdruk. De n-alkaan adsorptie voor $n = 7$, 8 of 9, uitgedrukt in aantal moleculen per m^2, bleek lineair toe te nemen met de dampdruk en was onafhankelijk van de ketenlengte n. Indien voorafgaand aan de adsorptiemetingen, methyl ($-CH_3$) groepen verankerd worden aan het silica oppervlak wordt een lagere n-alkaan adsorptie gevonden. De vorm van de gemeten adsorptie-isothermen suggereert dat n-alkanen tamelijk loodrecht adsorberen op kale silica terwijl ze veel vlakker gaan liggen op gemethyleerde silica. Alkanen bevochtigen kale silica volledig, op gemethyleerde silica wordt onvolledige bevochting gevonden. Samen met de gemeten isothermen geeft dit aan dat de bevochtiging van een oppervlak door alkanen sterk afhangt van de structuur van de SV alkaanfilm.
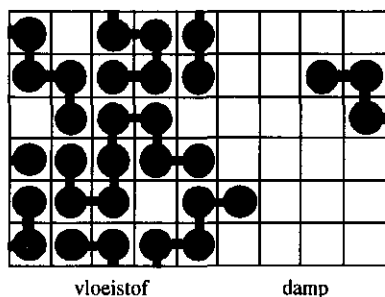
Om een beter inzicht te krijgen in het gedrag van alkanen aan grensvlakken is gebruik gemaakt van een statistisch-thermodynamische theorie die oorspronkelijk ontwikkeld is door Scheutjens en Fleer en is uitgebreid door o.a. Leermakers. In deze theorie worden ketenmoleculen (in dit geval n-alkanen) beschreven als een keten opgebouwd uit aan elkaar gekoppelde eenheden. Deze eenheden worden segmenten genoemd. Ieder segment stelt een C-atoom van een alkaanmolecuul voor. De ruimtelijke verdeling van de moleculen wordt beschreven door de ketens in een rooster te plaatsen (zie Fig. 2). Met deze theorie kan zowel de (evenwichts)structuur als de oppervlaktespanning van een oppervlak met alkaanmoleculen uitgerekend worden.

Berekeningen aan alkaan vloeistof-damp grensvlakken laten zien dat de uiteinden van de alkaanketens bij voorkeur uitsteken in de dampfase. Voor langere n-alkanen en bij lagere temperaturen is deze voorkeur sterker. De berekende LV grensvlakspanningen voor diverse n-alkanen bij verschillende temperaturen komen goed overeen met gemeten waarden.

vloeistof   damp

Figuur 2. Octaanmoleculen en hun vloeistof-damp grensvlak binnen een roostermodel. Octaan wordt voorgesteld als een keten van 8 segmenten, ieder segment vult precies één roostercel. De zwarte balken geven aan welke segmenten samen één molecuul vormen.

De adsorptie, structuur en oppervlaktespanningen van verschillende vaste oppervlakken die in contact staan met alkaandamp of alkaanvloeistof zijn met de theorie bestudeerd. In de adsorptieberekeningen is de invloed van adsorptie-energie verschillen tussen eind (CH_3) en midden (CH_2) segmenten op het adsorptiegedrag van n-alkanen onderzocht. De aldus berekende alkaan isothermen komen goed overeen met de gemeten curven. Daarnaast zijn n-alkaan randhoeken op verschillende onvolledig bevochtigende oppervlakken uitgerekend. Hierbij is gekeken naar de invloed van de temperatuur en de n-alkaanketenlengte op de randhoek. De berekende randhoeken nemen toe wanneer de temperatuur daalt of wanneer de ketenlengte van de bevochtigende alkaan stijgt. Verder blijkt dat chemische verankering van koolwaterstofketens aan een volledig bevochtigend oppervlak dat oppervlak slechter bevochtigbaar maken voor n-alkanen. Hierbij hebben korte verankerde ketens normaal gesproken een sterker effect op de randhoek dan langere.

Met de theorie is een beter inzicht verkregen in het mechanisme van bevochtiging op moleculair niveau. De structuur van de dunste geadsorbeerde laag die gevormd kan worden bij de verzadigde dampdruk (het SV grensvlak, zie Fig. 1b) kan sterk afwijken van die in bulk vloeistof, bijvoorbeeld doordat de geadsorbeerde moleculen plat gaan liggen op het oppervlak. In dit geval zal alkaanvloeistof als druppels op het oppervlak met de geadsorbeerde alkaanmoleculen blijven liggen. De theorie beschrijft zowel de vloeistof en damp fasen van n-alkanen als hun gedrag aan vloeibare en vaste oppervlakken op moleculaire en macroscopische schaal. Hiermee voorziet de theorie in een gemeenschappelijke benadering van adsorptie en bevochtiging waarbinnen thermodynamica, moleculaire aspecten en experimenten aan elkaar gekoppeld worden.

Curriculum Vitae

Lucas Jozef Maria Schlangen is op 21 Juli 1968 te Enschede geboren. In 1986 heeft hij het einddiploma Atheneum B aan het Boschveldcollege te Venray behaald en begon hij zijn studie Moleculaire Wetenschappen aan de Landbouwuniversiteit Wageningen. In November 1990 studeerde hij cum laude af in de Fysisch-chemische en Chemische oriëntaties van deze studierichting. Vanaf december 1990 was hij, in het kader van het EG project JOULE, voor vier jaar werkzaam als assistent in opleiding bij de vakgroep Fysische en Kolloïdchemie. Ten behoeve van dit project was hij van oktober 1991 tot oktober 1992 gedetacheerd aan het Institut Français du Pétrole te Parijs. Begin 1995 rondde hij het onderzoek af met het schrijven van dit proefschrift. Vanaf april 1995 is hij werkzaam op het Philips Natuurkundig Laboratorium te Eindhoven.